


For Reference

NOT TO BE TAKEN FROM THIS ROOM

Ex LIBRIS
UNIVERSITATIS
ALBERTAENSIS





Digitized by the Internet Archive
in 2023 with funding from
University of Alberta Library

<https://archive.org/details/Semary1972>

THE UNIVERSITY OF ALBERTA

NORMAL TUNNELING INTO MAGNETIC JUNCTIONS

by



MOHAMMAD ABDALLA SEMARY

A THESIS

SUBMITTED TO THE FACULTY OF GRADUATE STUDIES AND RESEARCH

IN PARTIAL FULFILLMENT OF THE REQUIREMENTS FOR THE DEGREE

OF DOCTOR OF PHILOSOPHY

DEPARTMENT OF PHYSICS

EDMONTON, ALBERTA

FALL, 1972

UNIVERSITY OF ALBERTA

FACULTY OF GRADUATE STUDIES AND RESEARCH

The undersigned certify that they have read, and recommend to the Faculty of Graduate Studies and Research for acceptance, a thesis entitled "NORMAL TUNNELING INTO MAGNETIC JUNCTIONS", submitted by Mohammad Abdalla Semary in partial fulfillment of the requirements for the degree of Doctor of Philosophy.

ABSTRACT

The S-d exchange interaction between the conduction electrons and the localized magnetic moments in dilute magnetic alloys was shown by Kondo to explain the resistivity minimum and its temperature dependence. The S-d exchange tunneling version of the Kondo scattering has been considered by Appelbaum and Zawadowski in order to explain the zero bias anomalies in the tunneling conductance of metal-metal oxide-metal junctions doped with magnetic impurities.

In this work the tunneling technique has been used to explore some information about the Kondo problem. This has been done by investigating the conductance characteristics of Al-I-Al junctions doped with Fe and Ni impurities. The dopant was introduced in a form of a layer like distribution in the Al electrode. The results show that, not only the impurities at the barrier interface are effective in producing the conductance anomaly, but also those located within a certain length inside the metallic electrode. This effective length can be associated with the Kondo coherence length of the magnetic dopant in the non-magnetic host metal. The results are explained in terms of Mezei and Zawadowski theory.

The first observation concerning the effect of the impurity-impurity interaction on the conductance anomaly was reported, and the results are compared with Gupta and Upadhyaya predictions.

Al-I-Ni (or Fe) junctions were prepared with the intention of observing fine structure which could be associated with the electron-magnon interactions or band structure effects, however, no experimental evidence was found for such predicted structure.

ACKNOWLEDGEMENTS

I wish to express my gratitude to Dr. J.S. Rogers, my research supervisor, for suggesting the project and for his encouragement and guidance.

I am deeply thankful to Dr. S.B. Woods, for his cooperation during different phases of this project.

I am grateful to the technical staff, who supplied liquid helium and liquid air and assisted in the construction of evaporators and cryostats.

I would like to thank Miss M.O. Flores for proof-reading the final manuscript and Mrs. Mary Yiu for her patience and fine typing performance.

I wish to record my thanks for the Department of Physics and the National Research Council of Canada for the financial assistance.

I like to thank Cairo University, Egypt, for granting me a study leave.

Finally, I thank my wife and my son for their understanding and patience during the past years.

TABLE OF CONTENTS

Chapter		Page
1.	INTRODUCTION	1
	1.1. Electron Tunneling	1
	1.2. Motivation of This Work	6
2.	THEORETICAL BACKGROUND	8
	2.1. Kondo Problem and Tunneling Anomalies	8
	2.2. The S-d Exchange Model of Zero Bias Anomaly	12
	(a) The Temperature and Energy Dependence	12
	(b) The Conductance Peak Anomaly in a Magnetic Field	18
	2.3. Strong Coupling Limit	19
	2.4. Interface Effect on the Conductance Characteristics	23
	2.5. Interacting Magnetic Impurities	25
	2.6. The Normalized Electron Density of States	26
	2.7. The Tunneling Conductance and the Renormalization Function	34
	2.8. The Anomalies and Kondo Coherence Length	39
3.	EXPERIMENTAL METHODS	45
	3.1. General Consideration	45
	3.2. Junction Preparation	49
	3.3. Thickness Measurements	51

Chapter		Page
3.	3.4. Production of Low Temperatures	56
	3.5. Conductance Measurements	58
4.	EXPERIMENTAL RESULTS AND DISCUSSIONS	60
	4.1. Small Conductance Peak	60
	(a) Temperature and Voltage Dependence	60
	(b) Magnetic Field Dependence	65
	(c) Concentration Dependence	68
	4.2. Tunneling Results with Interacting Magnetic Impurities	73
	4.3. Tunneling Results and Kondo Coherence Length	81
	4.4. Al-I-Fe or Ni Junctions	96
	4.5. Iron-Oxide Barriers	104
5.	SUMMARY AND CONCLUSIONS	111
	REFERENCES	113

LIST OF FIGURES

Figure		Page
2.1	Schematic representing A-I-B tunnel junction doped with a magnetic impurity. The localized state ϕ_d strongly overlap the wave function ϕ_A ; weak interaction with ϕ_B leads to exchange tunneling events.	13
2.2 (a)	Schematic diagrams of the different processes that contribute to the theoretical conductance of the Appelbaum model.	20
(b)	The process of Fig.2.2a in the presence of a magnetic field, after Shen and Rowell (1968).	
2.3 (a)	A tunnel barrier of height U doped with a single impurity at Z_0 .	24
(b)	$G^{(2)}$ as a function of the impurity position.	
(c)	The coefficient of the log as a function of the impurity position, after Appelbaum and Brinkman (1970).	
2.4 (a)	$G^{(2)}$ versus bias voltage at 1.6°K .	27
(b)	$G^{(2)}$ versus temperature at zero bias.	
(c)	$G^{(3)}$ versus bias voltage at 1.6°K .	
(d)	$G^{(3)}$ versus temperature at zero bias.	

- 2.3
cont'd Curves I, II, III, IV and V correspond to $W = 0, 10^{-4}, 2 \times 10^{-4}, -10^{-4}$ and 2×10^{-4} eV, respectively, after Gupta and Upadhyaya (1971).
- 2.5 (a) A-I-B junction with magnetic impurities within the coherence length ξ . 30
(b) The depression of the electron density of states within the coherence length, after Sóllyom and Zawadowski (1968).
- 2.6 (a) $R(V)/R_0 \equiv Z^{-1}$ versus reduced bias voltage V , at different reduced temperature t . 38
(b) Z versus E (dashed line), and the effect of self consistency on the energy at the minimum (solid line), after Sóllyom and Zawadowski (1968).
- 2.7 The relative change $\Delta\rho/\rho$ in the electron density of states due to (a) a single impurity, (b) an impurity layer as a function of r/ξ_Δ (taken from Mezei and Zawadowski (1971)). 43
- 3.1 (a) The resistance as a function of the film thickness at different substrate temperatures. 48
(b) The temperature dependence of the critical thickness t_c (taken from Chopra (1966), (1968)).

Figure		Page
3.2	(a) The oscillation of the single crystal; most of the mass displacement occurs at the crystal surface.	55
	(b) The circuit diagram of the single crystal monitor used in the present work.	
	(c) Single crystal holder; very light springs are used to provide elec- trical contacts with the crystals.	
3.3	The cryostat arrangement for the production of low temperatures.	57
4.1	The conductance versus voltage at 80 K (dashed line) and 4.2 K (solid line) of an Al-I-Al junction doped with Ni impurities at the barrier interface.	61
4.2	ΔG versus V at different temperatures.	62
4.3	The dependence of ΔG on bias voltage (open circles) and $\Delta G(V=0)$ on tem- peratures (solid points).	64
4.4	ΔG versus V characteristics in the presence of a magnetic field H . Curves a, b, c, d, e and f corres- pond to $H = 0, 20, 38, 55, 60$, and 66 ; $T \approx 1.7^\circ\text{K}$.	67

Figure		Page
4.5	G versus V for an Al-I-Al junctions doped approximately with (a) 1 A° ; (b) 2 A° ; (c) 3 A° ; (d) 5 A° ; and (e) 7 A° of Ni impurities at the barrier interface.	70
4.6	Conductance versus voltage for Al-I-Al junctions doped with Fe impurities. Doping is approximately (a) 0.5 A° ; (b) 1 A° ; (c) 1.5 A° .	74
4.7	Superconducting energy gap results for junctions (a), (b) and (c) of fig.4.6.	77
4.8	G versus V characteristics for junction (a) of fig. 4.6 at different temperatures.	78
4.9	Magnetic field results for junctions (a), (b) of fig. 4.6.	80
4.10	Preliminary run on Al-I-Al junction doped with Ni layer introduced at (a) 0 A° ; (b) 50 A° ; (c) 70 A° , and (d) 150 A° from the barrier interface.	84

Figure		Page
4.11	Conductance-voltage characteristics for Al-I-Al junctions, doped with $\sim 5 \text{ A}^\circ$ of Ni layer at $r = 11$, 21.5, 32.5 and 56.5 A° , Curves a, b, c and e respectively, Curve f, same as e with no impurities.	85
4.12	The energy gaps of Al, (a) undoped junction, (b) 3 A° of Ni dopant was introduced at $r = 50 \text{ A}^\circ$.	86
4.13	Curve (c) of fig. 4.11 at different temperatures, and $G(V=0)$ versus temperature.	88
4.14	The temperature dependence of the Conductance reduction $\Delta G/G^\circ$ for Al-I-Al junctions doped with different amount of impurities at different distances from the barrier-metal interface.	89
4.15 (a)	The conductance σ versus voltage V for Al-I-Al junctions with Sn particles in the barrier, $\sqrt{\langle r^2 \rangle}$ is the average radius of the Sn particle.	91
(b)	The temperature dependence of $\sigma(V=0)$, Zeller and Giaever (1969).	

Figure		Page
4.16	The conductance-voltage characteristics for Al-I-Al junctions doped approximately with (a) 2.5 A° ; (b) 2 A° ; (c) 1.5 A° ; (d) 0.5 A° and (e) 0 A° of Ni impurity layers at $r = 50 \text{ A}^\circ$.	93
4.17	The conductance reduction at zero bias $ \Delta G/G^\circ $ as a function of r ; Ni dopant is approximately $\square 5 \text{ A}^\circ$, 0.3 A° , or 2 A° . The solid lines $C e^{-r/\xi} [2 - e^{-r/\xi}]$ for $C = 1, 1.5$.	94
4.18	dG/dV versus V for an Al-I-Pb junction at 4.2°K . The peaks correspond to different excitations in the junction.	97
4.19	$G-V$ characteristics for Al-I-Fe junction at 4.2°K .	99
4.20	(dG/dV) versus V at 4.2°K for an Al-I-Fe junction.	100
4.21	$G-V$ characteristics at 4.2°K for an Al-I-Ni junction.	102
4.22	(dG/dV) versus V at 4.2°K for an Al-I-Ni junction.	103

Figure		Page
4.23	The dynamical resistance R versus V at different temperature for an $\text{Fe-Fe}_3\text{O}_4\text{-Al}$ junction (the tunnel barrier was formed in air at 100°C for about 10 minutes).	105
4.24	R versus V at different temperatures and $R(V=0)$ versus T for Fe_3O_4 barrier formed in a glow discharge of oxygen.	106
4.25	The normalized conductance σ_n versus voltage for $\text{Fe-Fe}_3\text{O}_4\text{-Pb}$ junctions (solid lines) and for $\text{Al-Al}_2\text{O}_3\text{-Pb}$ junction (circles).	108

CHAPTER 1

INTRODUCTION

1.1 Electron tunneling

In classical physics, a particle whose energy is less than the height of a potential barrier can never pass through, because the particle cannot be found in a space region where its kinetic energy is negative. On the basis of quantum mechanics, the particle behaviour is described in a probabilistic sense. Once it is represented by a wavefunction, the particle has a nonzero probability of penetrating through a classically forbidden region. This tunneling process is one of the simplest examples of a truly quantum mechanical phenomenon. The first application of tunneling was made by Oppenheimer (1928), in order to describe the autoionization of the excited states of atomic hydrogen in a strong electric field. The effect of the field is to distort the Coulomb potential wall, so that an electron would see a finite barrier through which it could tunnel. In fact Oppenheimer devised a simple time dependent formalism, which in due time became the basis of the transfer Hamiltonian method, Duke (1969). The next and almost immediate application was the analysis

of α -decay from heavy nuclei. The electron emission observed by Lilienfeld (1922) was explained by Fowler and Nordheim (1928).

The possibility that a tunnel current may flow between metals separated by an insulating layer was first considered by Frenkel (1930), nevertheless, the field of tunneling owes its present lively state to the discovery of the p-n diode by Esaki (1957), and tunneling through oxide layers by Fisher and Giaever (1961). The immediate effect of Giaever's work on the experimental aspect of tunneling was the stimulation of a sequence of measurements on both superconducting and normal metal-insulator-normal metal junctions. The early experiments led to the confirmation of the Bardeen-Cooper-Schrieffer-gap (1957), and square-root singularity in the electronic density of states of the weak coupling superconductors, the fascination of the Josephson effect, and the measurement of the details of electron-phonon interaction. A second consequence of Giaever's work was the development of a tunneling theory based on the transfer Hamiltonian model, which accounted for the many-body properties of the electrodes, Bardeen (1961). The extension of the model to look after the many-body effects in the barrier and normal electrodes is still in progress, Appelbaum and Brinkman (1969).

The main objective of the present investigation is the tunneling between two normal metal electrodes separated by a thin ($\sim 20 \text{ \AA}$) insulating barrier. The small size of the electron current in the junction is a manifestation of the weak coupling between the two electrodes. This coupling depends on the nature of the wavefunction in the barrier region. It is difficult, however, to treat the wavefunction in the barrier properly, because even weak interactions in the bulk have a nonperturbative effect on the electron wavefunction. We will first consider the interaction between the conduction electrons and the magnetic impurities, which introduces a rapid conductance change at the zero bias voltage, commonly called zero bias anomalies; and second, interactions which introduce conductance changes at higher bias voltages.

Essentially, there are two kinds of zero bias anomalies in the dynamical conductance characteristics of a metal-metal oxide-metal junction. The first one which was discovered by Wyatt (1964) on Ta-I-Al junction, consisted of a conductance peak at zero bias not greater than 10 % and typically of a few m.V. wide. It was analyzed in terms of a logarithmic singularity in the electron density of states, of Ta, around the Fermi energy. The second anomaly was discovered by Rowell and

Shen (1966), and it revealed a broad minimum in the conductance at zero voltage, having a width of the order of 100 m.V. The conductance reduction at zero bias is about 100 %. This anomaly is known as "a giant resistance anomaly".

Following Anderson's (1966) suggestion that the conductance peak anomaly is due to impurity states in the barrier, Appelbaum (1966) considered a model based on the Kondo interaction between the conduction electrons and magnetic impurity spins. The theory predicts the Zeeman splitting of the conductance peak in a magnetic field. The Zeeman splitting was observed by Shen and Rowell (1968). However both types of zero bias anomalies can be produced by doping the junction with the same magnetic dopant by only changing its amount. This strengthened the idea that the giant anomaly also has a magnetic origin. Sólyom and Zawadowski (1968) introduced a theory based on the influence of the electron impurity spin interactions on the electron dispersion relation, and hence, the tunneling conductance. They predict a large conductance reduction which varies with the position of the impurity in the metallic electrode. A Kondo coherence length, which could be determined from electron tunneling measurements, has been introduced by Mezei and Zawadowski (1971). The

different models of the zero bias anomalies are considered in Chapter 2.

Structures at higher bias voltage due to the interaction of the tunneling electron with different excitations in the barrier and the electrodes had been observed in different tunnel junctions, Duke (1969). Jacklevic and Lambe (1966) interpreted their measurement of step discontinuities in the conductance as caused by the excitation of vibronic states of adsorbed water molecules in the junction. At lower voltages, Rowell et al (1969) and Adler (1969), observed the excitations of vibrations of the oxide itself, which could be regarded as oxide phonons or vibrations of the oxide molecules. They also observed the characteristic phonon energies for the bulk normal Pb between 5 and 9 m.V. The effect of the electron-magnon interaction on the tunneling characteristics was investigated by Appelbaum and Brinkman (1969). The possibility of magnon excitation in the barrier was discussed by Duke et al (1969). Structure in Ni_xO_y has been observed by Adler and Chen (1971), and identified by Tsui et al (1971). Wyatt (1970) predicted that the spin band structure of Ni should be reflected in the zero bias conductance peak anomaly in the presence of a magnetic field. A beautiful tunneling technique as a new method for investigating spin dependent states in magnetic materials was introduced by

Tedrow et al (1971). Therefore, a common trend of most of the recent work, is towards the development of tunneling as a spectroscopic tool for probing the elementary and collective excitation spectra of solids.

1.2 Motivation of this work

With the knowledge that the zero bias anomalies are due to the interaction between the conduction electrons and non-interacting magnetic impurities at the barrier-metal interface of a tunnel junction; the questions arising are:

- 1) What is the effect of the interaction between the magnetic impurities on the conductance anomalies?
- 2) What is the effect of a magnetic impurity layer inside the metallic electrode on the conductance characteristics?

To shed some light on these questions, we prepared Al-I-Al junctions doped with Ni and Fe impurity layers at the barrier interface and inside the Al counter electrodes. The tunneling conductance anomalies of these junctions can provide information about the dependence of the electron density of states, of the doped electrode, on the position measured from the magnetic impurity layer and the effect of interacting magnetic impurities on the conductance anomalies.

Al-I-(Ni or Fe) junctions were prepared with the intention of observing fine structure which could be associated with the magnon characteristic frequencies, and band structure effects on the tunneling conductance behaviour.

The experimental methods used in this work are introduced in Chapter 3. In Chapter 4, the experimental results are discussed in terms of the existing theories, and the conclusion is contained in Chapter 5.

CHAPTER 2

THEORETICAL BACKGROUND

2.1 Kondo problem and tunneling anomalies

It has been confirmed experimentally that there is a one to one correspondence between the existence of the resistivity minimum and the localized magnetic moments in the dilute magnetic alloys. The correlation between the localized spins does not have an important role in the appearance of this phenomenon, but is a result of adding contribution from each spin. This led Kondo (1964) to assume that the resistance minimum is a direct consequence of the interaction between the spins of the localized and conduction electrons. The S-d model, which is due to Zener (1951), Kasuya (1956), and Yosida (1957), for a system of localized spins and conduction electrons was proposed to describe the phenomena. No assumptions concerning the band structure or the crystal symmetries of the host metals, nor the characteristics of the d-level, such as its location relative to the Fermi surface or the number of the d-electrons, has been introduced.

The perturbing Hamiltonian H' is given by

$$H' = - 2J\vec{S}\cdot\vec{\sigma} \quad , \quad (2.1)$$

where J is the exchange coupling energy, and \vec{S} and $\vec{\sigma}$ represent the spin of the localized magnetic moment and the conduction electron, respectively.

The transition probability per unit time from the initial state a to the final state b is given to the second Born approximation by

$$W(a-b) = \frac{2\pi}{\hbar} \{ H'_{ab} H'_{ba} + \sum_{c \neq a} (H'_{ac} H'_{cb} H'_{ba} + \text{C.C.}) / (\epsilon_a - \epsilon_c) \} \times \delta(\epsilon_a - \epsilon_b) \quad (2.2)$$

Assuming all the possible ways by which an electron \vec{k}_{\pm} scattered off the impurity to \vec{k}'_{\pm} or \vec{k}'_{\mp} , the transition probability is found to be

$$W = [6\pi J^2 S(S+1) C / 3\hbar N^2] [N + 4Jg(\epsilon_{\vec{k}})] \delta(\epsilon_{\vec{k}} - \epsilon_{\vec{k}'}) ,$$

$$\text{where} \quad g(\epsilon) = \sum_{\vec{q}} \frac{f_{\vec{q}}}{\epsilon_{\vec{q}} - \epsilon} . \quad (2.3)$$

$f_{\vec{q}}$ is the Fermi distribution function for the electron with energy $\epsilon_{\vec{q}}$, N is the total number of atoms in the crystal and C is the concentration of the impurity atoms. $g(\epsilon)$ is the function which describes the log T dependence of the resistivity in the dilute magnetic

alloys, provided that $J < 0$.^{*} $g(\epsilon)$ is also the same function which describes the $\log T$ dependence of the zero bias tunneling conductance anomaly.

The perturbation technique is not valid in the case of strong coupling or at low temperatures. Theoretical arguments, by Nagoaka (1965), show that a new physical state should be formed below a temperature T_k , the Kondo temperature, between the conduction-electron spin and the localized spin. The situation seems to be quite similar to the case of superconductivity, in which the perturbation treatment breaks down at the transition temperature T_c . Associated with T_k is a characteristic energy Δ , around the Fermi surface, over which the conduction electron spins are polarized by the impurity. The relation between $\Delta(T = 0^\circ\text{K})$ and T_k was found to be

$$T_k = 1.14 \Delta_0, \quad (2.4)$$

^{*} Coles (1964) observed a new type of temperature resistivity anomaly in alloys of Rh and Fe. Instead of having a minimum, the resistivity decreases more rapidly towards low temperatures. This phenomena could be explained in terms of Kondo theory if J is positive.

Δ_0 , like the superconducting energy gap, could be expressed in terms of a cut off energy D (of the order of the conduction electron band width), and the density of the conduction electrons ρ , as well as the strength of the exchange interaction J , i.e.

$$\Delta_0 = D e^{-N/|J|\rho} \quad . \quad (2.5)$$

Δ_0 is of the order of 2.5×10^{-4} e.V., and $T_k \sim 3^\circ\text{K}$, when $D = 5$ e.V. and $|J|\rho/N \approx 0.1$ are used in (2.5).

The cloud of spin polarization around the impurity atom is extended over a Kondo coherence length ξ_Δ , similar to the superconducting coherence length, and is given by

$$\xi_\Delta = \frac{v_F}{\Delta} \approx (\epsilon_F/\Delta) k_F^{-1} \sim 10^4 \text{ \AA} \quad , \quad (2.6)$$

where v_F , ϵ_F and k_F are the velocity, the energy and the wave vector at the Fermi surface. Equations (2.4), (2.5) and (2.6) reveal the similarity between the superconducting state and the correlated state between the conduction-electron spin and the localized spin below T_k . The quasi-bound state however appears gradually rather than suddenly at T_k .

Magnetic states localized near the interface of a tunnel junction may have an exchange coupling to the conduction electron in the electrode comparable in

magnitude to the coupling present in a dilute magnetic alloys. Appelbaum (1966), and Anderson (1966), have shown that Kondo scattering attenuated by the barrier transmission factor can transfer electrons across the barrier, an assisted tunneling process which contributes to the measurable current j . On the other hand S6lyom and Zawadowski (1968) and Mezei and Zawadowski (1971), using different approaches found that the Kondo coherence length is reflected in the tunneling characteristics of junctions doped with magnetic impurities. The different approaches to the theory of zero bias anomalies will be discussed in the following sections.

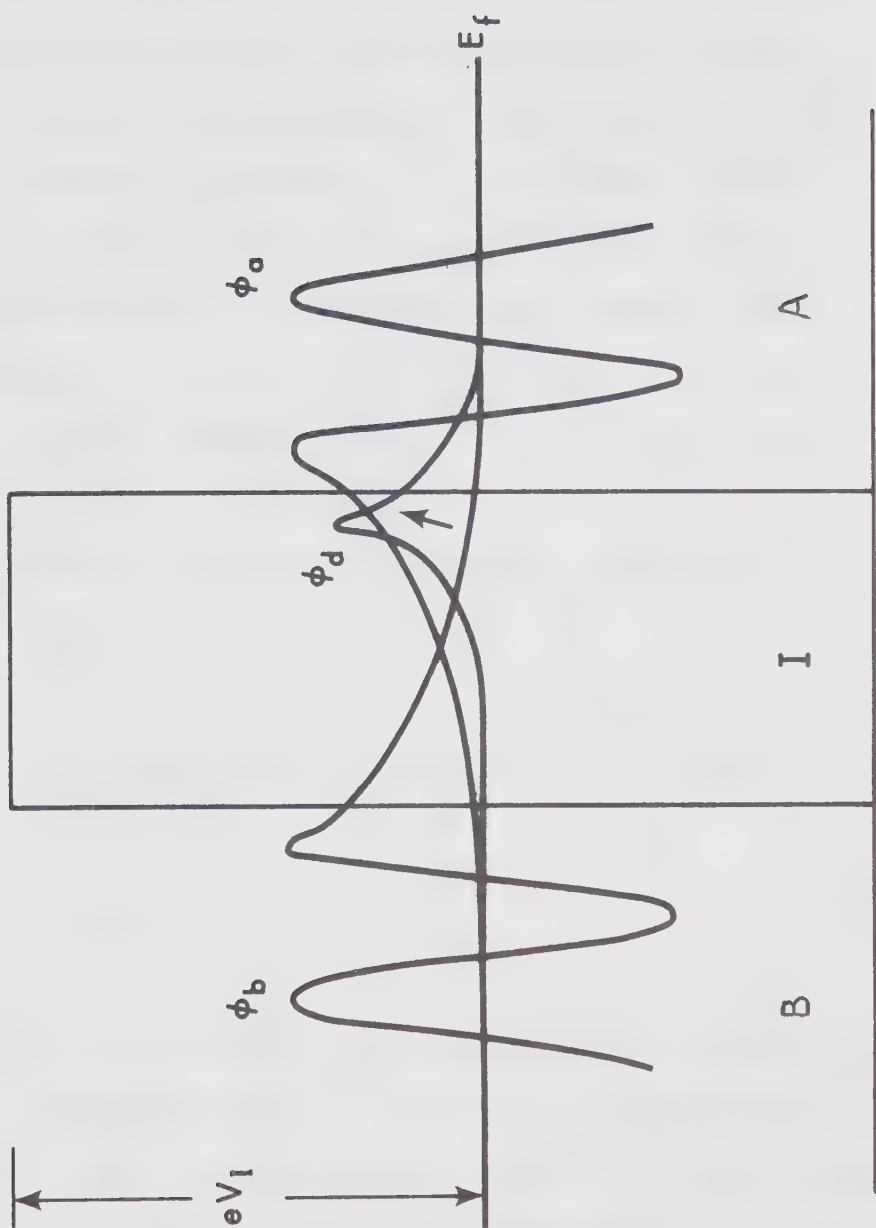
2.2 The S-d Exchange Model of Zero Bias Anomaly

(a) The Temperature and Energy Dependence

Consider a tunnel junction A-I-B, with magnetic impurities located close to electrode A. These impurities could be represented by non-interacting localized states with the bulk of their amplitudes in the barrier where the Coulomb self interaction cannot be screened off by the metallic electrons. A schematic diagram of the system is shown in fig. (2.1). As noted by Anderson (1966), the localized states ϕ_d act as a bridge between the exponentially tailing wavefunctions ϕ_a and ϕ_b of

Fig. 2.1

Schematic representing A-I-B tunnel junction doped with a magnetic impurity. The localized states ϕ_d strongly overlaps the wave function ϕ_A ; weak interaction with ϕ_B leads to exchange tunneling events.



the conduction electrons of the opposite sides of the junction, thus effectively decreasing the size of the barrier for those electrons which tunnel across the barrier by means of the localized states. As the coupling between the electrodes varies exponentially with the barrier thickness, a decrease of the effective thickness by a few angstroms can make the tunneling assisted by the impurities larger than tunneling due to direct overlap of the conduction electron states between sides A and B, even if the impurity concentration is low.

The Kondo exchange interaction (equation 2.1) can be written as:

$$H^J = -J \sum_{\vec{k}, \vec{k}'} [S_z (a_{\vec{k}+}^\dagger a_{\vec{k}'+} - a_{\vec{k}-}^\dagger a_{\vec{k}'-}) + S^+ (a_{\vec{k}-}^\dagger a_{\vec{k}'+}) + S^- (a_{\vec{k}+}^\dagger a_{\vec{k}'-})] \quad (2.7)$$

where $(a_{\vec{k}}^\dagger, a_{\vec{k}})$ and $(b_{\vec{k}}^\dagger, b_{\vec{k}})$ are the creation and annihilation operators for an electron of wave vector \vec{k} , in metals A and B respectively, and S^\pm are the raising and lowering operators for the z-projection of the localized spin operator S . H^J describes an electron in metal A, which can be scattered off the impurity and stays in metal A. An electron in metal A(B)

scattered off the impurity to metal B(A) and attenuated by the barrier, can be described by an exchange tunneling interaction H^{T_J} . H^{T_J} could be obtained from equation (2.7) by replacing a^\dagger by b^\dagger to get one term and a by b to get the other term, i.e.,

$$\begin{aligned}
 H^{T_J} = & - T_J \left[\sum_{\vec{k}, \vec{k}'} \{ S_z (b_{\vec{k}+}^\dagger a_{\vec{k}',+} - b_{\vec{k}-}^\dagger a_{\vec{k}',-}) + S^+ (b_{\vec{k}-}^\dagger a_{\vec{k}',+}) \right. \\
 & + S^- (b_{\vec{k}+}^\dagger a_{\vec{k}',-}) + S_z (a_{\vec{k}+}^\dagger b_{\vec{k}',+} - a_{\vec{k}-}^\dagger b_{\vec{k}',-}) \\
 & \left. + S^+ (a_{\vec{k}-}^\dagger b_{\vec{k}',+}) + S^- (a_{\vec{k}+}^\dagger b_{\vec{k}',-}) \} \right] \quad (2.8)
 \end{aligned}$$

Here T_J is smaller than J by a factor of the order of the barrier attenuation $e^{-\chi t}$, where χ is the decay constant and t the barrier thickness. The tunneling Hamiltonian is:

$$H' = H^J + H^{T_J} + H^{T+T_a} \quad , \quad (2.9)$$

where H^{T+T_a} is the elastic and inelastic part in which no spin exchange takes place.

The tunneling current $j(eV)$ for a single impurity is calculated from the following expression

$$j(eV) = e \sum_M P_M \left[\sum_{j,j} W_{1j} f(\epsilon_1) \{1 - f(\epsilon_j + eV)\} - \right. \\ \left. - \sum_{i,j} W_{ji} f(\epsilon_j + eV) \{1 - f(\epsilon_i)\} \right] , \quad (2.10)$$

where W_{1j} is given by equation (2.2), and P_M is the probability of a localized spin projection M . Following analysis similar to that of Kondo (1964), Appelbaum (1967) found that

$$W_{ij}^{(2)} \propto T_J^2 , \quad W_{ij}^{(3)} \propto T_J^2 J ,$$

and additional nonexchange terms $\propto (T+T_a)^2$. The first two terms correspond respectively to spin-flip, and anomalous third order Kondo scattering across the barrier. The tunneling conductance in zero magnetic field for C impurities is given by

$$G(T,V) = G^{(2)} + G^{(3)} ,$$

where

$$G^{(2)} = \frac{4\pi e^2}{\hbar} \rho_A \rho_B [T^2 + C\{2TT_a + T_a^2 + S(S+1)T_J^2\}] . \quad (2.11)$$

The third order term which determines the conductance peak for antiferromagnetic interaction ($J < 0$) between the localized spins and the conduction electrons is given by

$$G^{(3)} = -16\pi e^2 S(S+1)/\hbar \rho_A \rho_B C J T_J^2 F(eV) ,$$

$$F(\omega) = + \int_{-\infty}^{\infty} g(\epsilon) \frac{\partial f}{\partial \epsilon} (\epsilon - \omega) d\epsilon . \quad (2.12)$$

The function $g(\epsilon)$ is defined by equations (2.3) above.

The function $F(eV)$ can be numerically evaluated, however it was approximated by

$$F(eV) = - \rho_A \ln \left(\frac{|eV| + n\kappa_\beta T}{E_0} \right) \quad (2.13)$$

E_0 is a cut off energy, which has been introduced because the parameters ρ , T_J and J are assumed independent of energy. The constant n is found to be 1.35. The function $F(eV)$, and hence the conductance peak, increases logarithmically with decreasing bias voltage at zero temperature, and with decreasing temperature at zero bias voltage. At $V = n\kappa_\beta T$, the conductance saturates as eV decreases.

The following assumptions have been introduced in the above calculations.

1) The density of states $\rho(\epsilon)$ is constant, removed from the integrals within which it appears, and replaced by their values at the Fermi energy ϵ_F , $\rho(\epsilon_F)$. This has been justified by the fact that only electrons within few millivolts of ϵ_F on either side of the

junction take part in the tunneling for bias voltages of interest.

2) The contribution to the current from each localized state is additive. This is valid if one can neglect the spin-spin interaction among the localized spins. Appelbaum argued that the presence of a short mean free path at the barrier interface should have the effect of weakening the long range spin-spin interaction, therefore making the independent impurity assumption valid at even relatively higher concentration. These assumptions will be questioned in later discussion.

(b) The Conductance Peak Anomaly in a Magnetic Field

The T_J^2 term in $G^{(2)}$ is strongly affected by a magnetic field. If the tunneling electron of energy eV about the Fermi level flips the spin of the impurity, it must exchange Zeeman energy $z = g\mu_B H$ necessary to leave the impurity in an excited state. Now for $eV < z$ and $T \rightarrow 0$, $G_{sf}^{(2)} \rightarrow 0$, if all the tunneling electrons spin flip. This is to be expected on general physical grounds; for with the spins in their ground state ($\frac{z}{T} \rightarrow \infty$) an electron at energy eV on side A would have to tunnel into an energy state $(eV - z)$ on side B if it underwent a spin flip. This process is forbidden by the exclusion principle at $T = 0$ and $eV < z$. This

argument is not restricted to second order processes and is true to all orders in H' . However as discussed by Appelbaum and Kondo only $S/S(S+1)$ of the electrons spin flip; the remainder exchange spin with the impurity in a virtual intermediate state with zero net change of the spin of the electron as it tunnels from metal A to metal B. Shen and Rowell (1968) had presented a simplified picture of the Appelbaum model at $T = 0$, in the absence and presence of a magnetic field as clearly illustrated in figs. (2.2a,b). A more complete expression for $G^{(2)}$ at finite temperature is given by Shen as

$$G^{(2)} \propto T_J^2 \rho_A \rho_B [S(S+1) + \frac{\langle M \rangle}{2} \{ h(\frac{z + eV}{\kappa_\beta T}) + h(\frac{z - eV}{\kappa_\beta T}) \}] , \quad (2.14)$$

$$\text{where } h(x) := - \frac{1 + e^{2x} - 2x e^x}{(1 - e^x)^2} ,$$

and $\langle M \rangle$ is the average magnetization of the spins. Therefore $G^{(2)}$ is voltage and temperature dependent in the presence of a magnetic field, and constant in zero magnetic field.

2.3 Strong Coupling Limit

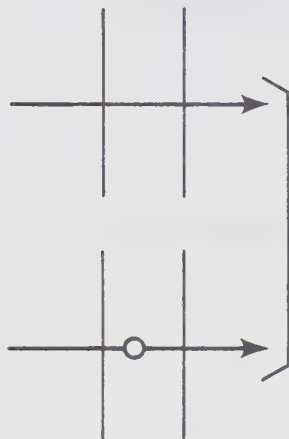
The previous theory does not explain the giant resistance peak anomaly observed in Cr junctions by Rowell and Shen (1966). It became essential to resort

Fig. 2.2

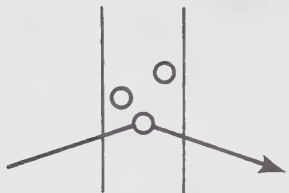
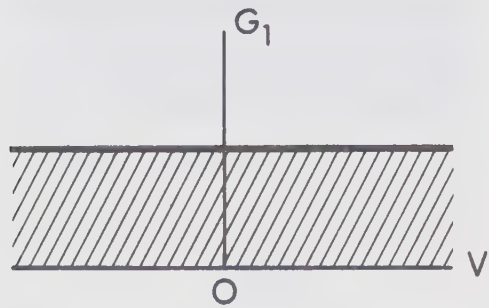
- (a) Schematic diagrams of the different processes that contribute to the theoretical conductance of the Appelbaum model.
- (b) The process of Fig. 2.2a in the presence of a magnetic field, after Shen and Rowell (1968).

APPELBAUM - ANDERSON MODEL

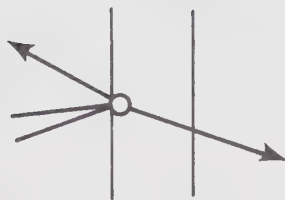
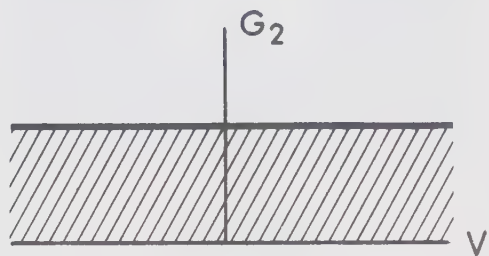
$H=0 \quad T=0$



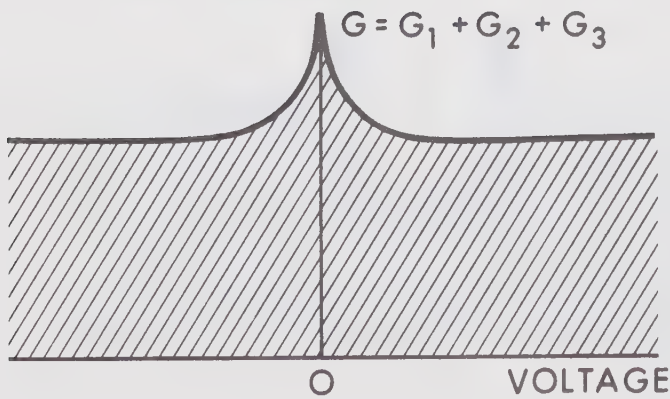
G_1



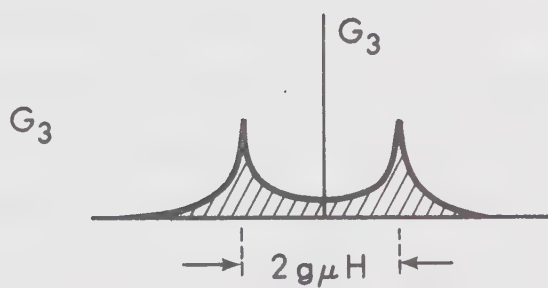
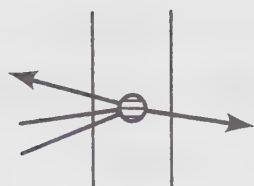
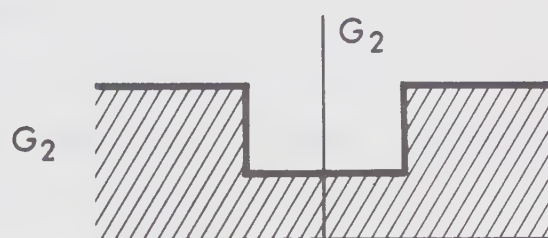
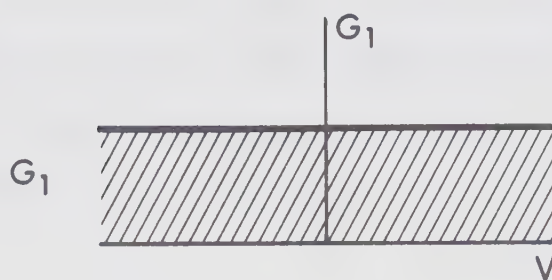
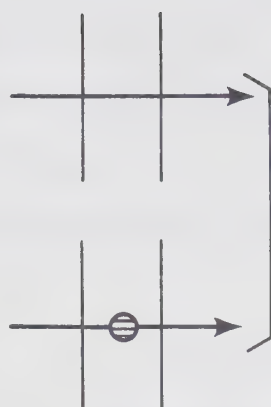
G_2



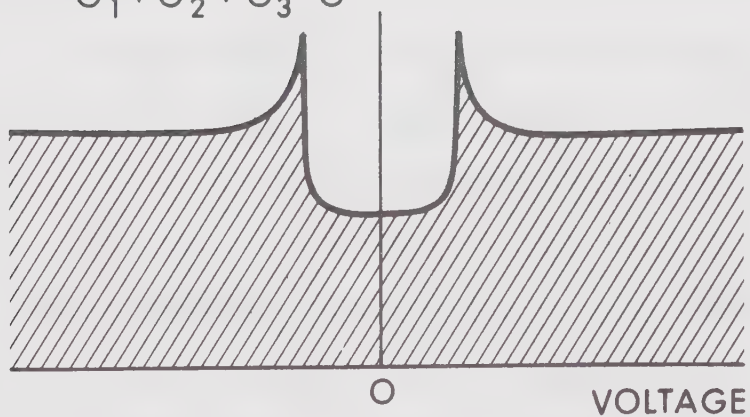
G_3



FIELD H APPLIED T=0



$$G_1 + G_2 + G_3 = G$$



to more powerful methods to account for the strong coupling regime which occurs in a tunnel junction with a large exchange coupling energy J , and consequently high Kondo temperature. Assuming one single impurity; the Hamiltonian of the system

$$H = H_0 + H_1 + H_2 + H_3 + H_4 \quad , \quad (2.15)$$

has the following meaning:

H_0 is the energy of the metallic electrons.

H_1 represents the usual tunneling through the barrier without spin flip, and is proportional to T .

H_2 corresponds to impurity-assisted nonmagnetic tunneling and is proportional to T_a .

H_3 describes the tunneling with spin flip (non local part of the exchange interaction) and is proportional to T_J .

H_4 describes the scattering off the impurity of an electron in the electrode back to the electrode and is proportional to J .

The current which proceeds through the localized states is calculated by neglecting H_1 , and by assuming $H_2 + H_4$ to be a small perturbation. Using a self consistent solution of the Kondo effect given by Nagaoka (1965) and a generalization of a method employed for superconducting tunneling by Ambergakar and Baratoff (1963), Appelbaum et al (1967) found that in the weak coupling limit the conductance $g^{w.c.}$ is given by

$$\left.
\begin{aligned}
g^{w.c.} &= g_{\text{const.}}^{w.c.} + g_{\text{anom.}}^{w.c.} , \\
g_{\text{anom.}}^{w.c.} &= g_{\text{anom.1}}^{w.c.} + g_{\text{anom.2}}^{w.c.} , \\
g_{\text{anom.1}}^{w.c.} &= 12\pi e^2 T_J^2 \rho_A \rho_B (J\rho_A) F(\text{eV}) , \\
g_{\text{anom.2}}^{w.c.} &= -6\pi^3 e^2 T_a^2 \rho_A \rho_B (J\rho_A)^3 F(\text{eV}) , \\
\text{where } F(\text{eV}) &= \int_{-\infty}^{\infty} \frac{\partial f(\omega + \text{eV})}{\partial \omega} \cdot \frac{\partial f(\omega')}{\partial \omega'} \ln \left| \frac{\omega - \omega'}{D} \right| d\omega d\omega'
\end{aligned}
\right\} \quad (2.16)$$

and D is the electron band width of order 5 eV. The two terms of g_{an} have identical voltage and temperature dependence, because the sign is different,

$g_{\text{anom.1}}^{w.c.}$ yields a conductance peak for $J < 0$, while $g_{\text{anom.2}}^{w.c.}$ yields a conductance peak for $J > 0$. In the strong coupling regime

$$\left.
\begin{aligned}
G_1^{s.c.} &= G_1^{s.c.} + G_2^{s.c.} , \\
G_1^{s.c.}(\text{eV}) &= \frac{4e^2}{\pi} \frac{T_J^2}{(J\rho_A)^2} \rho_A \rho_B \frac{\Delta^2}{(\text{eV})^2 + \Delta^2} ,
\end{aligned}
\right\} \quad (2.17)$$

and

$$G_2^{s.c.}(\text{eV}) = 4\pi e^2 T_a^2 \rho_A \rho_B \frac{(\text{eV})^2}{(\text{eV})^2 + \Delta^2} , \quad (2.18)$$

for $J < 0$.

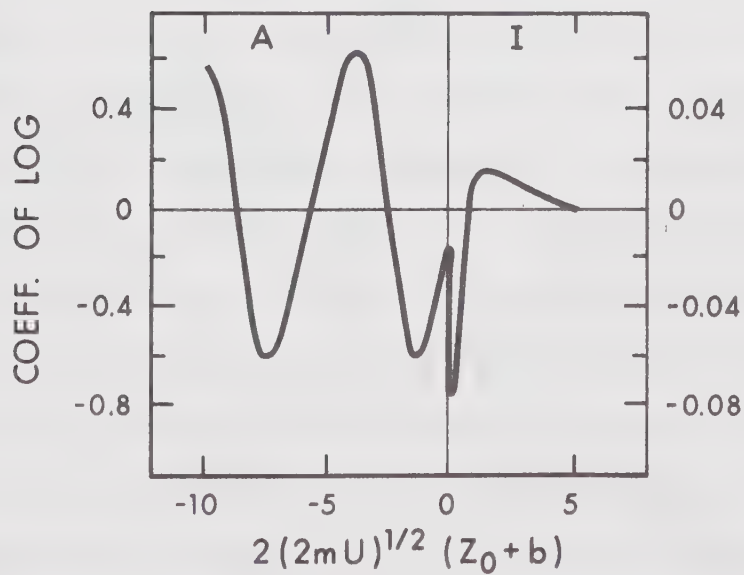
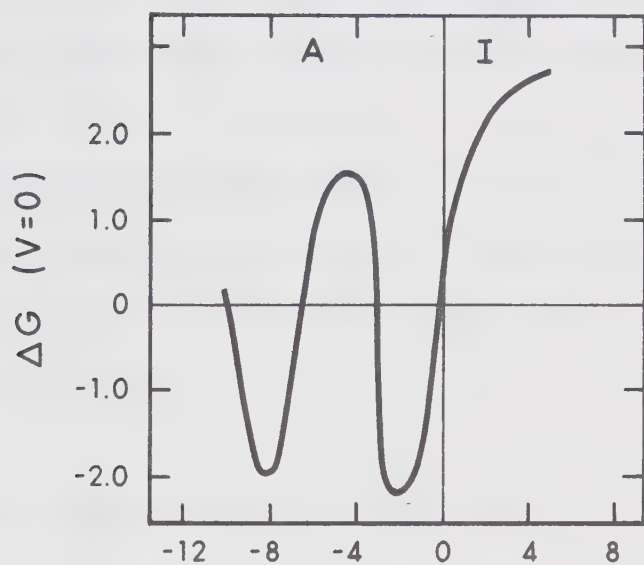
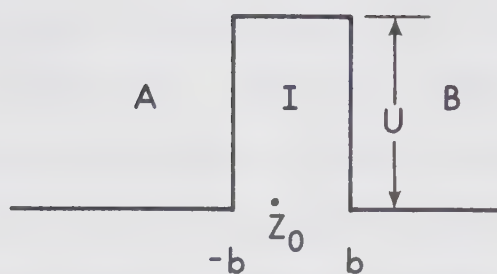
The relative importance of the various terms which contribute to the current depend on the relative size of T_a , T_J , and J ; parameters which are difficult to determine. In tunnel junctions where T_J terms are important, the conductance peak varies initially as $\ln \frac{D}{eV + \kappa_\beta T}$ and saturates to the value given by $G_1^{s.c.}(0)$ for $\kappa_\beta T$, $eV \lesssim \Delta$. If T_a terms are important the conductance dip varies as $\ln \left[\frac{|eV| + \kappa_\beta T}{D} \right]$ and eventually goes to zero at T and $V \rightarrow 0$. According to Appelbaum, the giant resistance anomaly could be explained when the T_a terms are important.

2.4 Interface Effect on the Conductance Characteristics.

Appelbaum and Brinkman (1970), assuming a single impurity near a sharp metal-barrier interface, studied the effect of the interaction between spins of the localized and conduction electrons on the tunneling conductance characteristics as a function of the impurity position. The tunnel junction shown in fig.(2.3a) has been decomposed into the left and right hand side problems. An expression for the current similar to that of Zawadowski (1967) has been derived by Appelbaum and Brinkman (1969); however, the approximation procedure is different and leads to qualitatively different results. It was found that the largest contribution to the

Fig. 2.3

- (a) A tunnel barrier of height U doped with a single impurity at Z_0 .
- (b) $G^{(2)}$ as a function of the impurity position.
- (c) The coefficient of the log as a function of the impurity position, after Appelbaum and Brinkman (1970).



conductance change, ΔG which comes from $G^{(2)}$ and $G^{(3)}$ terms, is sensitive to the position of the impurity relative to the interface. The $G^{(2)}$ term is an oscillating function of position, on the scale of $1/k_f$, when the impurity exists in the electrode, and of one sign when it is in the barrier. This is shown in fig. (2.3b).

The third order term $G^{(3)}$ which accounts for the zero bias conductance anomaly has the oscillating behaviour shown in fig. (2.3c).

A different theory which reflects the change in the conductance as a function of impurity position has been introduced by Mezei and Zawadowski (1971), and will be discussed later.

2.5 Interacting Magnetic Impurities

Gupta and Upadhyaya (1971) introduced a theoretical study of a tunnel junction containing interacting paramagnetic impurities. The current was calculated for one pair of impurities coupled by an interaction W . The density of pairs was assumed to be low enough such that the correlation between them could be neglected. The interaction W may be due to Ruderman-Kittel-Kasuya-Yosida (RKKY) interaction between the impurities via the conduction electrons, direct interaction, or indirect exchange interaction. Following the tunneling

Hamiltonian approach by Cohen et al (1962), they found that the second order contribution, $G^{(2)}$, has a temperature and bias dependence in zero magnetic field. In the case of an antiferromagnetic interaction, the maxima of $G^{(3)}$ occur at slightly different biasing voltages and temperatures when compared to the case of non-interacting impurities. The results of their calculations is shown in fig. (2.4).

2.6 The Normalized Electron Density of States

The main argument against the existence of a new assisted tunneling process, as pointed out by Mezei and Zawadowski (1971), could be the local behaviour of the exchange interaction in space in which case there is no new channel for tunneling. This corresponds to retaining in the tunneling Hamiltonian, equation (2.15), only the local terms H_0 , H_1 , H_2 , H_4 and dropping H_3 . Appelbaum (1967) argued that the nonlocal behaviour arises from the fact that the distinction between an electron from the left and right hand side necessarily breaks down in the junction, which has the effect of further breaking the local nature of the exchange interaction.

In this section we will consider a different approach which leads to different results. This new

Fig. 2.4

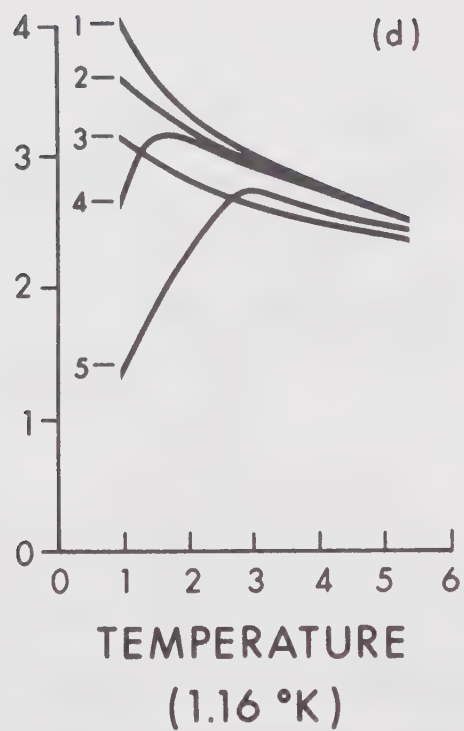
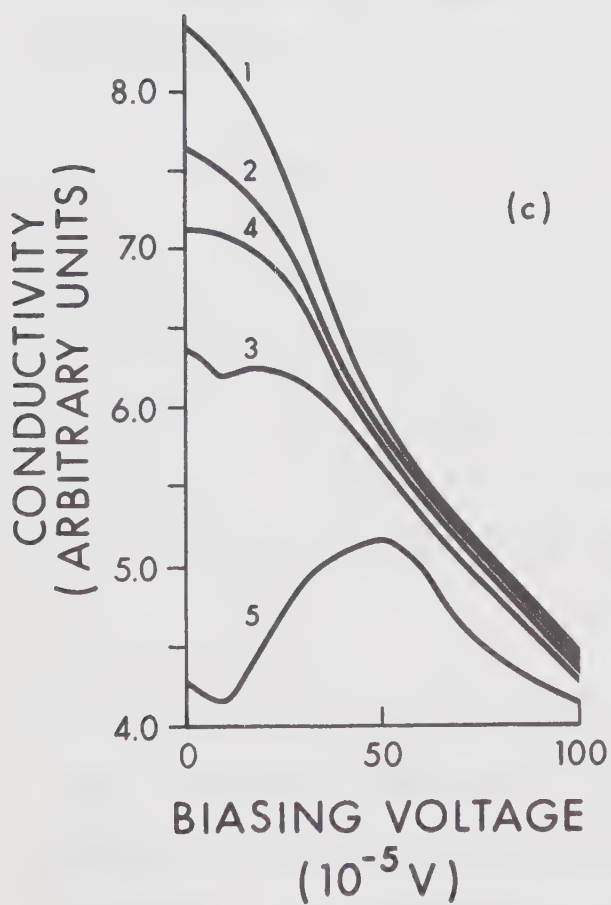
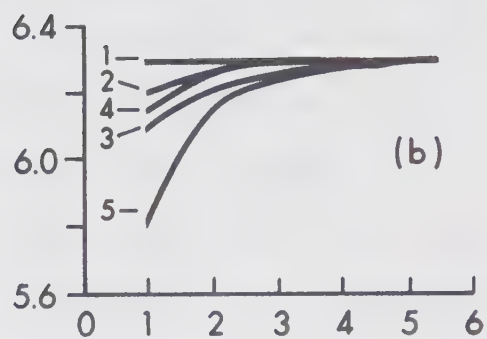
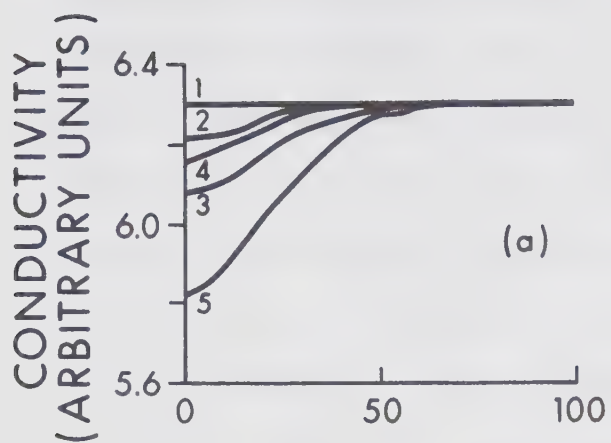
(a) $G^{(2)}$ versus bias voltage at 1.6°K .

(b) $G^{(2)}$ versus temperature at zero bias.

(c) $G^{(3)}$ versus bias voltage at 1.6°K .

(d) $G^{(3)}$ versus temperature at zero bias.

Curves 1, 2, 3, 4 and 5 correspond to $W = 0, 10^{-4}, 2 \times 10^{-4}, -10^{-4}$ and -2×10^{-4} eV, respectively, after Gupta and Upadhyaya (1971).



approach reflects the importance of the change of the electron energy spectrum in the barrier due to the interaction between the localized impurity excitations and the conduction electrons. The change in the energy spectrum will affect the amplitudes of electrons penetrating the barrier, and as a result the overlap of the wavefunctions of the left and right hand side electrons will be modified. This effect could be looked after by an energy dependent tunneling matrix element or a local density of states variation at the barrier.

Sólyom and Zawadowski showed that the current can be written as:

$$j \propto \int \rho_A \rho_B \{f_B - f_A\} d\epsilon \quad ,$$

an expression which has been used in the case of superconducting tunneling with the difference that ρ_α ($\alpha \equiv A, B$) represents the local density of states. The bulk density of states ρ is related to the local one through a renormalization function Z , such that

$$\rho_\alpha = Z\rho \quad .$$

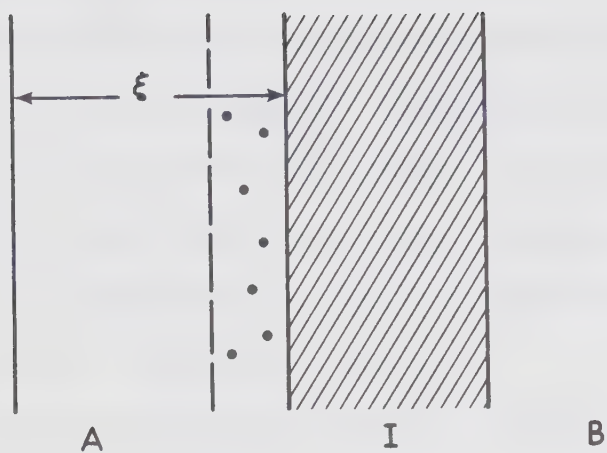
The function Z is obtained in terms of the life time of the conduction electrons. In the case of an S-d exchange interaction between paramagnetic impurities and conduction electrons, and taking into account the Kondo effect, the

life time of the electrons is very sensitive to the energy of the electrons relative to the Fermi energy. This energy dependence leads to the anomalous I-V characteristics of diodes containing magnetic impurities.

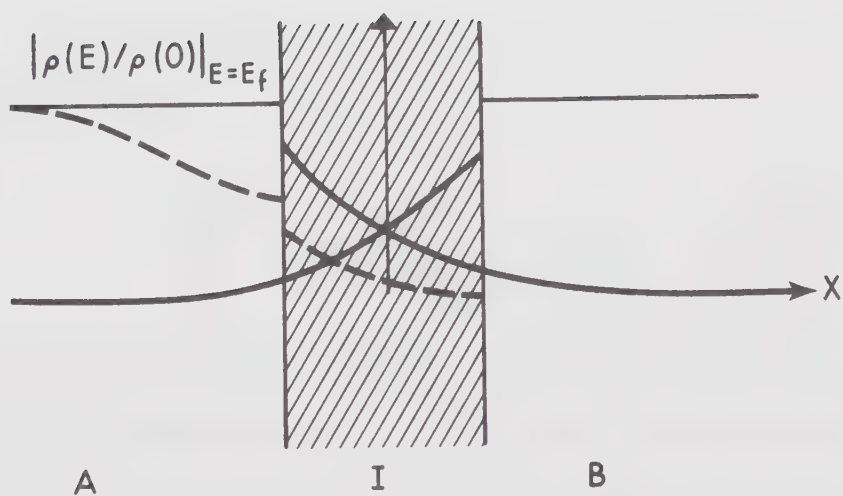
The local density of states as found by the authors, is also a function of the position of the impurities. An essential change in the current occurs, for impurity atoms situated on the metal oxide interface or in the next atomic layer. Because of the exponentially decreasing wavefunctions of the electrons in the barrier, the impurities located deeply inside the barrier give no contribution to the anomaly. Investigating the effect of the impurities in the metal, the concept of Kondo coherence length ξ was introduced as shown in fig. (2.5). Impurities within ξ measured from the barrier interface have an effect on the life time which is proportional to the impurity concentration. Therefore the electron density of states can be diminished by increasing the amount of evaporated impurities. This behaviour does not hold for arbitrary thicknesses or distributions of impurities; for example, in the special case when the impurities are homogeneously distributed in the metal electrode, the density of states is found to be the same as that of the pure metal.

Fig. 2.5

- (a) A-I-B junction with magnetic impurities within the coherence length ξ .
- (b) The depression of the electron density of states within the coherence length, after S6lyom and Zawadowski (1968).



(a)



(b)

It is indeed interesting to show that the present theory predicts a decrease of the local density of states compared with the unrenormalized one as a consequence of the effect of the paramagnetic impurities. Consequently, the tunneling current decreases in contrast with the Appelbaum tunneling Hamiltonian method, which gives a tunneling current contribution originating from the impurity assisted tunneling.

The calculation was based on a generalization of Bardeen's tunneling theory, (1961), (1962), to account for the many body interactions. The Green's function technique of the particular problem consisting of the solution of the left and right hand side problems was introduced by Zawadowski (1967), to describe the tunneling current. The expression for the local density of states is found to be

$$\rho_{\alpha}(k_{||}, E) = Z(E)\rho = \frac{\rho}{1 + \pi\rho \frac{1}{2\tau_{\alpha}(k_{||}, E)}} \quad . \quad (2.19)$$

τ is a quantity of relaxation time type and is defined in terms of the imaginary part of the self energy operator averaged over the position of the impurities, i.e.

$$\bar{\tau} \frac{1}{2\tau_{\alpha}(k_{||}, E)} = \bar{\sum}_{i\omega=E \pm i\epsilon; \alpha} (k_{||}) ,$$

and

$$\begin{aligned} \frac{1}{L_{\alpha}} \bar{\sum}_{\omega; \alpha} (k_{||}, v, v') &= \int d^3x \phi_{k_{||}, v; \alpha}(\vec{x}) \bar{\sum}_{\omega} (x) \phi_{k_{||}, v'; \alpha}(\vec{x}) \\ &= \frac{1}{L_{\alpha}} \int dx f_{k_{||}, v}^{\alpha}(x) \bar{\sum} (x) f_{k_{||}, v'}^{\alpha}(x), \end{aligned} \quad (2.20)$$

where L_{α} denotes the thickness of the metal. The matrix element is taken between eigenfunction states satisfying the Schrödinger's equation:

$$\left\{ -\frac{\nabla^2}{2m} + V_{\alpha}(\vec{x}) \right\} \phi_{\lambda, \alpha} = \epsilon_{\lambda, \alpha} \phi_{\lambda, \alpha} .$$

$\phi_{\lambda, \alpha}(\vec{x})$ could be written as:

$$\phi_{\lambda, \alpha}(\vec{x}) = \frac{1}{\sqrt{\Omega_{\alpha}}} e^{ik_{||} \cdot \vec{x}} f_{k_{||}, v}^{\alpha}(x) ,$$

where $f_{k_{||}, v}^{\alpha}(x)$ is the longitudinal component of the wavefunction, and Ω_{α} is the volume of metal on side α . The function $f_{k_{||}, v}^{\alpha}(x)$ is independent of v for x in the barrier and is given by

$$f_{k_{||}, v}^{\alpha}(x) \sim e^{\bar{k}_{\perp} x} , \quad x \in I ,$$

with $k_{\perp} \approx [2m(V + \frac{k_{||}^2}{m} - E_F)]^{\frac{1}{2}}$.

If the impurities are in the barrier, the self energy is independent of the quantum number v and could be written as:

$$\bar{\Sigma}_{\omega;\alpha} \approx \int |f^\alpha(x)|^2 \bar{\Sigma}(x) dx = \int |f^\alpha(x)|^2 \Sigma(x) c(x) dx ,$$

where $c(x)$ is the impurity concentration, and $\Sigma(x)$ is the self energy at the barrier due to a single impurity. The local nature of self energy is satisfied if the exchange interaction between the impurity and the conduction electron is described by the Kondo Hamiltonian which spreads over one atomic distance. As shown by Sályom and Zawadowski, the contribution of an impurity to the matrix element (2.20) is very sensitive to its position relative to the barrier interface, and the matrix elements are important only if they are taken between states in an energy interval ΔE , around the Fermi surface, where the largest contribution to the Kondo scattering occurs. The coherence length ζ is given by

$$\zeta = \pi v_F / \Delta E ,$$

where v_F is the Fermi velocity. It is estimated to be 80 \AA for $\Delta E \approx 20 \text{ meV}$.

Finally, a set of coupled equations has been obtained and should be solved in a self consistent

manner for all cases where $Z(E) < 0.8$ at some energy E . However, the self consistent solution is not feasible due to the fact that no analytic form of the scattering amplitude is available for an energy dependent density of states.

2.7 The Tunneling Conductance and the Renormalization Function.

Let us assume that $T = 0$, the impurities are on one side of the barrier, and the bulk density of states of the metals are constants on the two sides of the barrier. Then the expression for the current is

$$I(V) \propto \rho_A \rho_B \int_0^{eV} Z_A(E) dE .$$

The dynamical conductance and resistance are defined as

$$G(V) = \frac{dI}{dV} \propto Z_A(eV) ; \quad R(V) = G^{-1}(V) \propto Z^{-1}(eV) .$$

This is a good approximation at finite temperature provided that $\kappa_\beta T \ll eV$, and the variation of $Z(E)$ is small in intervals of $\kappa_\beta T$, i.e.

$$\left. \frac{dZ}{dE} \right|_{E=eV} \cdot \kappa_\beta T \ll Z(eV) .$$

For the calculation of Z , we need to know the scattering amplitude. The typical ones which are known in the literature are :

1) Abrikosov type (1965). The imaginary self energy due to one impurity is

$$\text{Im} \sum_{i\omega=E \pm i\epsilon} (R) = \mp \frac{\pi}{4} S(S+1) \frac{1}{\rho(R)} \left[\left(\log \frac{E_0(R)}{|E| + n\kappa_\beta^T} \right)^2 + \chi^2 \right],$$

where $\chi^2 = S(S+1)\pi^2/4$. The scattering amplitude has a maximum at $\pm E_0$ corresponding to the resonant scattering

$$E_0 = E_c e^{N/2J\rho}.$$

2) Suhl-Wong type (1967). There exists a maximum in the scattering amplitude with energy comparable with κ_β^T .

3) Nagaoka type (1965). A quasi bound state is formed and $\text{Im} \sum_{i\omega=E \pm i\epsilon}$ is given by

$$\text{Im} \sum_{i\omega=E \pm i\epsilon} = \mp \frac{1}{\pi\rho(R)} \cdot \frac{\Delta^2}{\Delta^2 + E^2}.$$

Using the Abrikosov scattering amplitude and considering the impurities as located in the metal yields

$$Z(E) = \left\{ 1 + \frac{1}{\gamma} \pi^2 S(S+1) \frac{N_i}{N_s} \left[\log \left(\frac{E_0}{|E| + n\kappa_\beta^T} \right)^2 + \chi^2 \right]^{-1} \right\}, \quad (2.21)$$

where $N_1 \approx \int c(R) [\overline{f(R)}]^2 dR$, N_s is the surface density of atoms, and γ is a parameter of the order of unity. If we introduce the following parameters,

$$t = \kappa_\beta T / E_0 ,$$

$$\varepsilon = eV / E_0 ,$$

$$a^2 = \frac{1}{\gamma} \frac{\pi^2}{4} S(S+1) \frac{N_1}{N_s} ,$$

expression (2.21) becomes

$$Z(E) = \frac{\log^2(nt+\varepsilon) + \chi^2}{\log^2(nt+\varepsilon) + \chi^2 + a^2} \lesssim 1 . \quad (2.21')$$

In the case of ferromagnetic coupling, $J > 0$, the energy dependence of $Z(E)$ is very small with small relative amplitude. The minimum of $Z(E) > 0.9$ for reasonable values of the parameters in equation (2.21'). In the case of antiferromagnetic coupling, $J < 0$, it is found that

$$\lim_{E \rightarrow 0} Z(E) = \lim_{E \rightarrow \infty} Z(E) = 1 \quad \text{at} \quad t = 0 ,$$

and the minimum of $Z(E)$,

$$Z(E)_{\min} = \frac{\chi^2}{\chi^2 + a^2} , \quad \text{occurs at} \quad E = E_0 .$$

The larger the constant a^2 , the higher the impurity

concentration, and the deeper the minimum. The characteristics of Z^{-1} for different t are shown in fig.(2.6a).

The resistivity maximum is then a result of the depression of the density of electron states around the Fermi energy. If the depression is large, the change in the energy spectrum of the electrons can be expected to cause an essential modification of the scattering amplitude also. In that case, a self consistent solution is needed. A crude approximation which may illustrate the consequences of self consistency could be arrived at by assuming that the renormalization function is weakly energy dependent. In this case the density of states occurring in the scattering amplitude at energy E could be replaced by the renormalization density of states taken at the same energy, i.e.

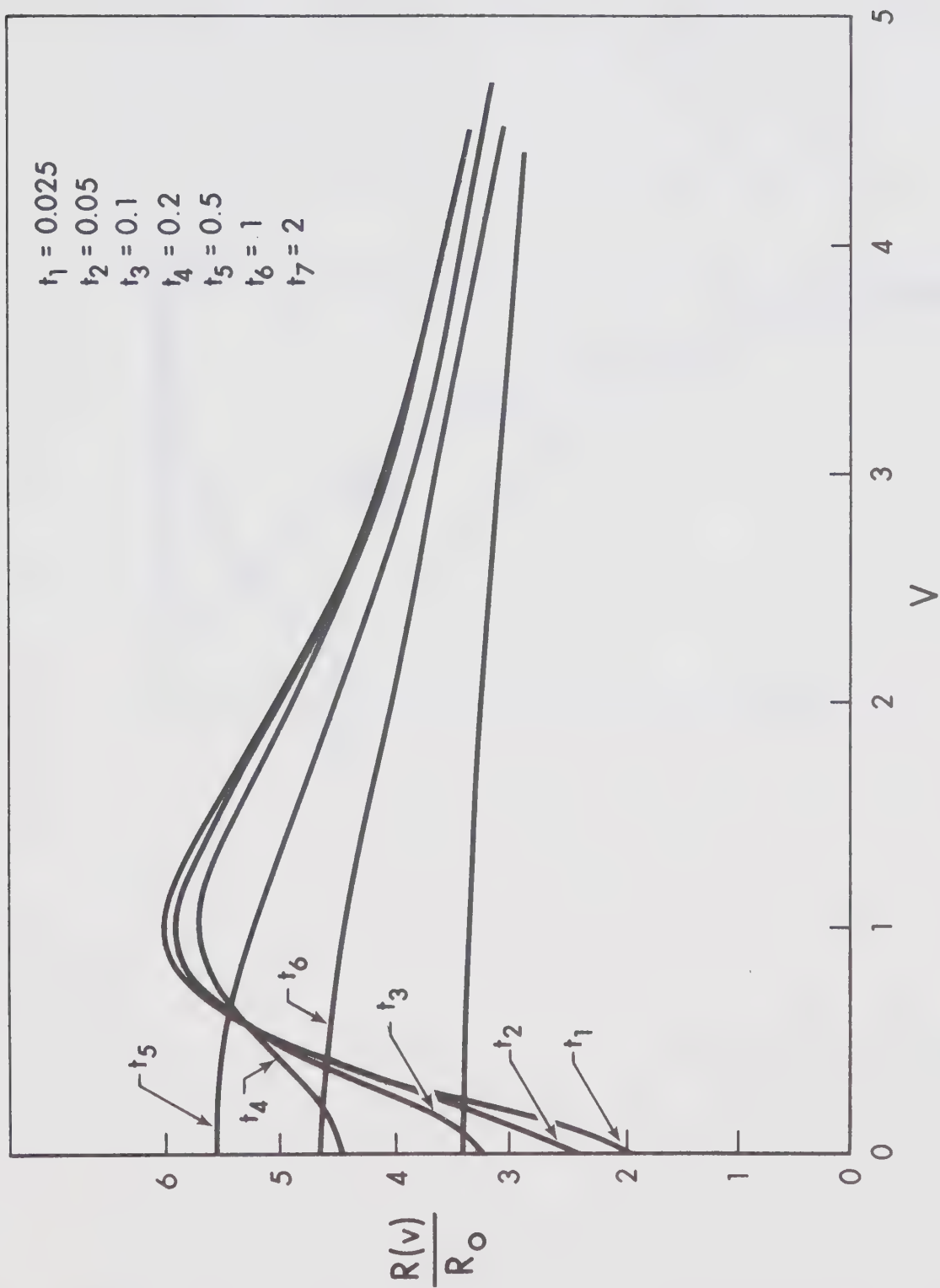
$$E_0 = E_c e^{-N/2J\rho Z(E)} .$$

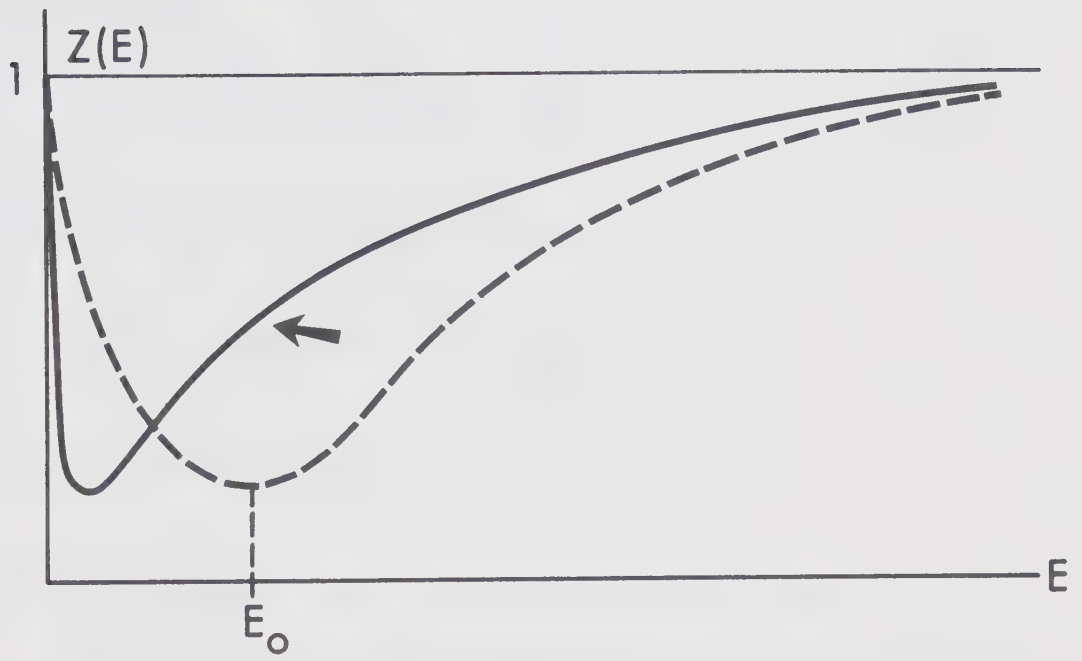
The above equation then indicates that the energy of the maximum E_0 is energy dependent. In fig. (2.6b), the renormalization function versus energy shows the self consistency effect. Note that E_0 is shifted towards zero, and only the maximum of the amplitude can be seen. For such high reduction in the conductance i.e. $Z(E) \ll 1$, the resistance $R(V)$ is found to be

$$R(V) \propto - \frac{2|J|\rho}{N} \log eV/E_0 ,$$

Fig. 2.6

- (a) $R(v)/R_0 \equiv Z^{-1}$ versus reduced bias voltage V , at different reduced temperature t .
- (b) Z versus E (dashed line), and the effect of self consistency on the energy at the minimum (solid line), after S6lyom and Zawadowski (1968).





(b)

and the results are not sensitive to the type of the scattering amplitude. However, the authors argued that it is still possible to distinguish between the scattering amplitudes on the basis of the height of the maximum. For example, the Nagoaka type of interaction gives

$$\text{Max. } R(V)/R(V=\infty) = \frac{1}{\gamma} \frac{N_1}{N_S} + 1 ,$$

while the Abrikosov type gives

$$\text{Max. } R(V)/R(V=\infty) = \frac{5}{\chi^2} \frac{N_1}{N_S} + 1 ,$$

which is larger than the above expression.

2.8 The Anomalies and Kondo Coherence Length

The effect of the paramagnetic impurity layer on the electron density of states of the host metal has been introduced in the previous sections in its connection with the zero bias tunneling anomalies. The result is that the electron density of states may be depressed by the resonant electron-paramagnetic impurity scattering in the vicinity of the impurity. Alternatively, the phenomena can be viewed as a strong destructive interference between the incoming and outgoing waves. In this section, we will discuss the Kondo coherence

length in more detail. As mentioned before, the electron spin polarization is damped out beyond a coherence length $\xi_{\Delta} = 10^4 \text{ \AA}$, Nagoaka (1965). Some other investigators have shown that the electron polarization consists of an oscillating part and a non-oscillating part. The latter has two ranges. The short range falls off beyond a cut off energy D , reflecting the band structure, and is characterized by $\xi_D \sim \frac{aE_F}{D}$ of the order of one atomic distance, where a is the lattice constant. The long range has the asymptotic form $-r^{-3} S(S+1) \log^{-2} r/\xi_{\Delta}$, where r is the distance measured from the impurity. Sólyom and Zawadowski (1968) pointed out that the cut off energy, which gives the coherence length, could be determined from the exchange coupling which is momentum dependent. This dependence may be stronger than the energy dependence of the bulk electron density of states. If one assumes that the range of energy Δ over which $J_{kk'}$ changes is such that $\Delta \ll D$, then $\xi_{\Delta} \gg \xi_D$. The spatial structure of the electron density of states is independent of the conduction-electron-paramagnetic scattering amplitude as found by Müller-Hartmann (1969). Therefore Mezei and Zawadowski (1971) assumed that the spatial structure is associated with the $J_{kk'}$ momentum dependence. Their mathematical model is based on the basic assumption of the Kondo Hamiltonian which is given by

$$\left. \begin{aligned}
 H &= H_0 - H_1, \\
 \text{where } H_0 &= \sum_{\vec{k}} \epsilon_{\vec{k}} a_{\vec{k}\alpha}^\dagger a_{\vec{k}\alpha}; \\
 H_1 &= - \sum_{\vec{k}, \vec{k}'} (J_{\vec{k}\vec{k}'}, /N) a_{\vec{k}\alpha}^\dagger \vec{\sigma}_{\alpha\beta} a_{\vec{k}',\beta} S.
 \end{aligned} \right\} \quad (2.22)$$

$J_{\vec{k}\vec{k}'}$, could be expressed in terms of Legendre Polynomials P_ℓ in the following way:

$$J_{\vec{k}\vec{k}'} = J_{\vec{k}\vec{k}'}^\ell = (2\ell+1)J_\ell P_\ell(\cos\theta_{\vec{k}\vec{k}'})F(k)F(k'), \quad (2.23)$$

where the angular momentum of the scattered state has the value ℓ , $\theta_{\vec{k}\vec{k}'}$ is the angle between the incoming and outgoing electrons, and J_ℓ is a coupling constant. The dependence on the absolute values of momenta is given by $F(k)F(k')$. The cut off function $F(k)$ was assumed to have a peak at momentum k_0 corresponding to an energy ϵ_0 , and can be represented by the simple analytic function,

$$F(k) = \frac{\Delta^2}{\Delta^2 + (\epsilon_k - \epsilon_0)^2},$$

where Δ is the energy domain over which $J_{\vec{k}\vec{k}'}$ varies. The change in the electron density of states, $\Delta\rho$ due to the impurity, can be described by an energy dependent scattering amplitude $t_\ell(\omega-i\delta)$, and a position dependent function $f(r)$ characterized by a coherence length ξ_Δ . $\Delta\rho$ was found to be

$$\Delta\rho \left\{ \begin{array}{ll} = -2c & ; \quad r, \ell = 0 \\ = 0 & ; \quad r = 0, \quad \ell \neq 0 \\ = c(k_0 r)^{-2} [\cos 2(k_0 r - \frac{\pi\ell}{2}) - 1] & ; \quad \ell(\ell+1)/k_0 \ll r \ll \xi_\Delta \\ = -c(k_0 r)^{-2} [e^{-r/\xi_\Delta} - \frac{1}{2} e^{-2r/\xi_\Delta}] & ; \quad \ell(\ell+1)/k_0 \ll r \sim \xi_\Delta \end{array} \right. \quad (2.24)$$

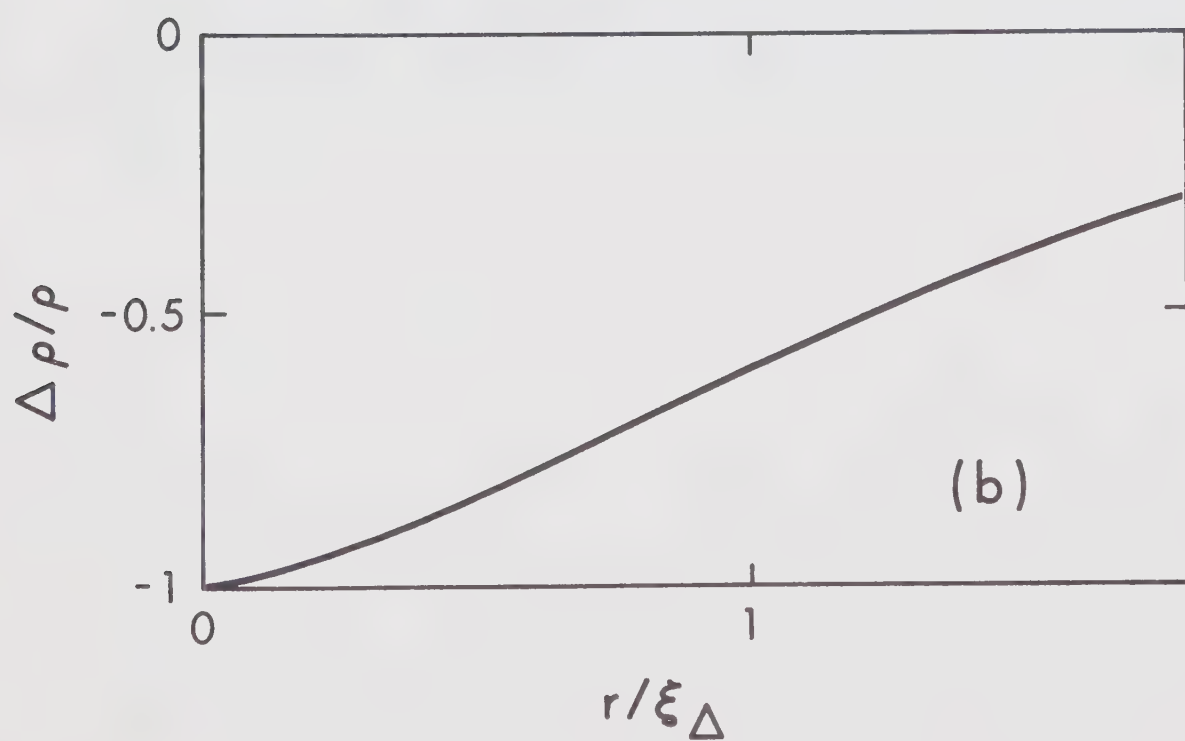
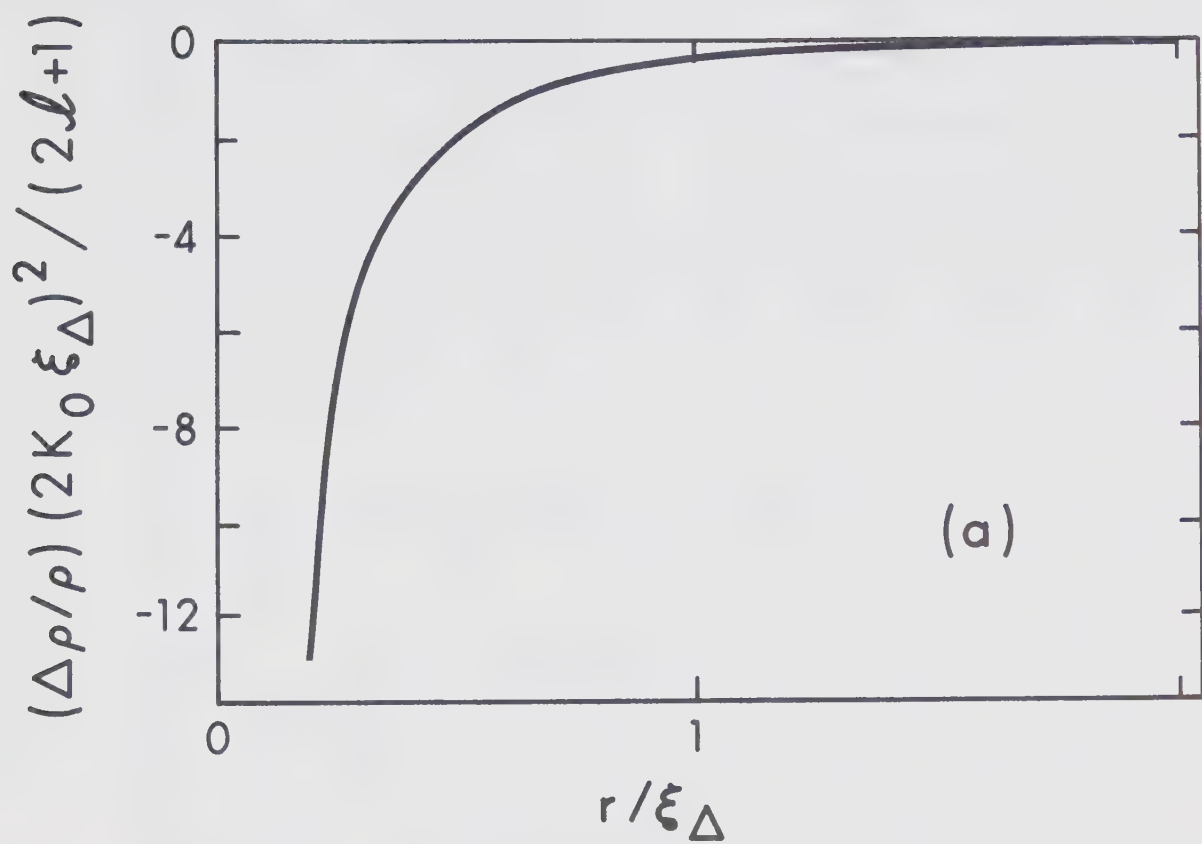
where $c = \frac{2\ell+1}{2} \pi \rho^2 \text{Im}[t_\ell(\omega - i\delta)]$, and r is measured relative to the position of the impurity atom. In the long range limit $r \gg \xi_\Delta$, a term corresponding to Friedel oscillations exists.

Equations (2.24) show that the change in the electron density of states has different features in the short and long range limits which are separated at distance corresponding to the coherence length ξ_Δ . In the short range region, the change is always negative. The amplitude of the depression has its maximum at the impurity site or at one atomic distance, depending on the type of scattering. With increasing distance, the change spreads over a distance which is determined by the coherence length, as shown in fig. (2.7a).

Mezei and Zawadowski (1971) extended their theory to the case of an impurity layer, where the effects become pronounced and can be observed by electron tunneling measurements. The impurities must be displaced

Fig. 2.7

The relative change $\Delta\rho/\rho$ in the electron density of states due to (a) a single impurity, (b) an impurity layer as a function of r/ξ_Δ (taken from Mezei and Zawadowski (1971)).



in one of the electrodes in a layer parallel to the junction surface at a distance r from the barrier interface. If r is less than ξ_{Δ} , the tunneling conductance characteristics will be anomalous. In their calculations the authors found that the spatial dependence of $\Delta\rho$ is similar to that of single impurity except for the lack of the r^{-2} factor, i.e.

$$\frac{\Delta\rho}{\rho} = \frac{G(r,0) - G^{(0)}}{G^{(0)}} \propto A(e^{-r/\xi_{\Delta}} - e^{-2r/\xi_{\Delta}}), \quad (2.25)$$

$r \sim \xi_{\Delta}$,

where $G^{(0)}$ is the conductance of the pure junction.

Fig. (2.7b) shows $\Delta\rho/\rho$ vs r/ξ_{Δ} at different energies ω/Δ . Therefore it is possible to determine the coherence length and to get information on the momentum dependence of the exchange coupling, by considering the functional form (2.25).

CHAPTER 3

EXPERIMENTAL METHODS

A large variety of methods for depositing thin solid films at rates ranging from a fraction of an angstrom per second to 10^6 Å⁰/sec. have been utilized and discussed in the literature, Holland (1963), and Chopra (1969). Several of these methods, notably thermal evaporation and sputtering, permit automatic monitoring and controlling of the rate of deposition and film thickness. The fact that the properties of the film and its structure depend on various deposition parameters will be considered in this section. In the rest of this chapter we will discuss the tunnel junction preparation, film thickness measurements, and the production of low temperatures.

3.1 General Consideration.

Interactions between deposition parameters.

The main parameters which are responsible for the film properties are the evaporant material (M), the deposition rate (V), the film thickness (t), the residual gas pressure in the vacuum system (P), and the substrate (S). All of these parameters interact with one another to a considerable extent. For example, the substrate

might be characterized by its temperature, its material and surface condition, its absorption of or reaction with various components of the residual gases at their respective partial pressures, and its interface properties with respect to the evaporated material. Taking into account all the interactions possible between the parameters M , Δ , t , P and S listed above would therefore result in a great quantity of parameters which would be difficult to survey. Because of these interactions, even at similar thicknesses, films of very different physical characteristics can be obtained.

Generally the process of film formation is a diffusion controlled process which can be divided into four main stages, Uyeda (1942), Levinstein (1949), Poppa (1967).

- (a) Nucleation and growth of nuclei.
- (b) Coalescence of grains.
- (c) Formation of islands and channel systems.
- (d) Formation of continuous and uniform layers.

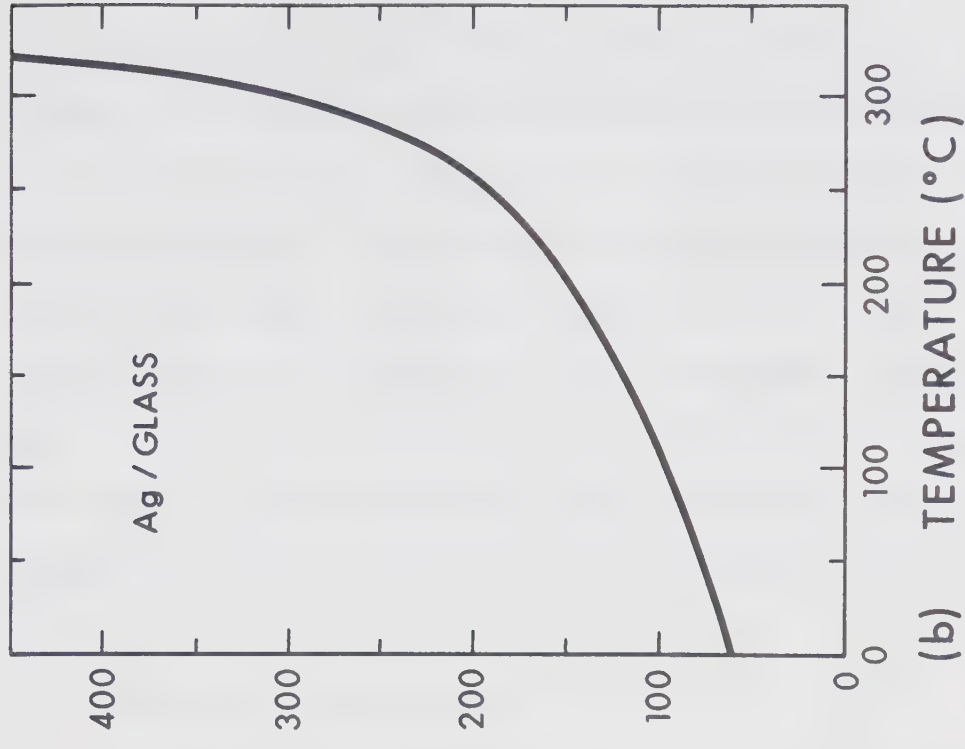
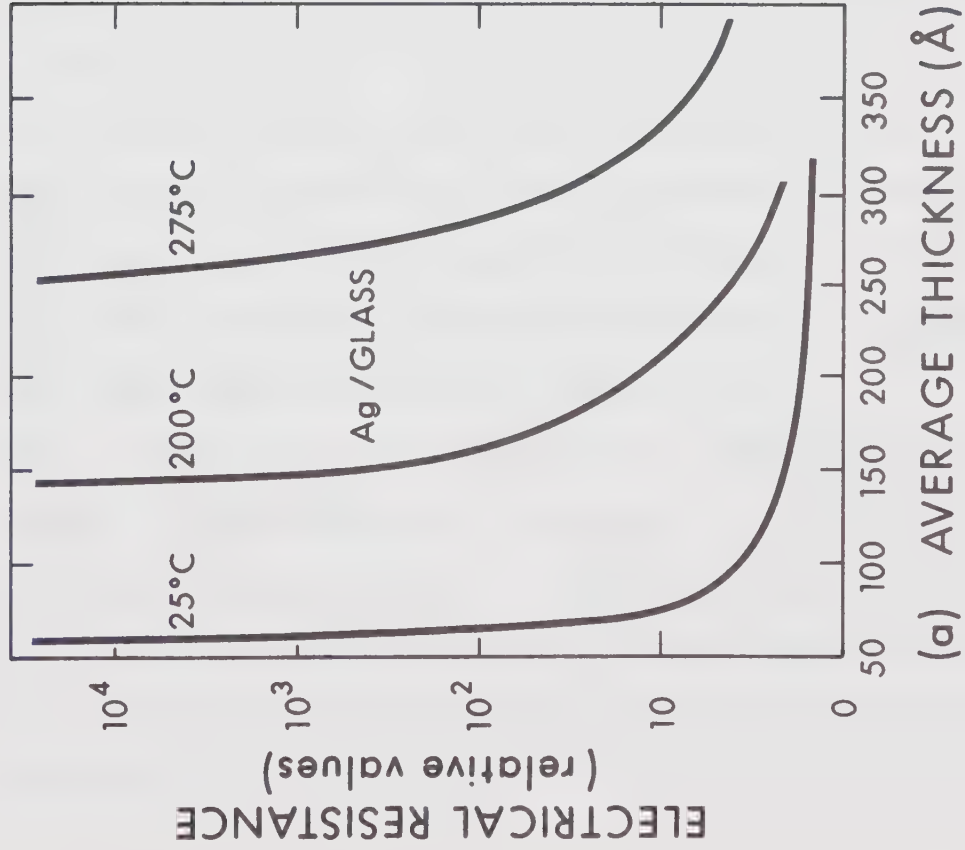
Investigations, performed mainly on indium by Pôcza (1967), show that there are two kinds of coalescence; b(1) the shape of coalesced grains does not change up to a certain size, beyond which the grains flatten and the built in grain boundaries are observed; b(2) the influence of the residual gases (P) might impede the growth of the grains in each of the above stages, and due to the nucleation

on the coating covering the surface of the grains, the growth stages of the vacuum deposited film begin all over again.

The effect of the substrate temperature on the electrical resistance behaviour during the coalescence stage of Ag films evaporated at a rate of 1 to 5 Å/sec. on glass is shown in fig. (3.1a), after Chopra (1966), (1968). The temperature dependence of the critical thickness t_c at which electrical continuity is attained is shown in fig. (3.1b). These curves show the sharpness of the coalescence transition from a discontinuous to an electrically continuous structure. Both the width of the transition and the critical thickness t_c increase with substrate temperature. Higher mobility and hence higher agglomeration is obtained for films of low melting materials on smooth and inert substrates. The high surface mobility deposits of Ag and Au condensed on pyrex glass slides at 25°C become electrically continuous at an average thickness of about 50 Å. On the other hand films of W, Ta, Ge, Si and various metal oxides deposited on several substrates at 25°C reach continuity at an average thickness of several angstroms. Any process bringing about an increase in the initial nucleation density and hence lesser agglomerations results in electrical continuity at a smaller thickness. For example, using pre-nucleation centers such as Bi₂O₃ or

Fig. 3.1

- (a) The resistance as a function of the film thickness at different substrate temperatures.
- (b) The temperature dependence of the critical thickness t_c (\AA°) (taken from Chopra (1966), (1968)).



SiO₂ on glass increases the nucleation density of Au films, and thus the films attain electrical continuity at 20 Å² as compared with 60 Å² on clean glass. This method is useful for obtaining ultrathin continuous films. Al films, have been reported to be electrically continuous at 15 Å² thick, Vrba and Woods (1971). The continuity of the Al films between 20 Å² and 100 Å² is important in the analysis of the tunneling conductance characteristics to be presented in Chapter 4.

3.2 Junction Preparation

The methods of junctions preparation which were adopted in this work had the following primary objectives.

- (i) Fabrication of the junction entirely in the controlled environment of a vacuum chamber, so that the junctions would be reproducible from sample to sample and the composition of the barriers would be unmodified by the contaminants of laboratory air.
- (ii) Control and determination of different film thicknesses in the different junctions.
- (iii) An identical barrier oxide for a set of junctions to facilitate the comparison of their characteristics.

The types of junctions used in this work are the following:

- (1) $\text{Al-Al}_2\text{O}_3\text{-Al}$ doped with Ni or Fe impurities at different distances r from the barrier interface. The location of the impurities r varies between 0 and 150 \AA .
- (2) $\text{Al-Al}_2\text{O}_3\text{-Ni}$ (or Fe).
- (3) $\text{Fe-Fe}_x\text{O}_y\text{-M}$, where M is Al, Sn, Pb or Fe counter electrodes.

The Al films were evaporated from tungsten baskets using Al wires of 99.999 % purity. Ni and Fe dopant and films were evaporated using bare filaments made of Ni strips and Fe wire of 99.99 % purity.

A typical junction preparation proceeded in the following manner:

A base Al film about 1000 \AA thick was evaporated and oxidized in a glow discharge [Miles and Smith (1963)], of 0.1 torr. of oxygen, for a time between 5 and 15 minutes, to obtain a junction resistance between 50 and 150 ohms. The high voltage electrode was adjusted to provide 1 m.a. of ionization current. Six Al films of different thicknesses (r) were deposited at a rate of 2 \AA/sec. in order to obtain an electrically continuous film at small thickness. Immediately after that a Ni or Fe impurity layer was deposited, which was followed by a thick Al film to complete the junction. The dynamic resistances of the six junctions at a bias

voltage of 250 m.V. were almost the same, an indication that the Al_2O_3 barrier is uniform, and that Ni does not change the junction resistance. For comparison, one of the junctions was not subjected to the magnetic impurity atoms.

Thermal oxidation has been also used to grow Fe_xO_y barrier, Tomashov (1966), and Al_2O_3 in case of an Fe counter electrode. The mass equivalent thickness of the deposited films was estimated from exposure times and crystal thickness monitor readings which will be discussed in the following section.

3.3 Thickness Measurement

Thickness is one of the most significant film parameters. It may be measured either by in situ monitoring of the rate of deposition, or after the film is taken out of the deposition chamber. Techniques of the first type, often referred to as "monitor" methods, generally allow both monitoring and controlling of the deposition rate and film thickness. Several reviews of the subject have appeared in the literature, Behrndt (1966) and Steckelmacher (1966). A sensitive method is based on measuring changes in the resonant frequency of quartz crystal oscillator with mass loading when operated in a particular mode of

vibration. A quartz crystal monitor for monitoring and controlling the rates of both the deposition and the evaporation of metals, nonmetals, and multicomponent films has become universally accepted and is at present the only most important monitor for thin film technology. The use of a quartz crystal as a thin film monitor was first proposed by Sauerbrey (1959), who made an extensive investigation of the various parameters of the monitor. The monitor utilizes the thickness shear mode of a piezoelectric crystal. A $35^{\circ} 20'$ quartz, called the AT cut, is generally used because of its low temperature coefficient ($\pm 5 \times 10^{-6}$ between -20 and $+60^{\circ}\text{C}$) for the resonant frequency. The standard method of operating an AT cut crystal is by perpendicular excitation using metal electrodes. The crystal then vibrates as shown in fig. (3.2a), so that most of the shear action takes place in the crystal interior, and most of the mass displacement occurs at or near the crystal surface. Adding a thin, uniform layer of any material to one surface of the crystal is therefore equivalent to increasing the crystal thickness (d) by an amount

$$\delta d = \frac{m}{\rho_q A}, \quad (3.1)$$

where m/A is the area density of the deposit, and ρ_q

is the volume density of quartz. Since the fundamental frequency of the crystal is related to its thickness by

$$f \cdot 2d = c_{\perp} = 3340 \text{ m/sec} , \quad (3.2)$$

the frequency shift δf due to deposited material is given by

$$\frac{\delta f}{f} = - \frac{2f}{c_{\perp}} \cdot \frac{m}{\rho_q A} , \quad (3.3)$$

provided $\delta f \lesssim 0.01 f$.

Warner and Stockbridge (1963), and others, have found by independent mass determinations that this last expression gives a correct ($\pm 1\%$) description of the monitor behaviour even if the crystal is masked and lightly damped at its periphery in order to make electrical, thermal, and mechanical contact.

If the crystal monitor results are combined with film thickness measurements obtained with a Tolansky interferometer, it is possible to determine the average film density. Hartman (1965) found that Al films attain 80 % of bulk density at $t \approx 250 \text{ \AA}$, and 97 % of bulk density at $t \geq 1000 \text{ \AA}$. Hartman has found Al film densities to be somewhat variable while Au films attain bulk density even when thin.

Table (3.1) shows results obtained for Al, Ni and Fe during the course of the work reported here. The uncertainties given are of interferometric and geometric origin

Table (3.1). The density ratio $\rho_{\text{film}}/\rho_{\text{bulk}}$ calculated from the single crystal monitor readings and the optical measurements.

Material	Thickness (\AA)	Density ratio ($\rho_{\text{film}}/\rho_{\text{bulk}}$)
Al	1200	$0.90 \pm 5 \%$
	1500	1.04
	1800	0.80
Ni	1200	$1.10 \pm 10 \%$
Fe	300	$0.93 \pm 10 \%$
	1200	$0.90 \pm 10 \%$

Low film densities are generally attributed to voids in the film since electron diffraction patterns reveal the bulk lattice spacing for the crystallites of the film. Film thicknesses quoted in the remainder of this work will be mass equivalent thicknesses relative to films about $1 \text{ K } \text{\AA}$ thick.

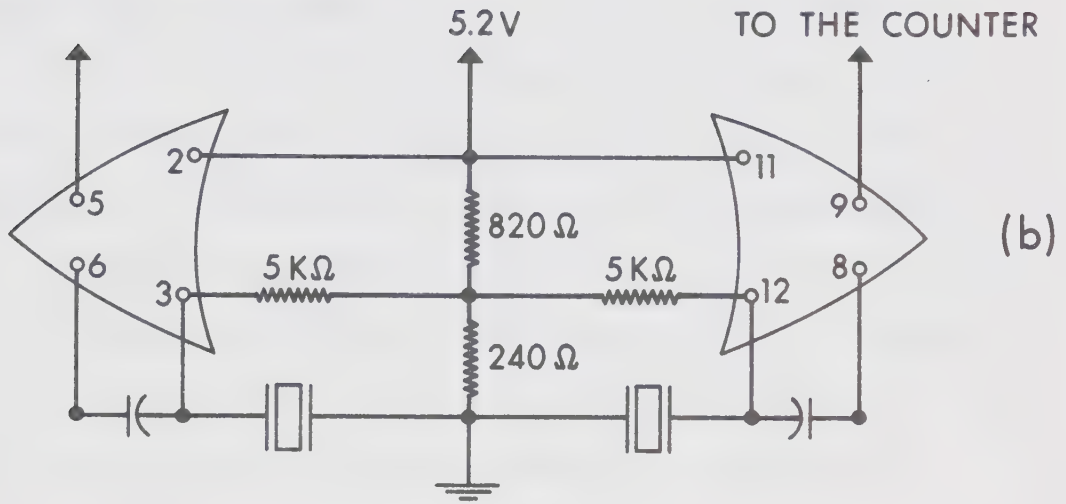
Fig. 3.2

- (a) The oscillation of the single crystal; most of the mass displacement occurs at the crystal surface.
- (b) The circuit diagram of the single crystal monitor used in the present work. The integrated circuit is Motorola MC 1024P.
- (c) Single crystal holder; very light springs are used to provide electrical contacts with the crystals.

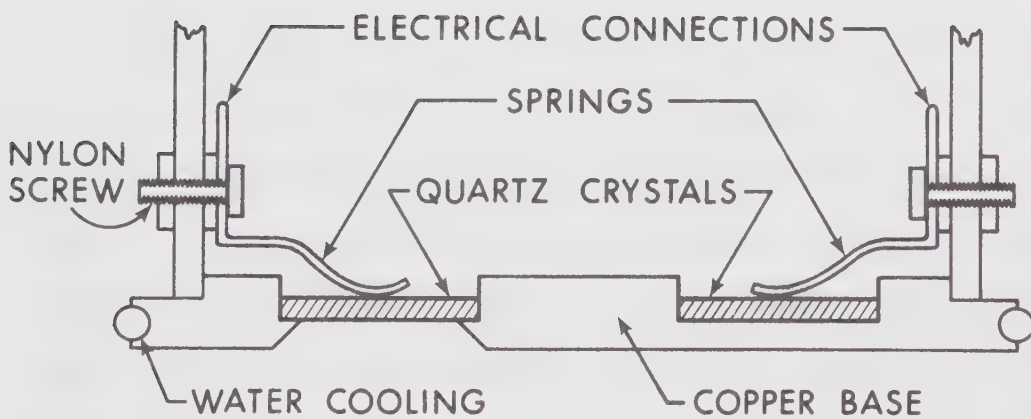


QUARTZ CRYSTAL

(a)



(b)



(c)

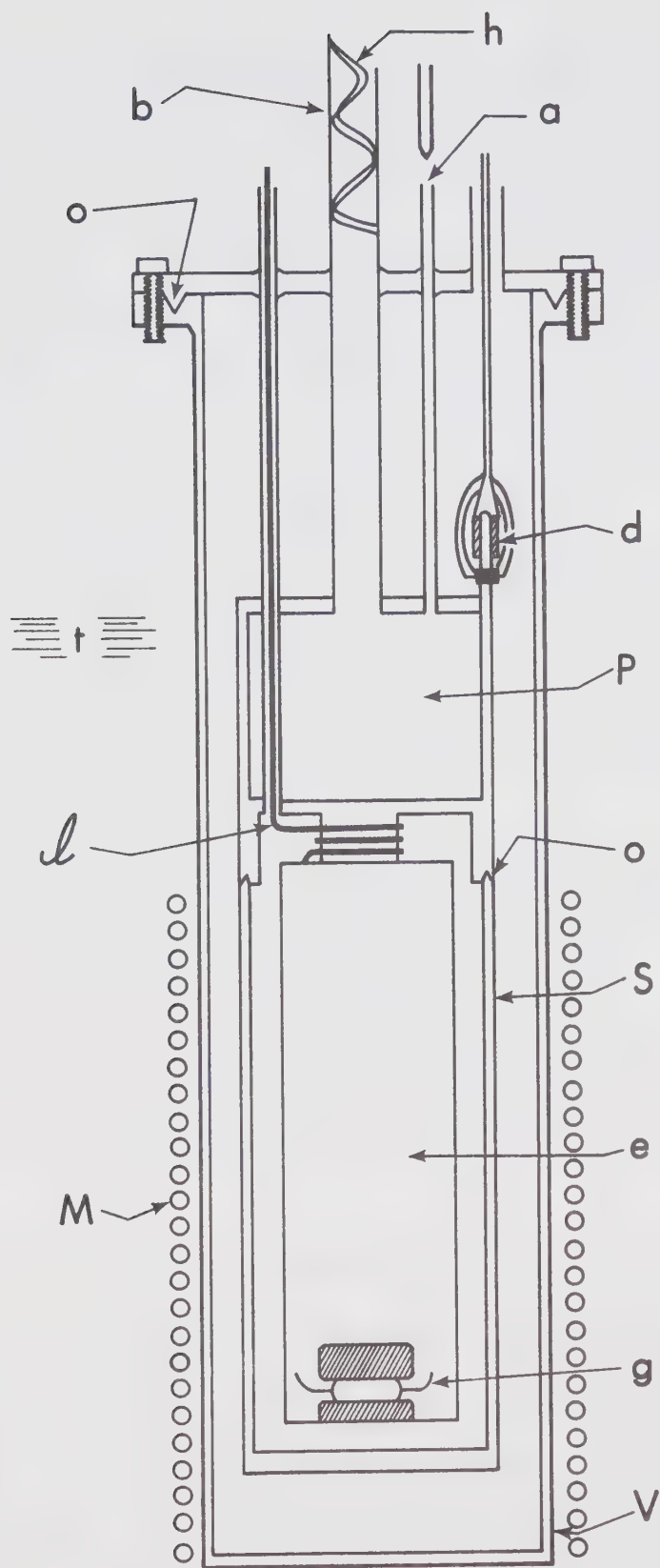
The circuit diagram of the single crystal monitor used in this work is shown in fig. (3.2b). The crystals are mounted in a water cooled copper jacket, and a silver coating was used to provide electrical contact with the crystal. Contact to the coating is secured by light spring clips as shown in fig. (3.2c). The outputs of the oscillators are connected to the inputs of a counter timer device (Monsanto, model 100A), which could measure the frequencies f_1 and f_2 of the oscillators, or, with a small modification, the ratio f_1/f_2 as a function of the deposition time. The frequency f_1 is constant at about 5 M Hz/sec. while f_2 changes as a function of the deposited metal on the surface of the crystal.

3.4 Production of Low Temperatures

The experimental arrangement used in this work is shown in fig. (3.3). The letters denote the following: (P) is the pumping chamber and is provided with a needle valve (a) to allow the desired amount of liquid nitrogen or liquid helium inside. A stainless steel tube (b), provided with the thermal shield (h), connects (P) to a diffusion pump. By pumping over the liquid helium, a temperature of 1°K could be maintained. A regulating valve to control the pressure above the helium changes the temperature between 1 and 4.2°K . Elevated temperatures up to 70°K could be maintained using an electronic

Fig. 3.3

The cryostat arrangement for the production of low temperatures.



controller which senses the resistance of a $220\ \Omega$ speer carbon resistor (d). (S) is the sample chamber, which contains the sample holder (e) and the germanium thermometer (g). The vacuum chamber (v) is connected to a diffusion pump. A pressure of 5×10^{-7} torr. is needed to shield the sample chamber from the liquid helium bath (t). The cryostat was designed to fit in the core of a 20 K.G. superconducting magnet (M). Indium O ring (o) plus apieson grease # N were used for vacuum sealing. The grease makes it possible to separate the cans from their caps without damage of the indium rings, and it is possible to use the seals 4 or 5 times before they have to be repaired.

For temperature measurements the germanium thermometer # 904 was calibrated by Dr. Rogers between 1°K and 60°K , and by Dr. Woods between 4.2°K and 12°K . The bridge used for the measurement of the resistance of the germanium thermometer was designed by Dr. Rogers.

3.5 Conductance Measurements

The dynamical conductance and its voltage derivative dG/dv are measured as a function of the bias voltage v at different temperatures. The conductance bridge used for this purpose is described by Rogers (1970). In a typical measurement, the junction was

cooled to 1°K , which is the limit of the pumping system. Superconducting energy gap traces were recorded to confirm that tunneling was the dominant transport mechanism in the junction. Any metallic bridges in the oxide barrier would lead to serious structure in the gap region. A magnetic field parallel to the junction films was applied and increased until the conductance versus voltage plot showed no evidence of the superconducting state. With the electrodes in their normal state, the bridge was balanced at a suitable bias voltage. The off balance signal of the bridge is proportional to the conductance change in the junction produced by varying the bias, the temperature, or higher magnetic fields, and is plotted by the x-y recorder with the required sensitivity.

CHAPTER 4

EXPERIMENTAL RESULTS AND DISCUSSIONS

4.1 Small Conductance Peak

The typical conductance versus voltage characteristics of an Al-I-Al junction doped with a small amount of Ni impurities at the barrier interface, is shown in fig. (4.1). The total conductance G can be written as

$$G = G_0 + \Delta G ,$$

where G_0 is the temperature independent background conductance, and ΔG is the 4 % conductance peak anomaly around the zero bias. The observation of a conductance peak anomaly due to magnetic impurities at the barrier interface was important to justify the basic assumption given by Anderson (1966), that the localized magnetic impurity states are the origin of the phenomena.

a) Temperature and Voltage Dependence

The conductance versus bias voltage, at different temperatures, is shown in fig. (4.2). It was pointed out by Wyatt (1964), that the conductance at zero bias depends on temperature as $-\ln T$ and that the voltage

Fig. 4.1

The conductance versus voltage at 80 K (dashed line) and 4.2 K (solid line) of an Al-I-Al junction doped with Ni impurities at the barrier interface.

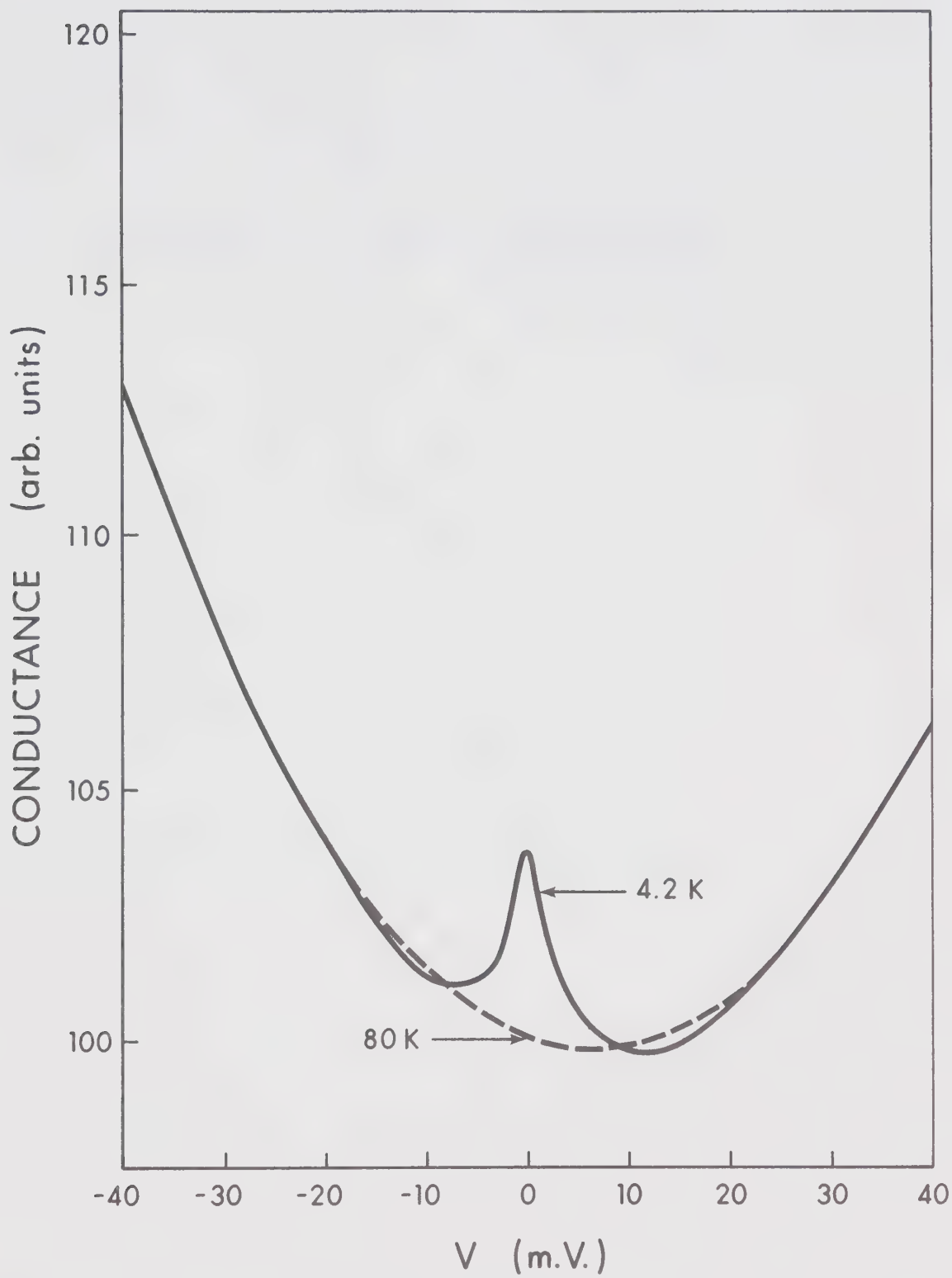
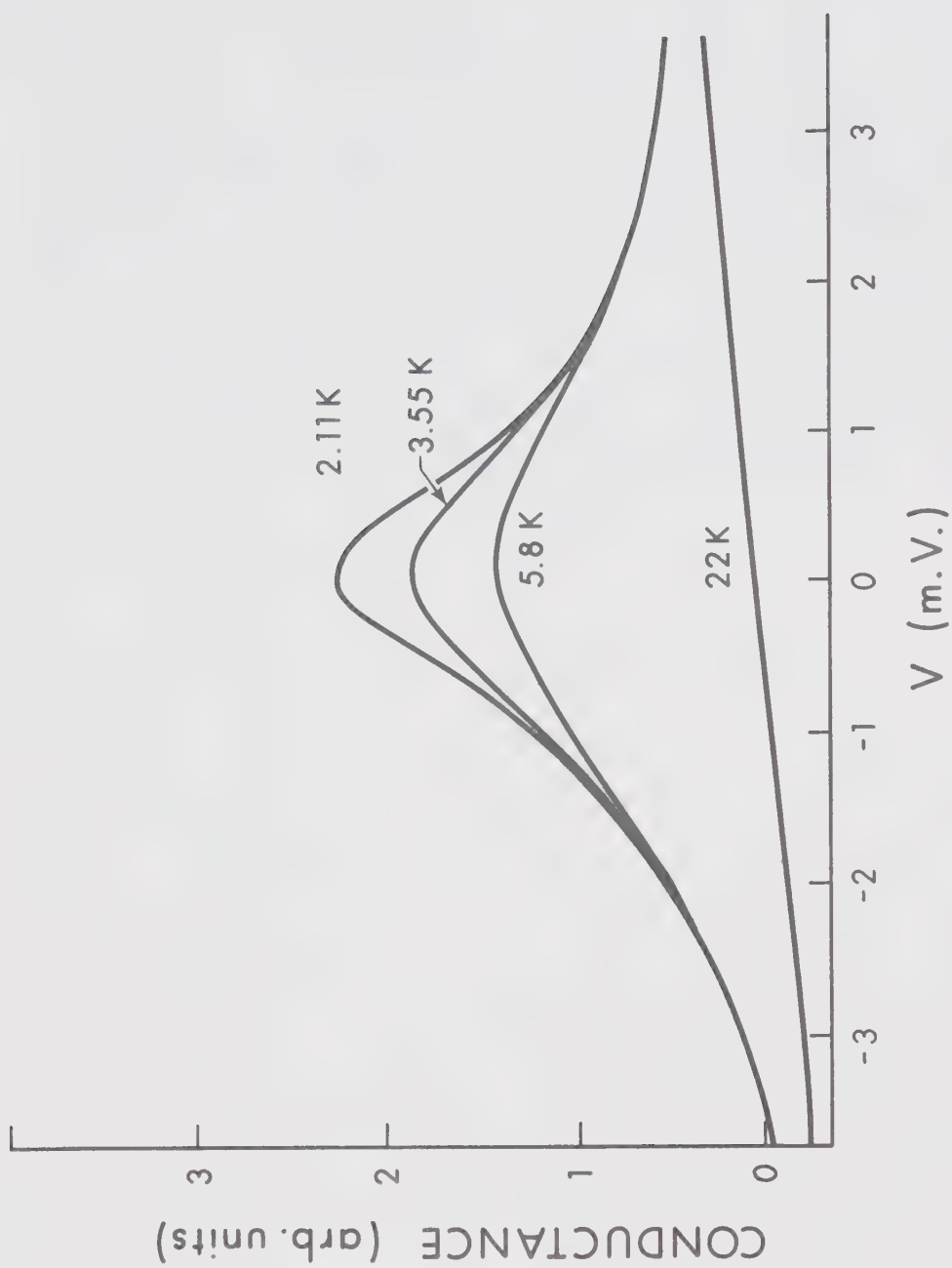


Fig. 4.2

ΔG versus V at different temperatures.



dependence of the excess anomalous conductance above the background was (for $eV \gg \kappa_\beta T$) also logarithmic. This excess conductance is identified with the $G^{(3)}$ term discussed before. A plot of the voltage dependence of $G^{(3)}(V)$ at 2.1°K and the temperature dependence of $G^{(3)}(0)$ is shown in fig. (4.3). The voltage dependence drops below a linear logarithmic plot at low voltage because of $\kappa_\beta T$ smearing. The temperature dependence should fit on the voltage dependence for $eV \gg \kappa_\beta T$ if n in the expression

$$G^{(3)} \propto \ln [|eV| + n\kappa_\beta T] / E_0 = F(eV) ,$$

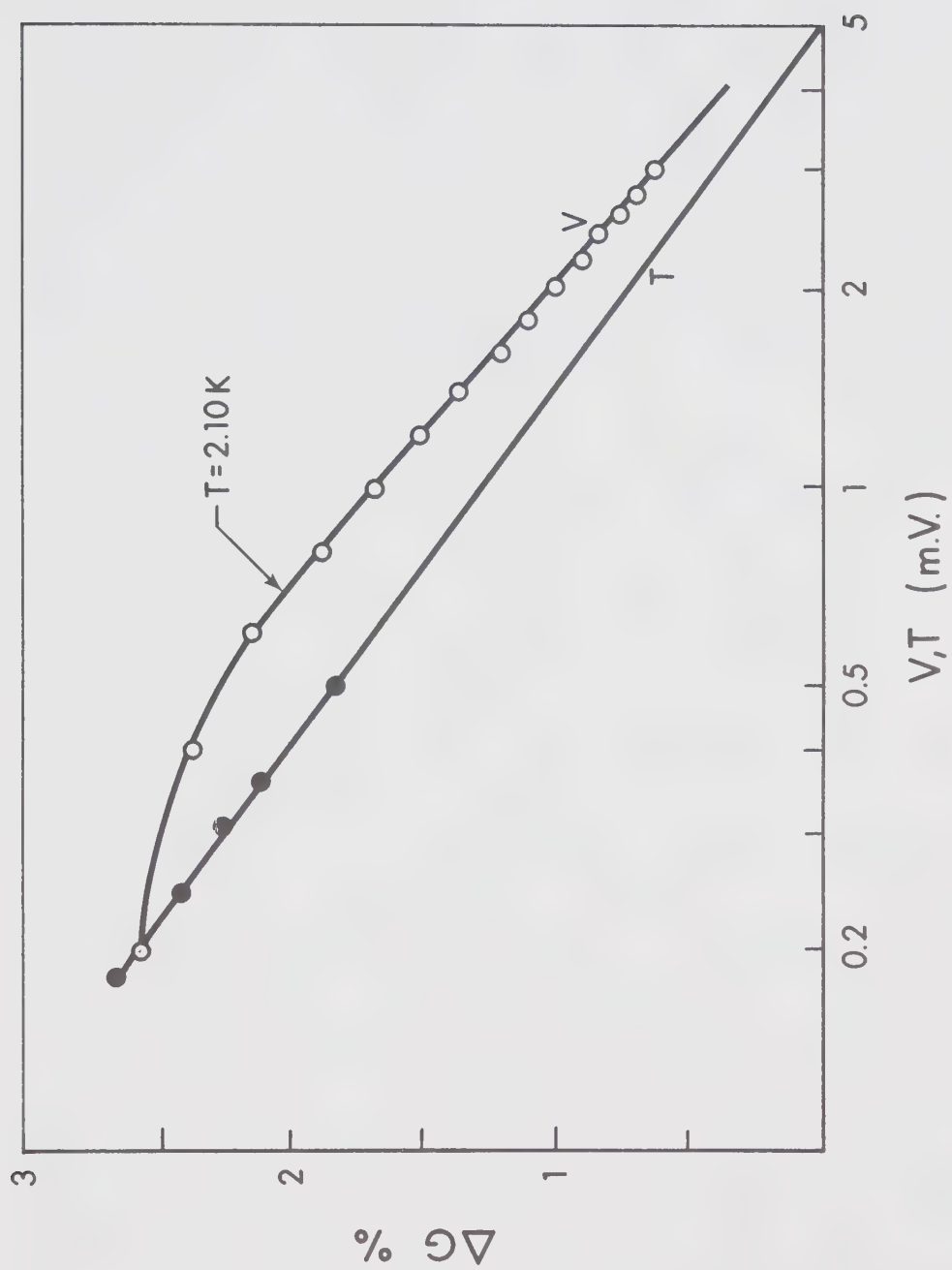
is unity. From the displacement of the temperature points we found that $n = 1.5 \pm 0.1$, and $E_0 = 5 \text{ m.V.}$ Shen and Rowell (1967) found that $n = 1.35 \pm 0.15$ for Ta-I-Al and Sn-I-Sn junctions. Nielsen (1969) found that n should be 10 at $T = 0.36^\circ\text{K}$, and at higher temperatures a different value should be chosen. A more accurate representation of $F(eV)$ was introduced by Wolf and Losee (1970), where

$$F(eV) = -\rho \ln \left(\frac{|eV|^2 + (n\kappa_\beta T)^2}{E_0^2} \right)^{\frac{1}{2}} ,$$

with a best value of $n = 1.84$. Numerical calculations by Appelbaum gives $n = 1.35$, where the earlier phenomenological model used by Wyatt (1964) gives $n = 1.1$.

Fig. 4.3

The dependence of ΔG on bias voltage (open circles) and $\Delta G(V=0)$ on temperatures (solid points).



b) Magnetic Field Dependence

It is difficult to regard the above results as a critical test of the Appelbaum theory. Zawadowski (1968), using a different approach, arrived at the same energy and temperature dependence, however with a conductance peak for ferromagnetic interaction ($J > 0$) between the conduction electron and the localized magnetic impurity states. A critical test of the theory is possible if one investigates the prediction made by Appelbaum for the effect of a large magnetic field at very low temperatures on tunnel junctions doped with a low enough impurity concentration to meet the conditions of the theory. Due to experimental limitations and difficulties it was not possible at this stage to carry out the experiment under these optimum conditions. However, the results available to us will give some information on the magnetic behaviour of Al-I-Al junctions doped with Ni impurities. As explained before the second order transition probability, $W_{ij}^{(2)}$, produces a conductance $G^{(2)}(V, H)$ corresponding to the spin flip process, which becomes inelastic in the presence of a magnetic field. The tunneling electron must supply the excitation energy $g\mu_B H$ to the impurity spin. Thus one expects a well in the $G^{(2)}$ term. The $G^{(3)}$ term, which includes the Kondo-Appelbaum integral function, shows splitting as well with two peaks located at $\pm g\mu_B H$.

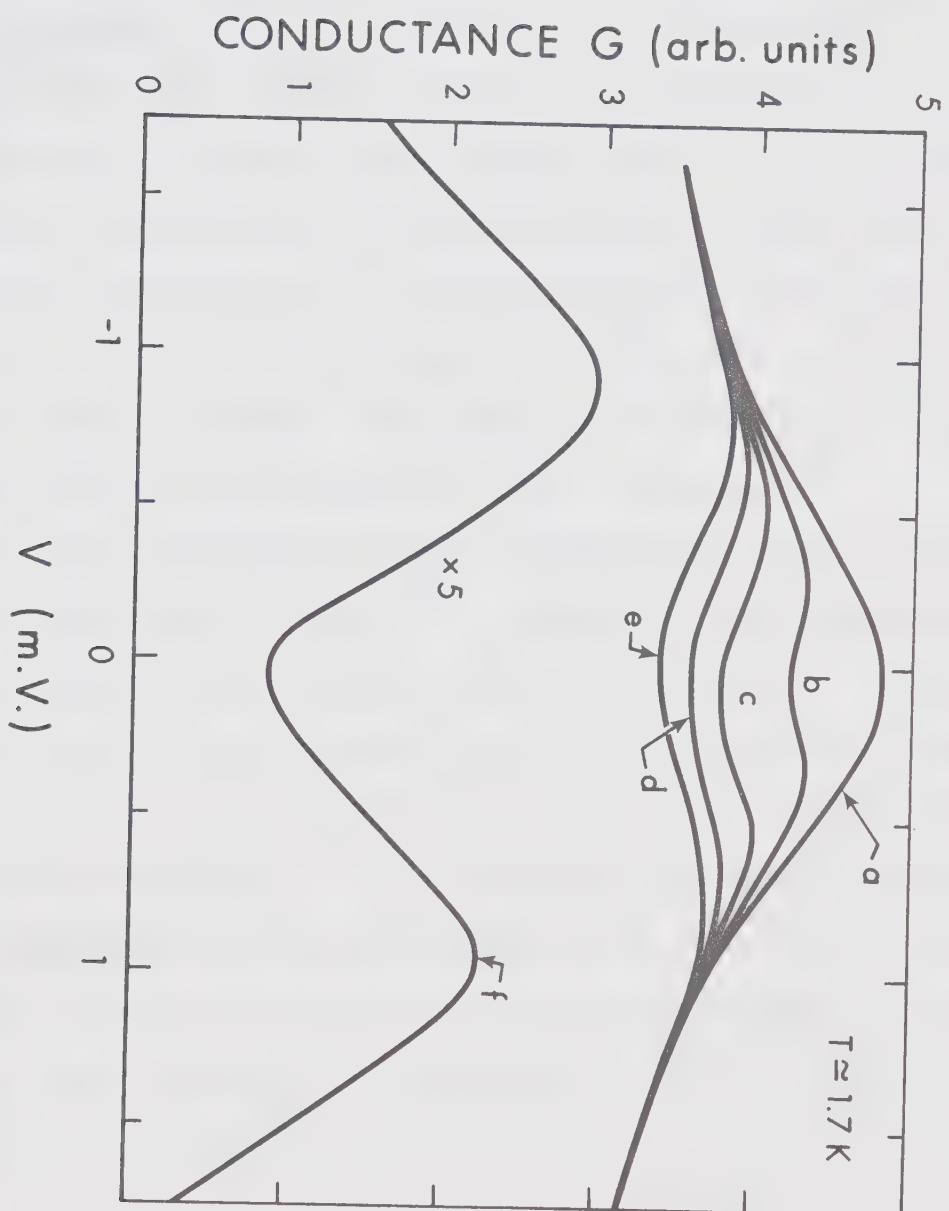
Experimental results at 1.5 - 1.7°K of a junction doped with Ni impurities in the presence of the magnetic field^{*} is shown in fig. (4.4). The effect of the field is first to reduce the height of the peak as if the temperature was being increased. At 30 KG, a dip in the conductance starts to appear. The magnitude of the dip increases by increasing the magnetic field and starts to saturate at relatively higher fields as explained by Appelbaum.

The effect of $\kappa_{\beta}T$ smearing is serious in this experiment. For example, if $g = 1$ and $H = 45$ KG, then $g\mu_B H = 0.26$ m.V.; and if the smearing h of the tunneling characteristics is $3.5 \kappa_{\beta}T$, then at 1.5°K, $h = 0.13$ m.V., which smears the conductance well to a dip. Wolf and Losee (1970) found that the expression (2.14), obtained by Shen for the temperature broadened conductance well, is not applicable for their data. In their study of Schottky barrier anomalies at 1.3°K and 150 KG, they found that an extension of Appelbaum's theory to include the magnetic field-induced life time broadening substantially improved the agreement with the experimental conductance line shape at higher fields. They predict for the $G^{(2)}$ term a field dependent broadening $\Gamma = \pi(J\rho)^2 z$, and a measured gyromagnetic ratio $g = g_0 - 2|J\rho|$, where J and ρ are the exchange coupling and

^{*} I wish to acknowledge the use of Dr. Woods' high field solenoid.

Fig. 4.4

ΔG versus V characteristics in the presence of a magnetic field H . Curves a, b, c, d, e and f correspond to $H = 0, 20, 38, 55, 60$, and 66 KG; $T \approx 1.7^\circ\text{K}$.



density incorporated in Appelbaum theory, and g_0 is the ion g-factor in zero magnetic field. According to their calculations, the amplitude of the $G^{(3)}$ term is reduced in magnetic fields ≥ 50 KG and could be neglected, i.e. the magnetic field quenches the Kondo scattering. The value of z and Γ could be determined from the location and the half width of the peak of dG/dV in high magnetic fields. The magnetic field available to us at the time of the experiment did not exceed 60 KG. In this field, one could still observe the field broadening effect on the peaks located at the Zeeman energies, fig. (4.4). Experimental difficulties in the determination of $dG(V)/dV$ necessitated large conductance peaks due to relatively small amounts of dopant. It was not possible to produce such junctions with Ni impurities. Even then the errors in the values z and Γ will be rather large because $dG(V)/dV$ could not be measured electronically with high accuracy. It is clearly impossible to extract unambiguous exchange parameters from fig. (4.4). However the g-factor, determined from the estimation of the peak separation versus magnetic field, was found to be 2.0 ± 0.2 .

c) Concentration Dependence

The tunneling conductance versus voltage characteristics, at 4.2°K , of Al-I-Al junctions doped with

different amounts of Ni impurities at the oxide interface are shown in fig. (4.5). The results indicate that,

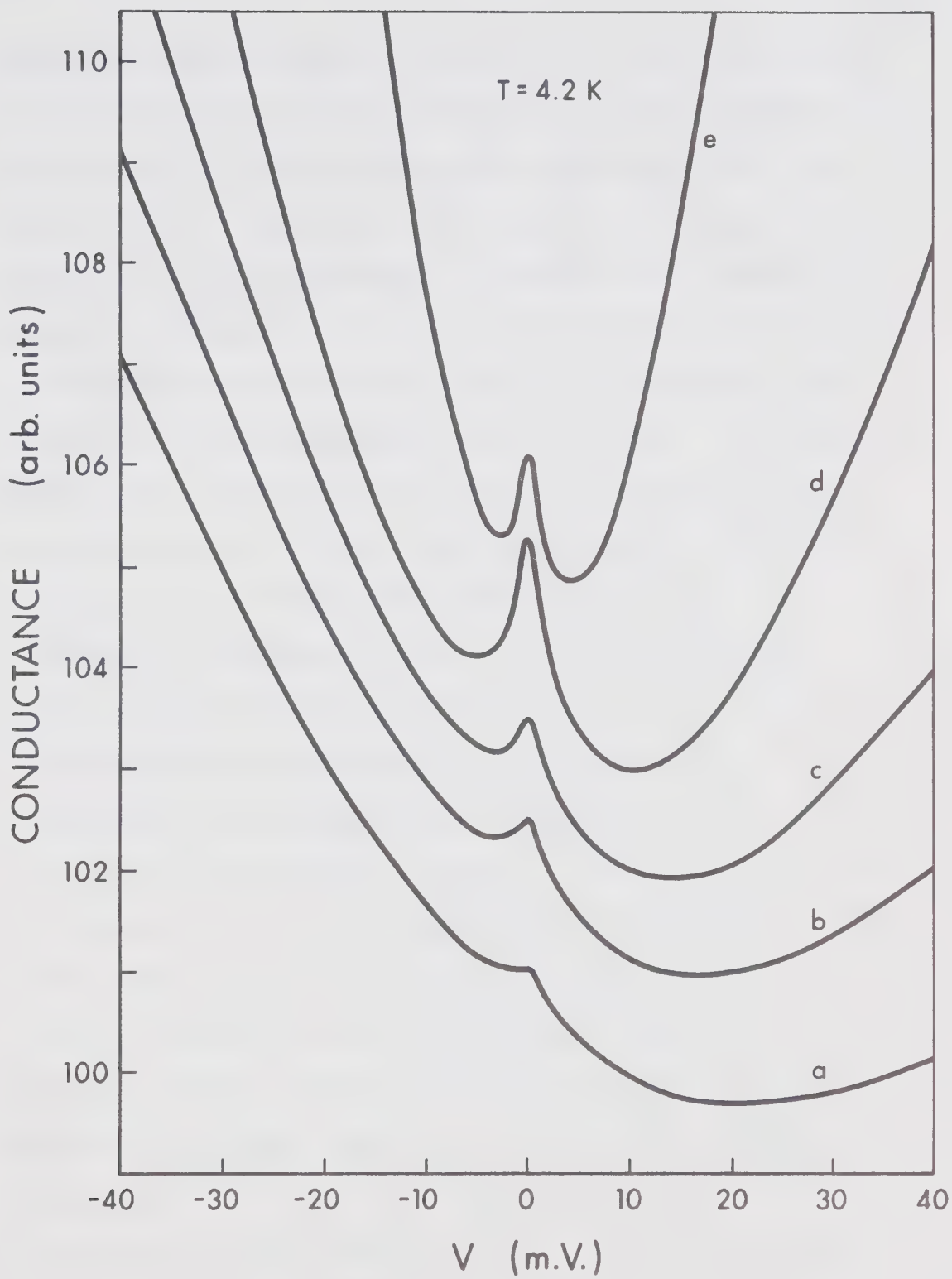
(a) - The conductance peak increases first with the impurity concentration and then decreases at higher concentration; (b) - The background conductance increases rather rapidly, and at relatively high concentration the conductance peak is superimposed on a resistivity maximum at zero bias. This behaviour has been observed in many other junctions. As far as (a) is concerned Nielsen (1970) found a reduction of the conductance peak upon increasing the amount of Cr dopant from 0.1 to 5 Å² and its absence beyond a thickness of 6 to 8 Å² of cobalt; the thickness range for the conductance peak of Ti dopant is between 0.3 Å² and 63 Å². He attributed this behaviour to the interaction between the impurities which minimizes the free exchange of electrons and impurity spin moments. However, the correlation between the impurity spins is not the only mechanism which leads to the decrease of the conductance peak anomaly. Appelbaum (1970) found theoretically that the conductance anomaly due to a single impurity is a function of its position relative to the barrier interface, and could be written as

$$\Delta g^{(3)} = A(R) \ln \frac{|eV| + n\kappa_{\beta} T}{E_0} ,$$

where E_0 is a cut off energy, $A(R)$ is large and positive

Fig. 4.5

G versus V for an Al-I-Al junctions doped approximately with (a) 1 A° ; (b) 2 A° ; (c) 3 A° ; (d) 5 A° ; and (e) 7 A° of Ni impurities at the barrier interface.



when the impurity lies in the barrier, zero when it is at the interface and oscillates when it is located in the metal. In the case of random distribution, the conductance at zero bias will depend on the effective position of the impurities. Therefore one expects to observe a conductance dip at a high enough concentration of impurities deposited on the Al_2O_3 interface. This behaviour is not reflected in our results. The conductance peak still exists at about 10 \AA^0 impurity layer thickness, which is large enough to move the effective position of the impurities from the barrier to the electrode. Neugebauer (1959) found that Ni layers become ferromagnetic at a thickness of 3 \AA^0 . It seems then possible to associate the small decrease of the conductance peak anomaly upon increasing the Ni dopant with a weak correlation between the magnetic impurities.

As far as (b) is concerned, the behaviour of the conductance versus bias voltage for heavily doped junctions could be explained by the strong coupling theories. There are two theories for the tunneling electrons strongly coupled to the magnetic moments. Sóllyom and Zawadowski (1968) showed that the resistance versus bias voltage behaves similar to the reciprocal life time of the scattered electrons as a function of energy. Using Abrikosov's solution for the scattering

amplitude, the resistance exhibits a peak at a finite voltage $E_0 > \kappa_\beta T$, and the effect of increasing impurity concentration is to shift E_0 towards the zero bias. They had also shown that the background conductance is slightly temperature dependent. This is in qualitative agreement with our results, fig. (4.5). However their theory does not include the spin flip process, and therefore is not adequate to explain the observed Zeeman splitting. Appelbaum et al (1967) predicted a small conductance peak if the spin flip process is dominant and a large resistance peak if the non-magnetic assisted tunneling process is important. However, the two anomalies have the same energy range, and therefore are mutually exclusive. Our results show that the two anomalies could be produced simultaneously, and could not be explained by a single theory. This means that the assisted tunneling process and the reduction in the electron density of states should be treated simultaneously. Using a Green's function decoupling technique Appelbaum showed the possibility of such a treatment. Mezei and Zawadowski, however, indicated that if both phenomena are present, they will produce an interference cross term which yields an asymmetric contribution to the resistance anomaly while the experimental results show fairly symmetrical $R(V)$ characteristics. Therefore one of the phenomena

should be neglected. The alternative explanation offered by the authors is that the impurities in the barrier will affect the electron density of states to produce a conductance peak and those in the metal will be responsible for the resistance peak. In order to test this argument the effect of an impurity layer introduced inside the metallic electrode should be investigated. This effect is discussed in Sec. 4.3.

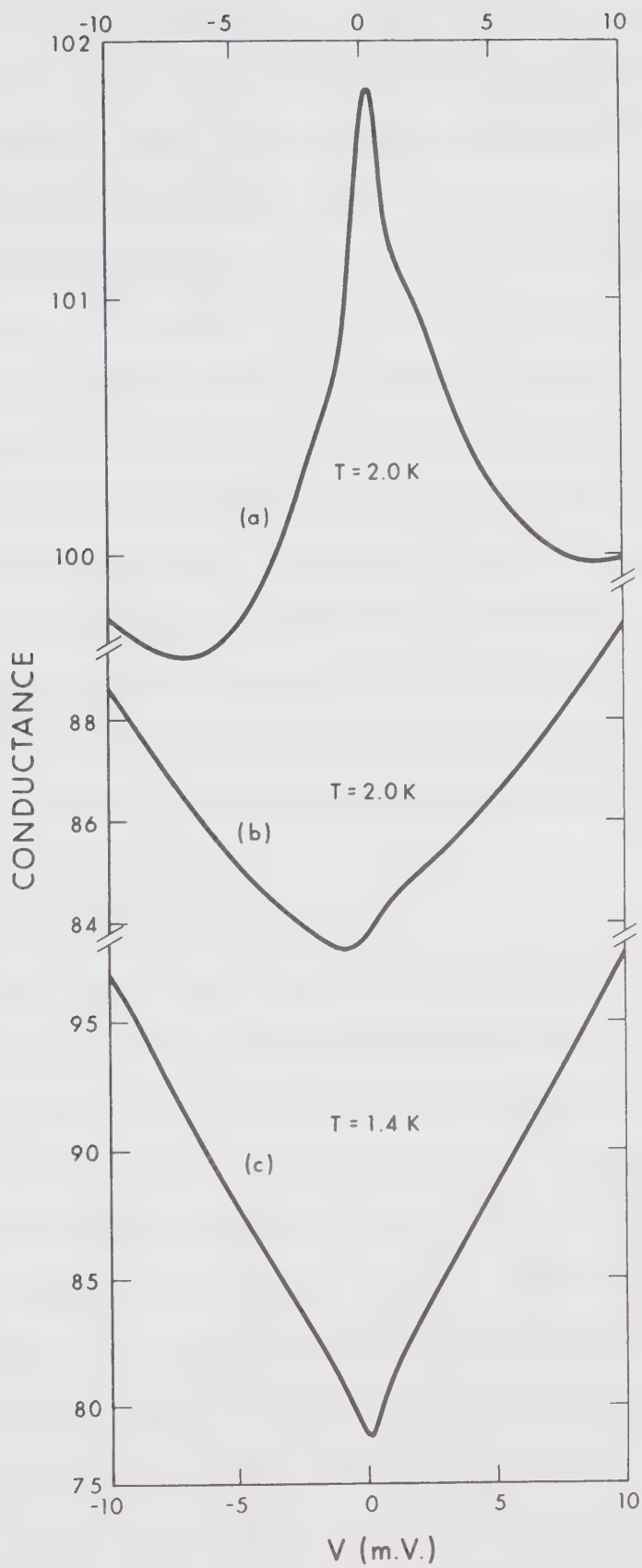
We believe that the strong coupling theories are not at present practically reliable, and they have not worked out in the presence of a magnetic field. Our experimental results show, however, that less than a monolayer of Ni impurities at the barrier interface can produce a conductance peak anomaly which could be fairly explained by Appelbaum theory.

4.2 Tunneling Results with Interacting Magnetic Impurities

Fig. (4.6) shows typical results of the conductance characteristics of Al-I-Al junctions doped with three different concentrations of Fe impurities. In contrast with Ni results, a very small amount of Fe (less than one monolayer) produces a conductance peak at zero bias; curve (a). The peak disappears at 1 \AA^0 of Fe, and a small conductance dip starts to show up, curve (b). A large conductance reduction (resistance peak anomaly)

Figure 4.6

Conductance versus voltage for Al-I-Al junctions doped with Fe impurities. Doping is approximately (a) 0.5 A° ; (b) 1 A° ; (c) 1.5 A° .



is observed at 1.5 \AA thick. This overall conductance behaviour has been observed before in some other junctions by Mezei (1967), and Lythall and Wyatt (1968).

Nielsen (1970) found that the first few evaporated layers of Cr impurities on the top of an Al_2O_3 barrier were not able to produce a conductance peak. The Cr was partially oxidized by the excess oxygen at the interface of the barrier. The oxidation state can prevent the free exchange of conduction electron and impurity spin moments. This has been confirmed experimentally when a large conductance reduction due to a magnetic oxide was observed and attributed to the formation of an additional barrier at the barrier interface. The bias range of this reduction was given by

$$V_0 = (d+t)\phi/t ,$$

where t and d are the thicknesses of the Al_2O_3 and the added magnetic oxide barrier, and ϕ is the height of the added barrier. The conductance characteristics of the undoped junction should be retained at bias voltages $V > V_0$. If one associates 30 m.V. for the barrier height of Fe_xO_y as obtained from the work of Isin et al (1968), and uses 20 \AA for the Al_2O_3 thickness, then one should observe the pure junction characteristics at 40 m.V. This is not the case in our results. We observed a conductance peak at low concentration, and an

anomaly which is even stronger than that of Al-I-Fe junctions. Therefore one could assume that the tunneling anomalies are due to magnetic Fe impurities rather than a magnetic oxide.

Abrikosov and Gorokov (1961) studied the effect of the magnetic impurities on the superconducting state. They found out that the S-d exchange scattering makes the life time of the Cooper pairs finite in contrast to the ordinary potential scattering where the life time remains infinite. Due to this depairing effect, the critical temperature T_c decreases. The finite life time of the pairs causes an energy spread proportional to the inverse life time and thus broadens the BCS density of states curve. The pair breaking effect on the superconducting density of states and the transition temperature of the Al electrode is shown in fig. (4.7). This illustrates that the S-d interaction is the origin of the zero bias anomalies observed in the normal tunneling characteristics.

The conductance peak versus bias voltage at different temperatures is shown in fig. (4.8). At 4.2°K a broad conductance peak located at a bias voltage slightly different from zero was observed. An additional narrow peak ($\sim 1 \text{ m.V.}$) is formed at 2°K and starts to split at 1.52°K .

Fig. 4.7

Superconducting energy gap results for junctions (a), (b) and (c) of fig. 4.6.

CONDUCTANCE (arb. units)

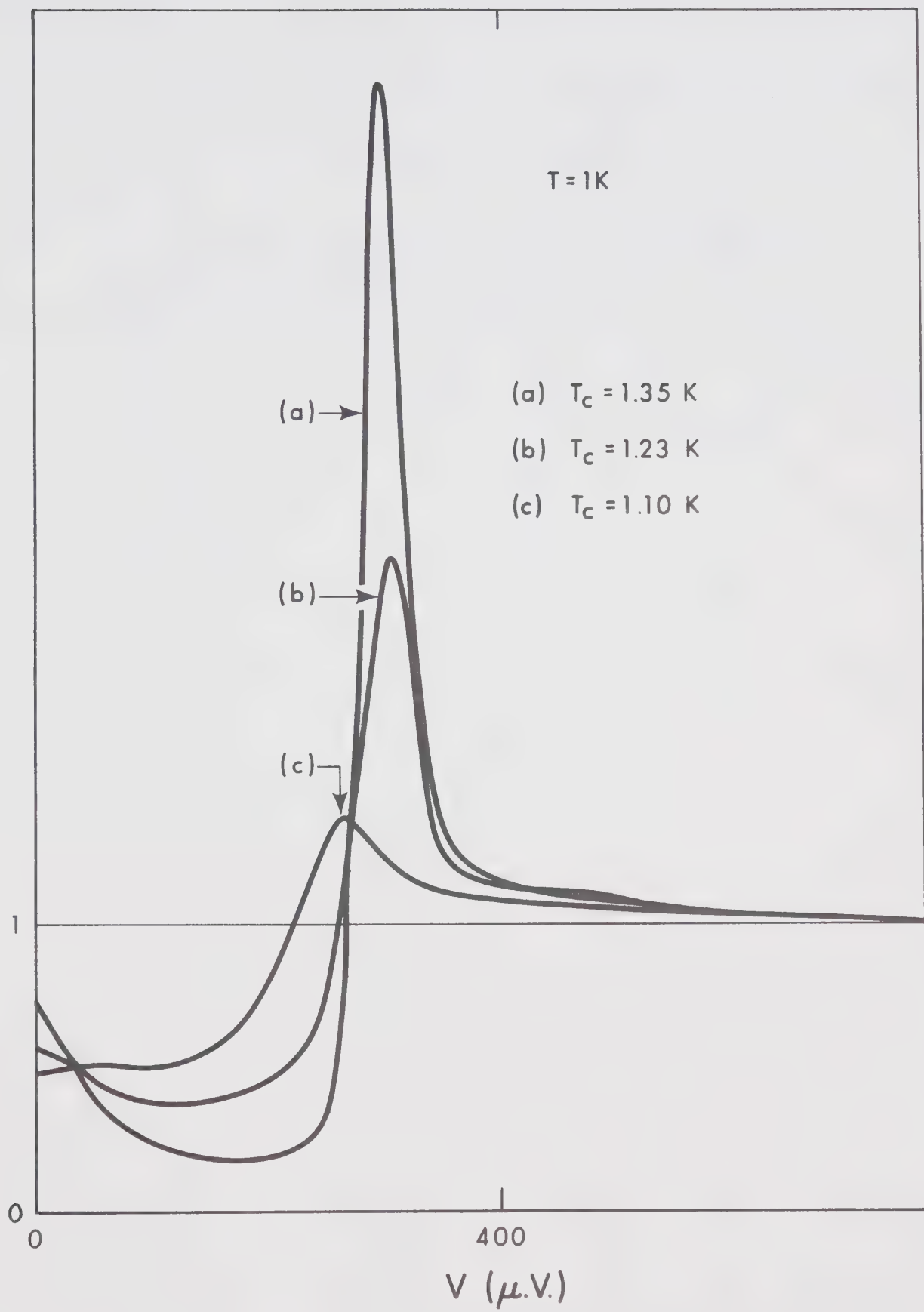
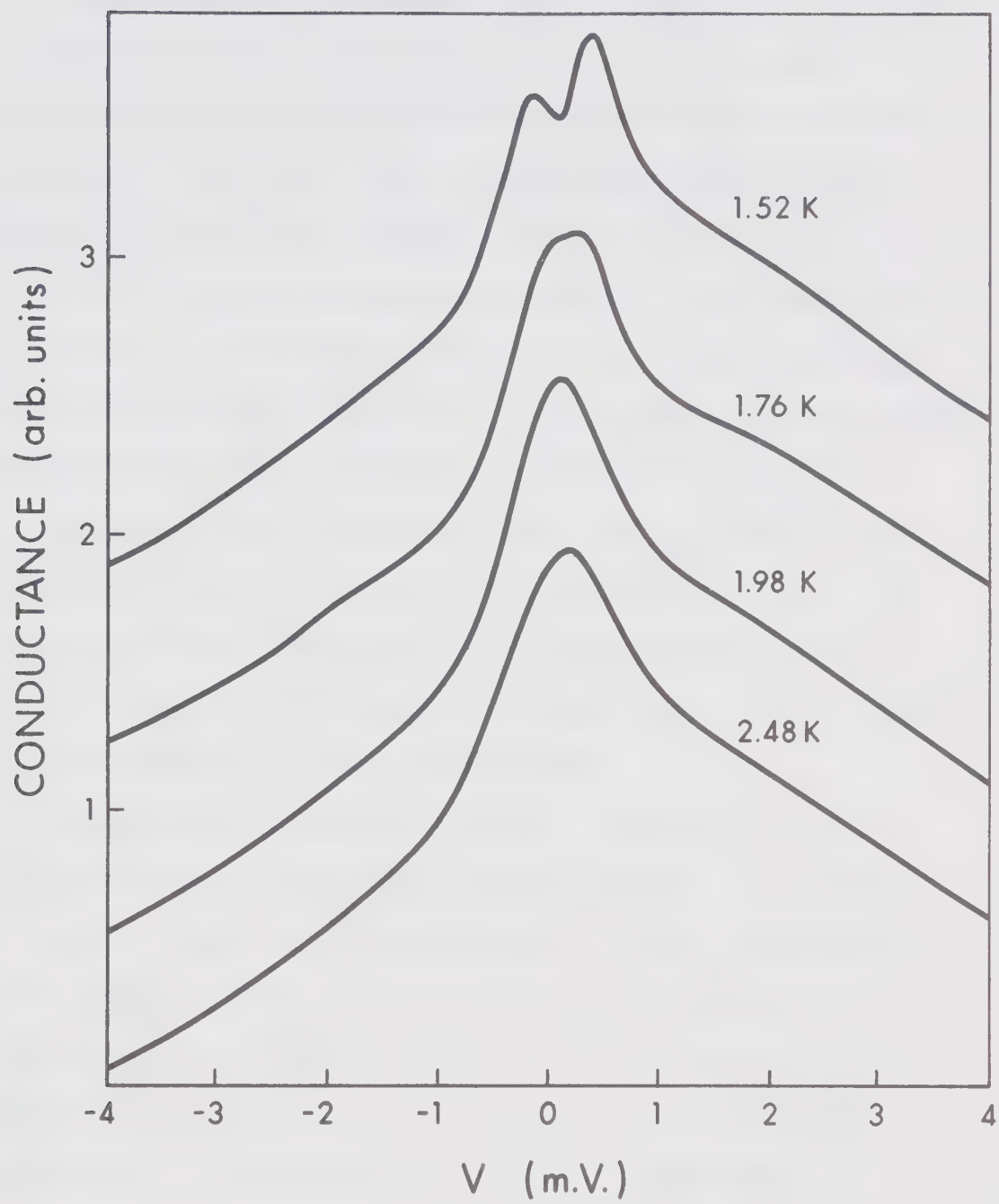


Fig. 4.8

G versus V characteristics for junction (a) of fig. 4.6 at different temperatures.

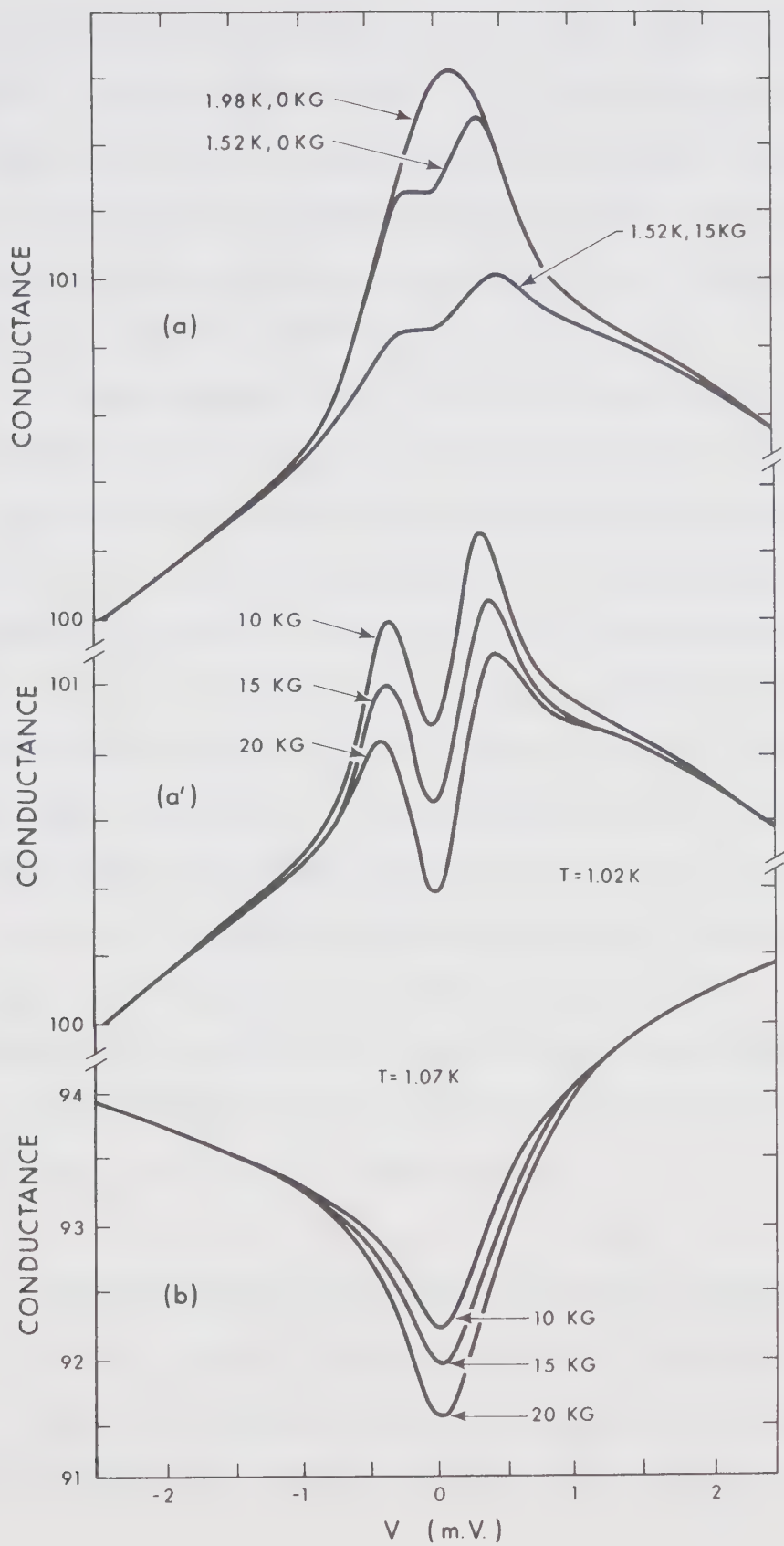


Appelbaum and Brinkman (1969) studied the effect of electron-magnon interaction on the conductance characteristics of simple metal-oxide-transition metal junctions. They found that an additional peak in the conductance should be formed with a width of about one tenth of the maximum magnon frequency. This peak could also split at low enough temperature and zero magnetic field due to magnon creation. In the case of Ni counter electrodes the peak should occur between 2 and 5 m.V. The additional peak, shown in fig. (4.6), cannot be associated with the magnon renormalization effect on the conductance characteristics since the impurities are less than one monolayer thick and the peak disappears upon increasing the Fe concentration.

Gupta and Upadhyaya (1971) extended the S-d Appelbaum model to account for the effect of the weak interaction between the impurities on the conductance peak anomaly. They found that the conductance peak could even have Zeeman splitting in the absence of an applied magnetic field due to the magnetic impurity correlation. Results at 1°K and in the presence of a magnetic field (to quench the superconductivity, fig. (4.9a,a')) seem to assist this idea. The effect of the field is to reduce the magnitude of the additional conductance peak and slightly affect its splitting.

Fig. 4.9

Magnetic field results for junctions (a), (b)
of fig. 4.6.



Similar results have been observed with intermediate impurity concentration, curve (b), but the dip becomes stronger and wider as one expects for closer impurities. To our knowledge the magnetic field effect on a conductance dip has not been reported in the literature except in a lightly doped p-n junction.

It would appear then that the interactions between the magnetic impurities in a barrier become important at surprisingly low impurity concentrations, and that they may be a contributing factor to the zero bias conductance dip which is often obtained with higher impurity concentration. This is the first observation of the interacting magnetic impurity effect on the tunneling conductance anomaly. Other work, using Fe as a dopant, has been reported by Christopher et al (1968); they did not observe a conductance peak at impurity concentrations of less than a monolayer. Their junction, however, was different in that the oxide barrier was grown thermally in air. For higher concentration they observed our results of a resistance peak anomaly.

4.3 Tunneling Results and Kondo Coherence Length

So far, we have observed a small conductance peak and a large conductance dip in tunnel junctions doped with two different species of different amounts at the

barrier interface. The regions of agreement with the existing theories have been introduced. The small conductance peak shows Zeeman splitting in a magnetic field, and has the logarithmic temperature and energy dependence as predicted by Appelbaum. We further associate the rapid increase in the conductance with the strong coupling theory of Zawadowski et al. Knowing then that the origin of the zero bias anomalies is due to the interaction between the conduction electrons and the magnetic impurities at the barrier interface, it became important to investigate the effects of the impurities which are introduced inside the metallic electrodes. These effects can reasonably be considered as local disturbances in the conductance electron wavefunctions, rather than modification of the tunneling matrix element such as impurity assisted channels. Since the electron tunneling conductance anomaly can be regarded as a measure of the change in the electron density of states at the barrier interface, it is then possible to study this change as a function of the impurity position and obtain some information about the existence of the Kondo coherence length.

In this experiment we introduced the Ni impurities in a form of a layer like distribution inside the metal and at different distances r from the barrier interface.

The first run was performed to determine the suitable range of thin Al thickness, and the impurity concentration, and is shown in fig. (4.10). The geometry of the high voltage glow discharge was modified to produce a uniform Al_2O_3 barrier over the whole length of the base Al surface. Typical conductance-voltage characteristics of one set of junctions doped with about 5 \AA^0 of Ni impurities are shown in fig. (4.11). The distance of the Ni layer from the interface varies between 10 and 60 \AA^0 . A sharp dip which approaches zero conductance has been observed in all heavily doped junctions. That current is due to the tunneling process over a wide range of bias voltage is obvious from the 0-II excitations at 118 m.V. and from the Al superconducting energy gap characteristics shown in fig. (4.12). The energy gap reflects some proximity structure between the thin and thick Al films decoupled by the magnetic impurities. The double sharp peaks are probably due to energy gaps of two junctions in parallel which are formed because the width of the Ni impurity layer is smaller than that of the Al films. We do not observe a gap for films less than 20 \AA^0 thick, in agreement with the measurements of Townsend et al (1972). The absence of the superconductivity in ultrathin Al films is due to the existence of magnetic impurities. The energy gap characteristics of our junctions are left for further investigations.

Fig. 4.10

Preliminary run on Al-I-Al junction doped with Ni layer introduced at (a) 0 Å⁰; (b) 50 Å⁰; (c) 70 Å⁰; and (d) 150 Å⁰ from the barrier interface.

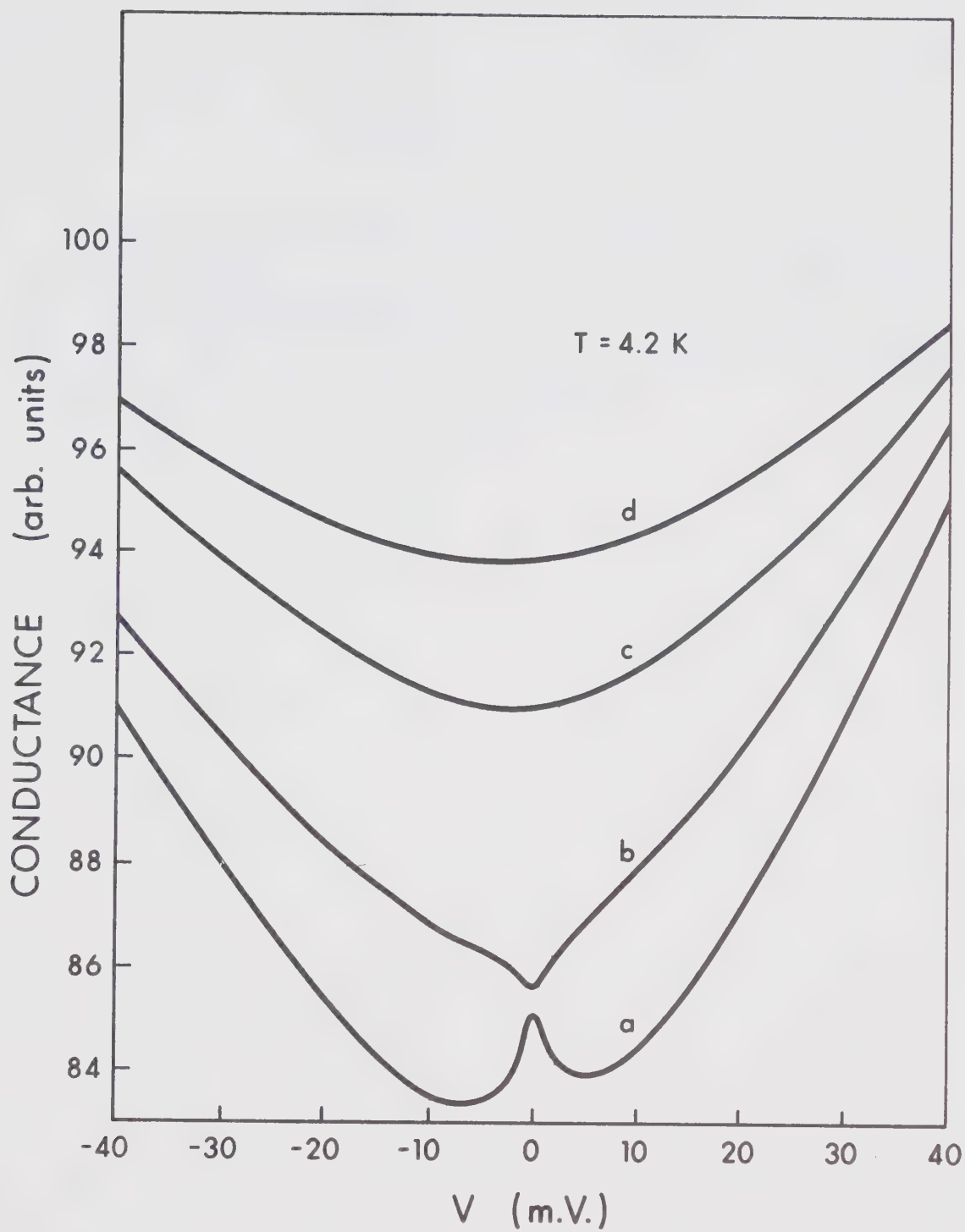


Fig.4.11

Conductance-voltage characteristics for Al-I-Al junctions, doped with $\sim 5 \text{ A}^\circ$ of Ni layer at $r = 11$, 21.5, 32.5 and 56.5 A° , Curves (a), (b), (c) and (e) respectively, Curve (f), same as (e) with no impurities.

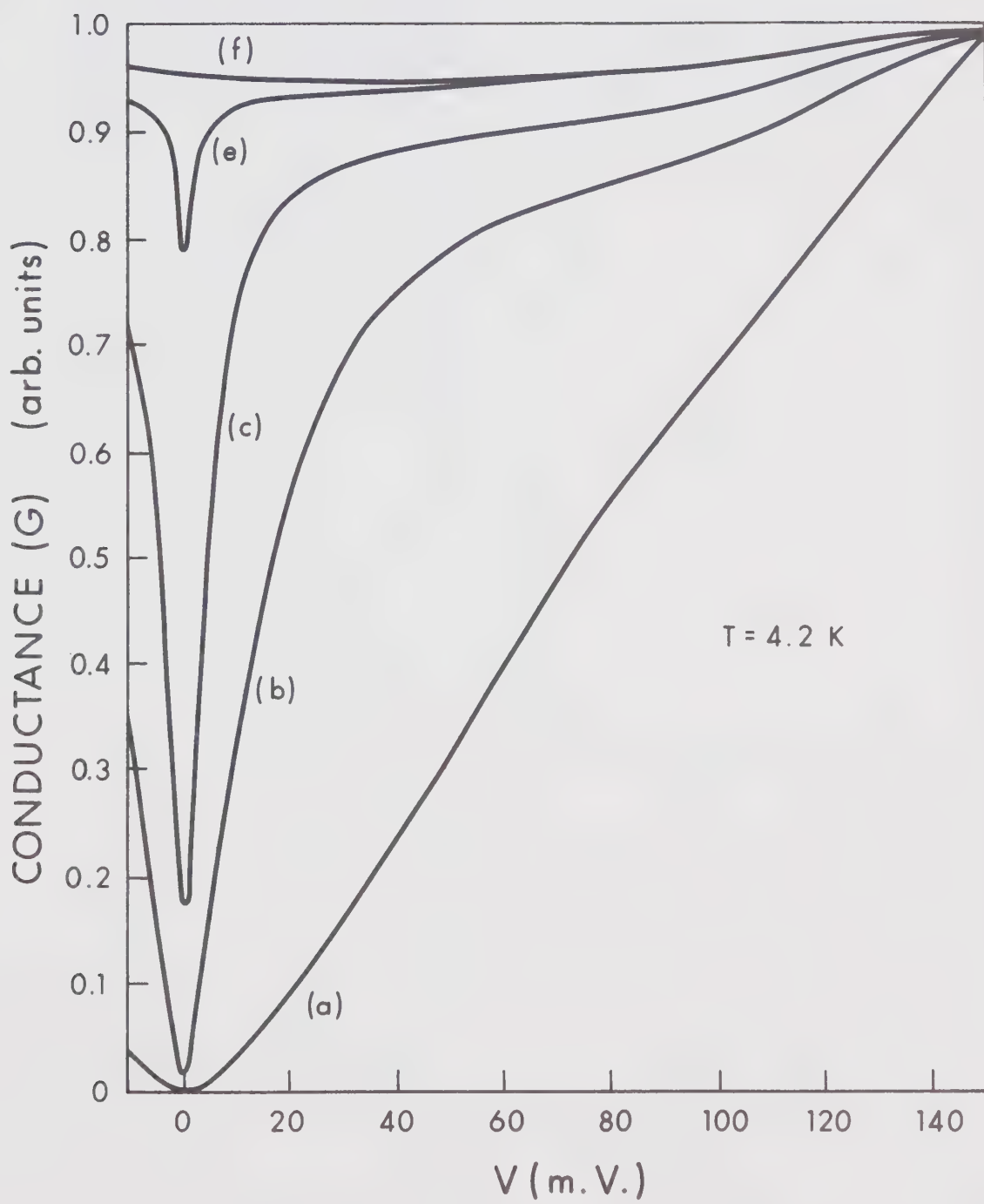
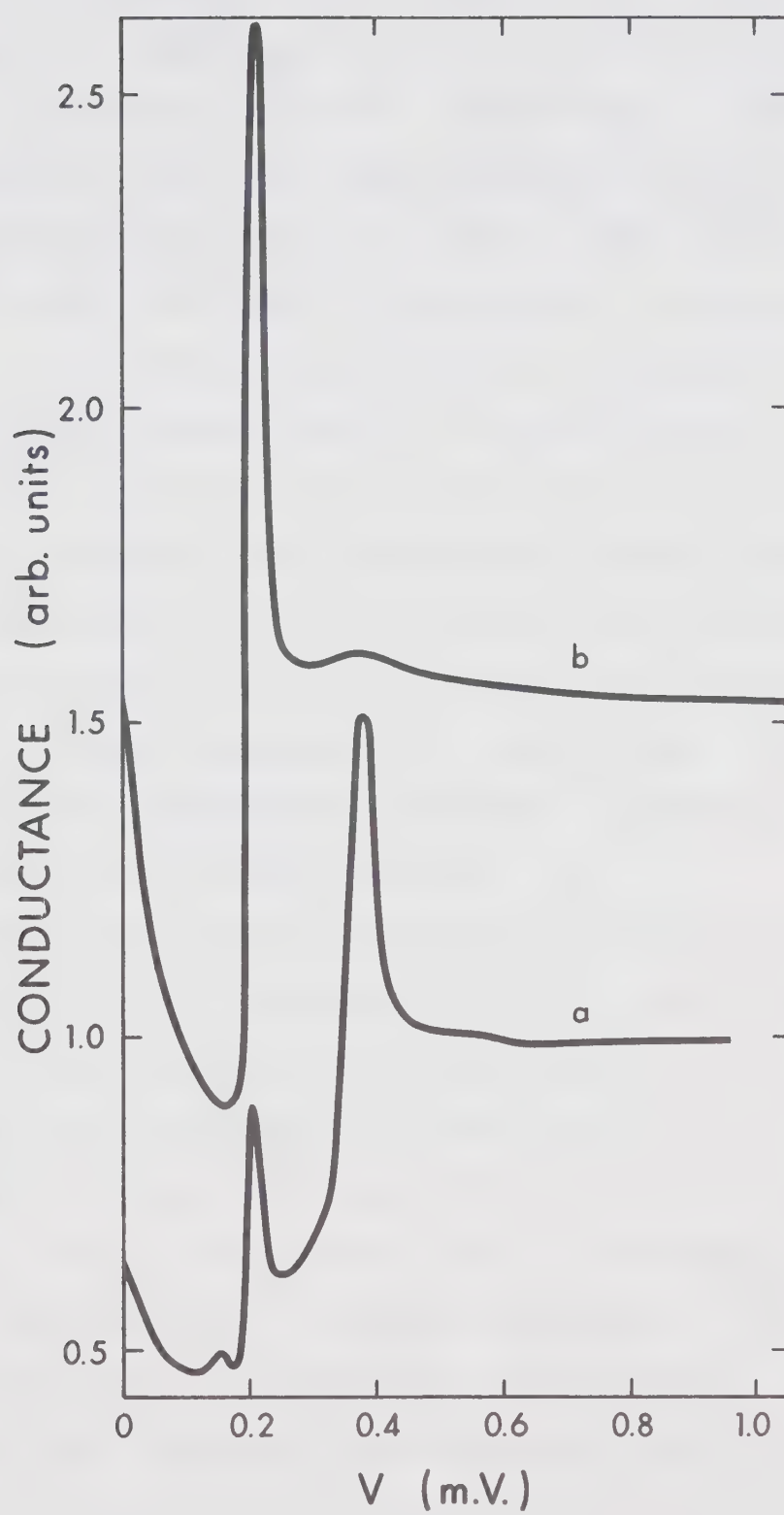


Fig. 4.12

The energy gaps of Al, (a) undoped junction,
(b) 3 \AA^0 of Ni dopant was introduced at $r = 50 \text{ \AA}^0$.



Ni is a suitable dopant because of its high resistance against oxidation, and its low diffusion coefficient in Al. It has been confirmed, theoretically by S6lyom and Zawadowski (1968) and experimentally by Rowell and Shen (1966) and Dumoulin et al (1970), that the dilute magnetic alloy electrodes do not produce a conductance anomaly. The effect of diffusion was investigated by remeasuring the conductance of the same junction three months later, and a change of 10 to 15 % was observed. Therefore diffusion could be neglected during the half an hour necessary to cool the junction down to 80°K.

Curve (c) of fig. (4.11) at different temperatures, and $G(V=0)$ versus temperature is shown in fig. (4.13). The logarithmic temperature dependence of different sets of junctions is shown in fig. (4.14).

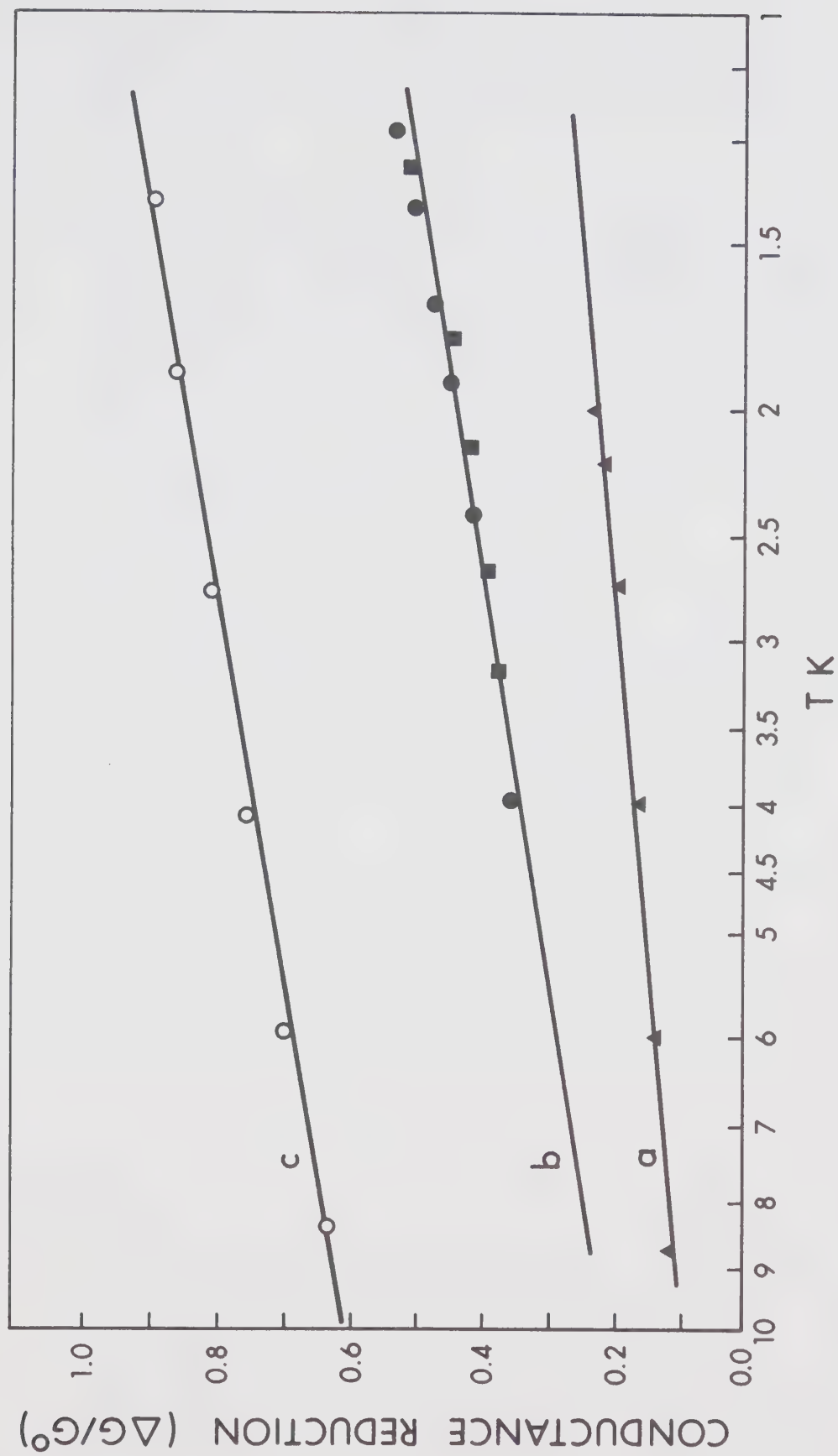
Giaever and Zeller (1968) have produced a sharp conductance dip by including in an Al_2O_3 matrix small metal particles which act as an intermediate state for tunneling. The conductance of their junction has linear dependence on energy and temperature as shown in fig. (4.15a,b), Zeller and Giaever (1969). The magnitude of the conductance dip is slightly dependent on the size of the particles in the range of 38 Å to 110 Å. On the other hand the energy gap characteristics of the particles show a step like increase in the conductance

Fig. 4.13

Curve (c) of fig. 4.11 at different temperatures,
and $G(V=0)$ versus temperature.

Fig. 4.14

The temperature dependence of the conductance reduction $\Delta G/G^0$ for Al-I-Al junctions doped with different amount of impurities at different distances from the barrier-metal interface.

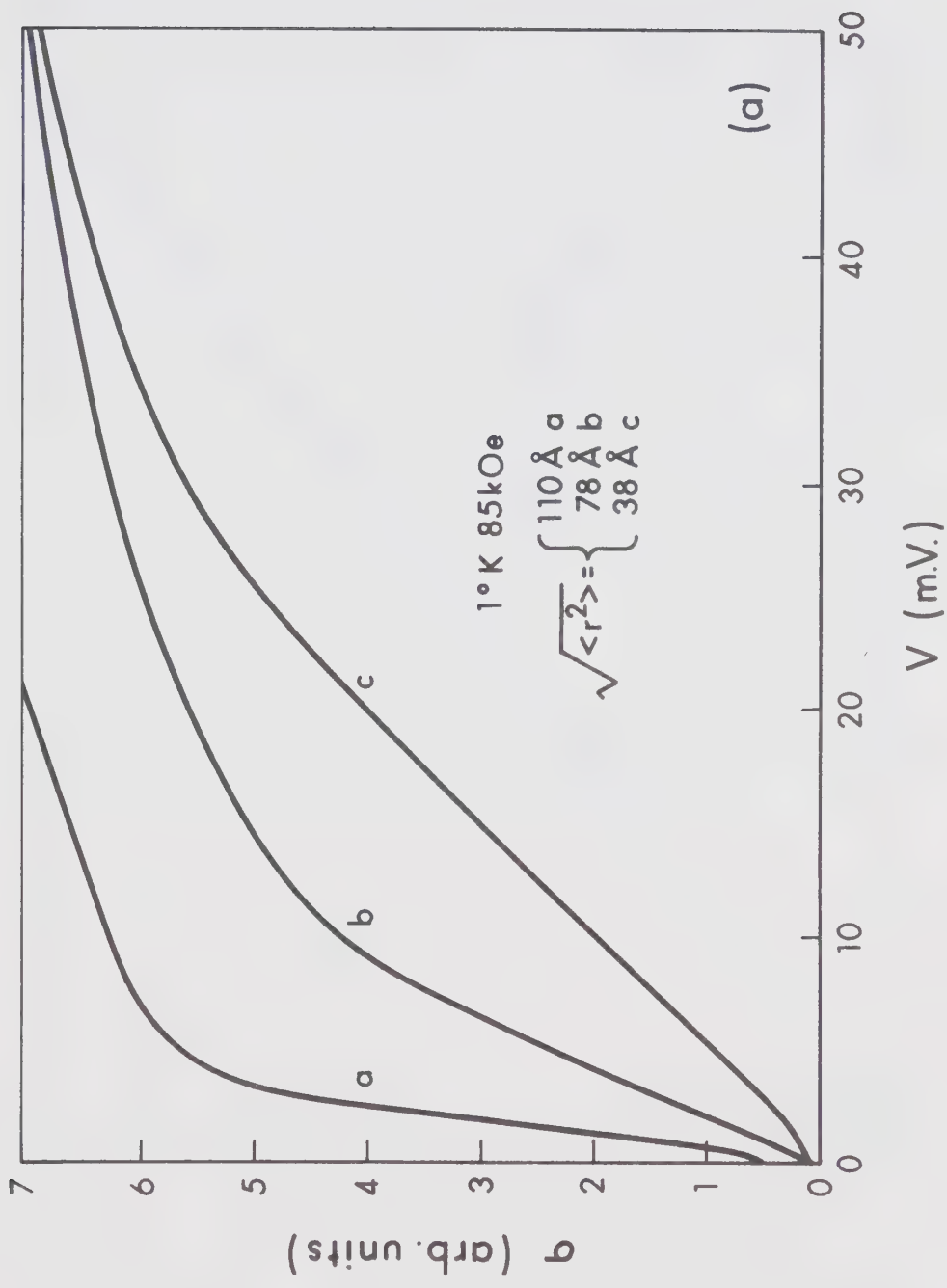


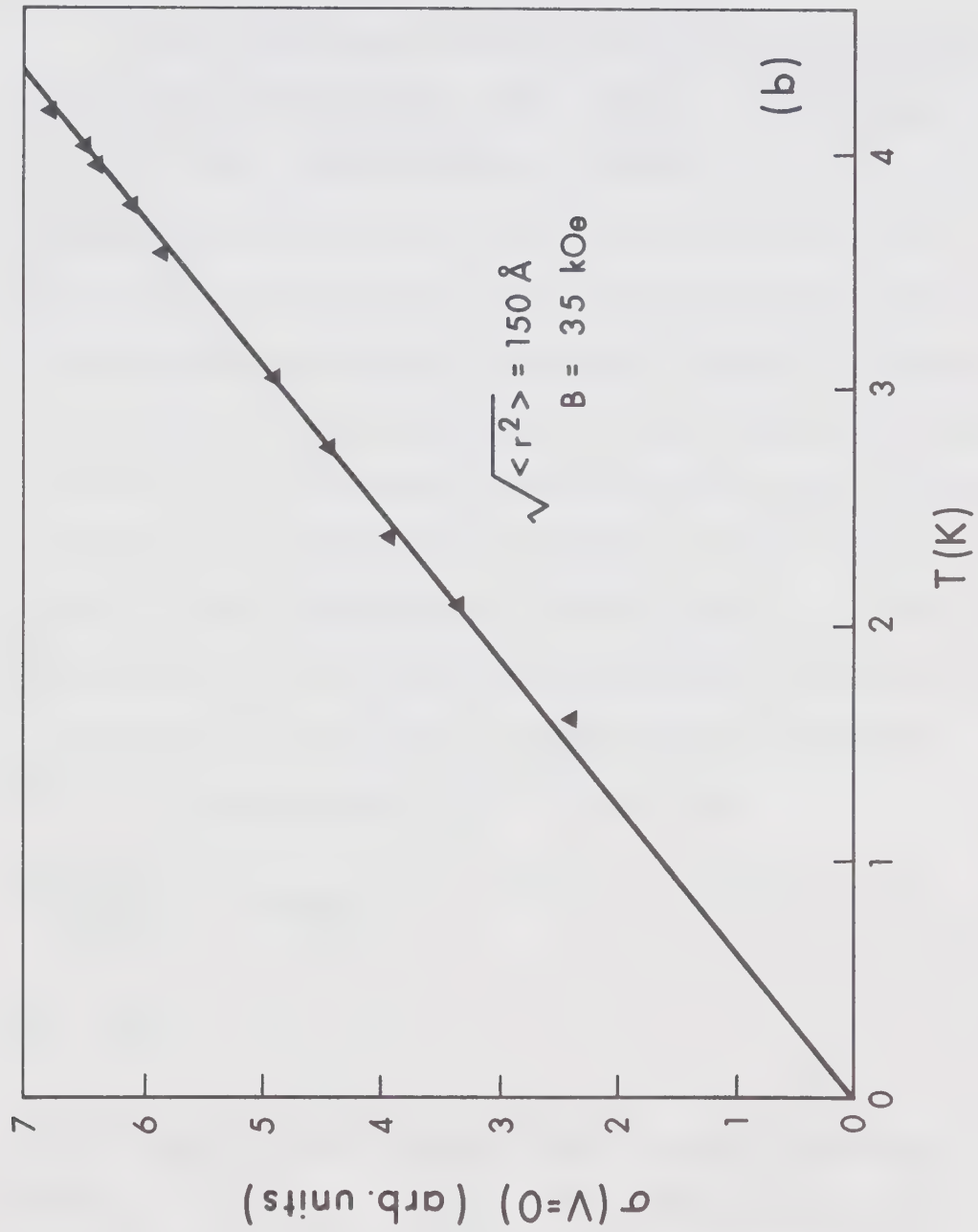
density of states, Zeller and Giaever (1971), but not a peak which is quite different from the results shown in fig. (4.12).

The Giaever-Zeller model is based on the formation of tiny capacitors in the barrier. This requires the existence of a barrier between the imbedded particles and the junction electrodes. In our junctions the oxide is not likely to be formed between the thin and thick Al films during the 20 seconds between their successive evaporations in a vacuum of 10^{-6} torr. Mezei (1969) has done an experiment in which the thin Al film was evaporated and subjected to a background vacuum of 2×10^{-5} torr. for 1 to 27 minutes. Control measurements showed that no insulation developed beyond the experimental resolution of 10^{-4} Ω/mm , and no decrease in the optical absorption of the thin Al layer occurred beyond the detection limit of 0.5 %, indicating an oxidation of less than one atomic layer. As mentioned before, Sec.(3.1), the critical thickness at which the deposited films become electrically continuous depends on the deposition parameters. The slow evaporation rate of a reasonably high melting point material on a substrate at 300°K temperature substrate covered with prenucleation centers, such as Al_2O_3 , would produce ultrathin electrically continuous films. Electrical continuity of Al films 15 Å thick has been reported by Vrba and Woods (1971). Therefore, one expects that the

Fig. 4.15

- (a) The conductance σ versus voltage V for Al-I-Al junctions with Sn particles in the barrier.
 $\sqrt{\langle r^2 \rangle}$ is the average radius of the Sn particle.
- (b) The temperature dependence of $\sigma(V=0)$, Zeller and Giaever (1969).





Al films 20 \AA thick are electrically continuous. As a result the intermediate state tunneling through particles is not present in our junctions.

The conductance versus voltage characteristics of junctions doped with small amounts of Ni impurities at 50 \AA from the interface is shown in fig. (4.16). Preliminary results show that the conductance dip increases linearly with impurity concentration at low concentrations and more rapidly at higher concentrations.

The position dependence of the conductance reduction $|\Delta G/G^0|$ for sets of junctions doped with different amounts of Ni impurities is shown in fig. (4.17). G^0 refers to the conductance of pure junctions. One common feature is that the impurity layers are only effective if they are within 60 \AA of the barrier interface.

Mezei and Zawadowski (1971) found that,

$$\left. \begin{aligned} \frac{\Delta G(d, V=0)}{G^0} &= \frac{\Delta \rho(d, 0)}{\rho^0} = C e^{-r/\zeta_{\Delta}} [2 - e^{-r/\zeta_{\Delta}}], \\ C &= \frac{\pi \rho^0}{2} \text{Im } T(\omega - i\delta) = 1, \end{aligned} \right\} \quad (4.1)$$

in the case of the unitary limit scattering amplitude, where $T = 2i/\pi\rho_0$. At higher impurity concentration, the unitary limit is enhanced by the reduced density of states in the impurity layer. Equation (4.1) is represented by the solid line in fig. (4.17), for $C = 1, 3/2$, and

Fig. 4.16

The conductance-voltage characteristics for Al-I-Al junctions doped approximately with (a) 2.5 A° ; (b) 2 A° ; (c) 1.5 A° ; (d) 0.5 A° and (e) 0 A° of Ni impurity layers at $r = 50 \text{ A}^\circ$.

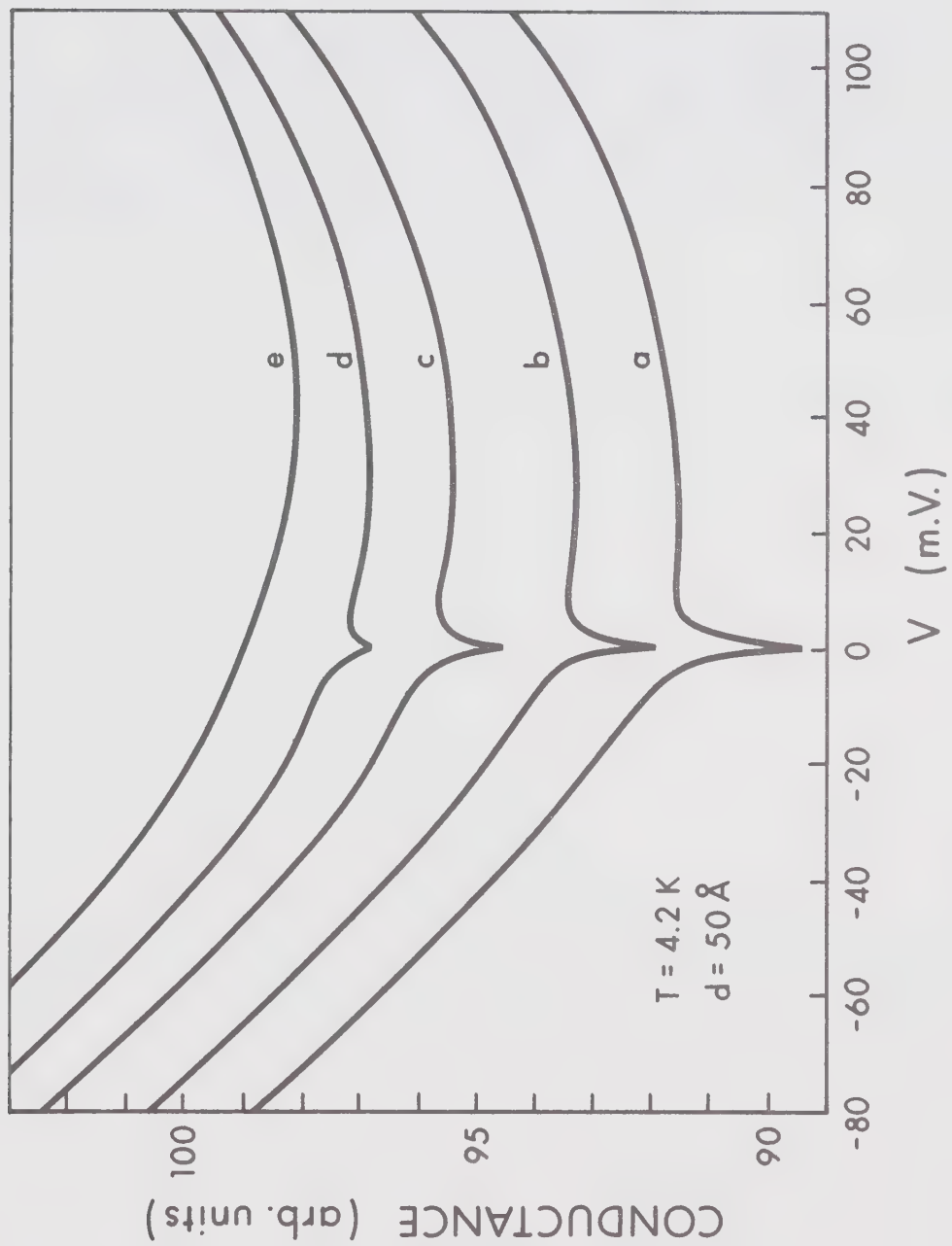
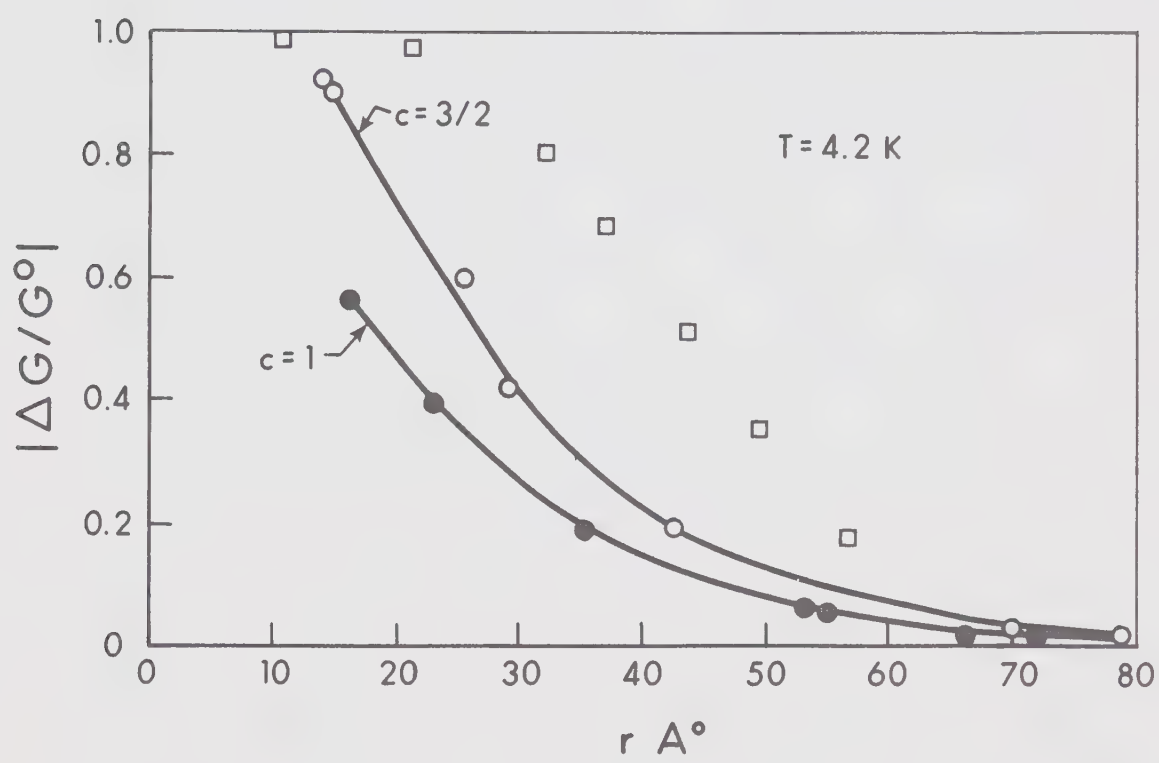


Fig. 4.17

The conductance reduction at zero bias $|\Delta G/G^0|$ as a function of r ; Ni dopant is approximately $\square 5 A^0$, $\circ 3 A^0$, $\bullet 2 A^0$. The solid lines represent $C e^{-r/\xi} [2 - e^{-r/\xi}]$ for $C = 1; 1.5$.



$\zeta_{\Delta} = 16 \text{ \AA}$. The results which fit the predicted relation are those of impurity layers 3 \AA thick. For higher impurity concentration, a self consistent treatment as well as inclusion of barrier interface effects may be necessary to explain the spatial behaviour of the conductance reduction.

In conclusion, we have observed a large conductance reduction, which depends on the position of the impurity layer in the counter electrode. The maximum depression takes place at zero bias for impurities closer to the interface, an indication that a magnetic impurity layer in a non-magnetic host metal is a source of the giant resistance peak anomaly. The observed reduction could be associated with a Kondo coherence length of about 16 \AA for a Ni monolayer in Al. The actual coherence length will be somewhat larger than 16 \AA if the Al films consist of islands not decoupled by an oxide barrier from the counter electrode. The existence of a coherence length of the order of $5\text{--}50 \text{ \AA}$ may be regarded as confirmed by experiments made on different alloy systems. Golibersuch and Heeger (1969) concluded from the analysis of their NMR data that a conduction-electron polarization of the range of 9 \AA exists around the impurities. Edelstein (1969) found conduction electron states inside the superconducting energy gap of a Kondo dilute alloy. He assumed that each impurity is surrounded by a radius

$r = 7.6 \text{ \AA}$, of spin compensated states, where the superconductivity is destroyed. Mezei's (1969) work could be explained by a coherence length of $20 - 50 \text{ \AA}$.

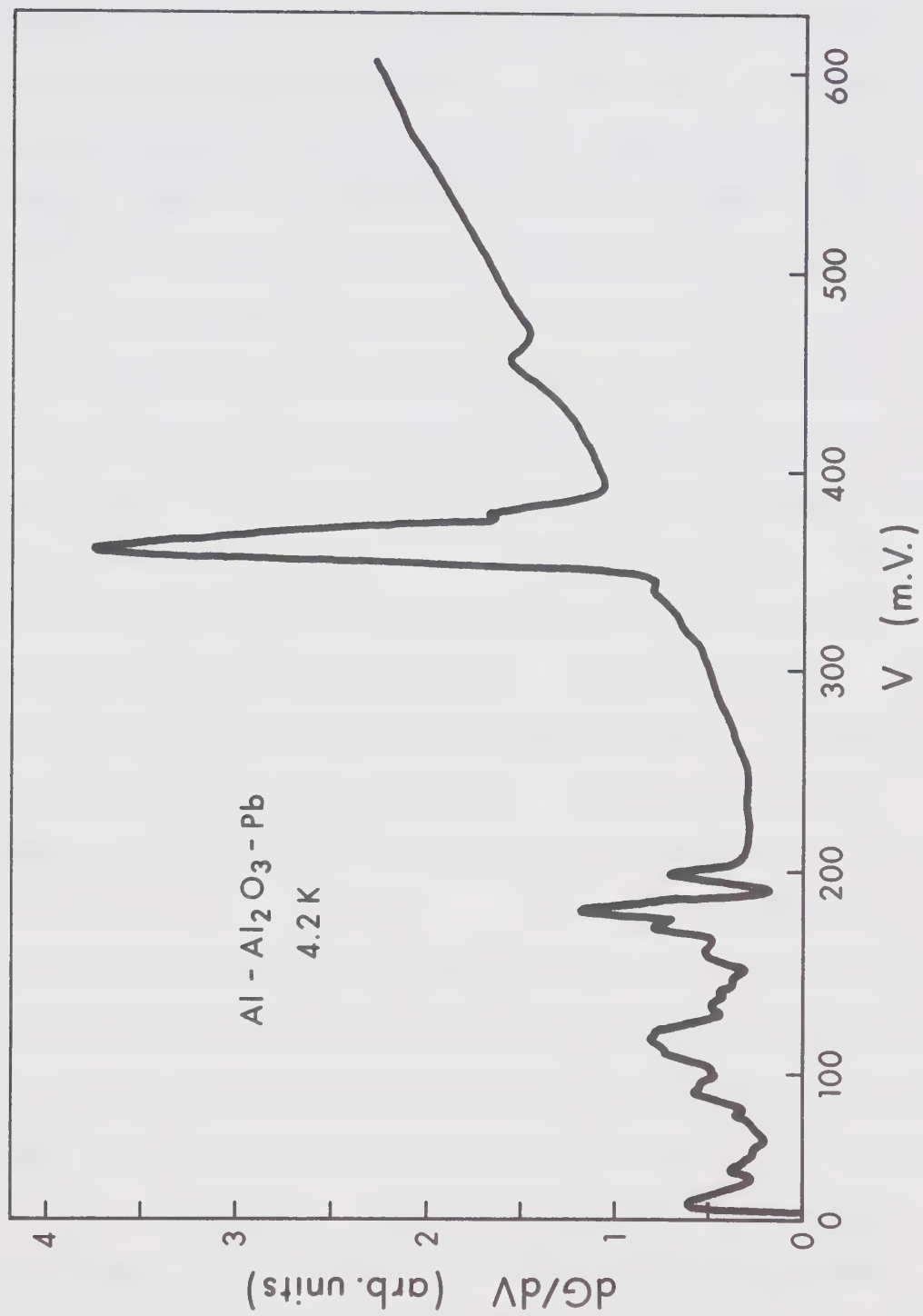
Further work is obviously necessary before reliable values for coherence lengths are obtained, but the results reported here suggest that it may well be possible to do so.

4.4 Al-I-Fe or Ni Junctions

Various structures in the conductance of normal metal tunnel junctions have been identified as due to the interaction of electrons with magnetic or non-magnetic impurities in the oxide or with phonons of the oxide or metal electrodes, to self energy corrections, to the tunneling probability, and to band structure effects. The conductance derivative dG/dV versus bias voltage V of an Al-I-Pb junction is shown in fig. (4.18). The peaks correspond to the excitations of the transverse and the longitudinal phonons of the oxide barrier and the vibrational modes of some of the molecules contaminating the barrier. Very recently structure of NiO was discovered by Adler and Chen (1971) and identified by Tsui et al (1971) as magnon excitations superimposed on the background conductance of Nickel single crystal tunnel junctions. Magnons could also be reflected in the tunneling characteristics as a conductance dip which

Fig. 4.18

dG/dV versus V for an Al-I-Pb junction at 4.2°K . The peaks correspond to different excitations in the junction.



varies as $(\text{eV})^3$, Bennett et al (1969), or as an additional conductance peak which has a half width of one tenth of the maximum magnon frequency. This peak is a result of the interaction between magnetic impurities in the barrier, which are coupled to the bulk magnetization of the electrodes, and the conduction electrons.

We prepared Al-I-Fe or Ni junctions to see if it is possible to observe variations in the density of states of the d-band of Ni near the Fermi energy, excitations of spin waves by tunneling electrons or self energy effects due to the interaction with other excitations. The conductance and its derivative versus voltage characteristics of an Al-I-Fe junction is shown in fig. (4.19) and (4.20). The tunneling mechanism is the dominant process in our tunnel junction because of the observation of the Al superconducting energy gap and the 0-H excitation at 118 m.V. However, the conductance increases rapidly with bias voltage, which could mask the weak superimposed structures. The conductance has a parabolic dependence on the bias voltage up to 0.6 volts, with deviations around the origin, which could be due to changes in the electron density of states available for tunneling. The excitation of magnons could lead to an increase in the conductance for bias voltages up to 100 m.V., as pointed out by Rowell (1969). The prediction of the renormalization effects in the

Fig. 4.19

G-V characteristics for Al-I-Fe junction at
4.2°K.

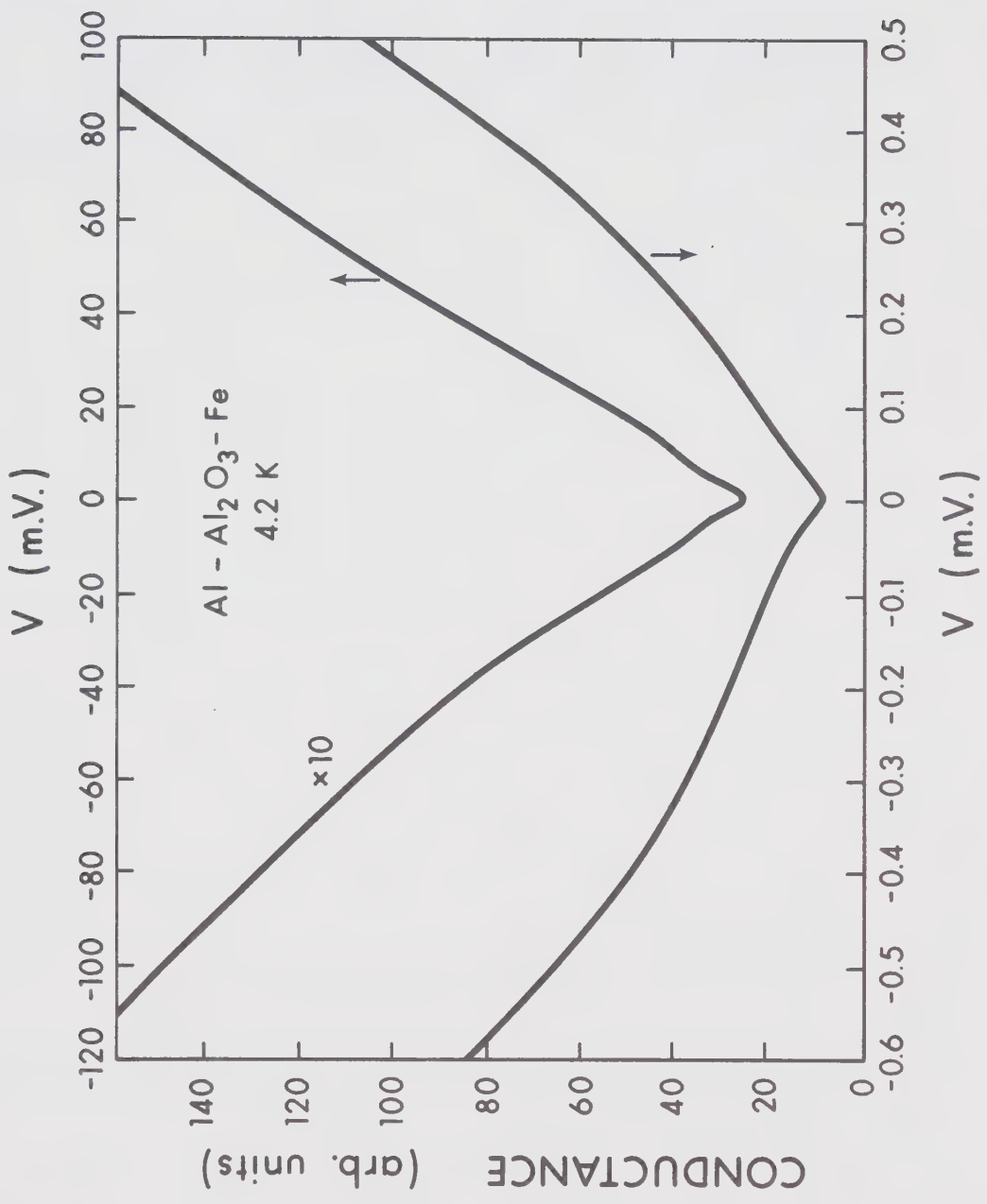
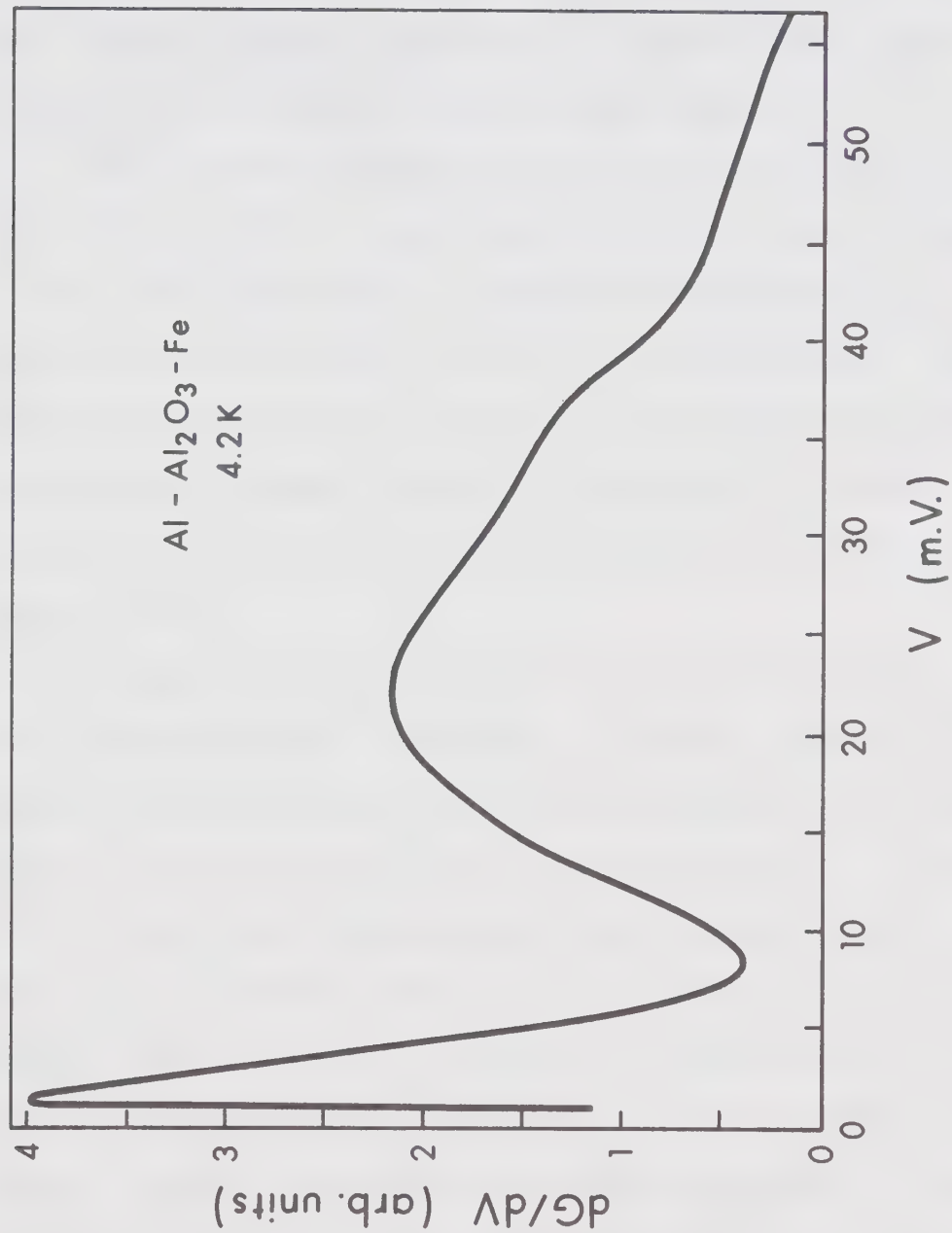


Fig. 4.20

(dG/dV) versus V at 4.2°K for an Al-I-Fe junction.



form of an additional peak or structure which could be associated with the magnon excitation has not been observed in our junctions. Rochlin et al (1970) did not observe magnon structure in their Cr-CrO-M junctions, though the CrO forms a well behaved barrier.

We observed strong structures between 20 and 40 m.V. which could be associated with the phonon modes of Fe. The structure is probably smeared by the phonon structure of Al which occurs in the same range. The phonon structure of Al is rarely observed in Al-I-Al junctions. We were not able to produce Sn-SnO-Fe junctions in order to resolve the Fe phonon structure beyond doubt.

Figs. (4.21) and (4.22) show the conductance and its derivative as a function of the bias voltage of an Al-I-Ni junction. In the low voltage range, there exist a 4 % conductance change from -100 m.V. to 100 m.V., and a small conductance dip at zero bias. Similar observations have been reported by Rowell (1969) while Chen and Adler observed a 5 % conductance dip around the zero bias. It is too early to associate these changes with magnon-assisted tunneling or band structure effects, since deformations of the oxide or impurities at the barrier interface could possibly produce such characteristics. The peak at 120 m.V. is due to the O-H impurity excitation, though it has

Fig. 4.21

G-V characteristics at 4.2°K for an Al-I-Ni junction.

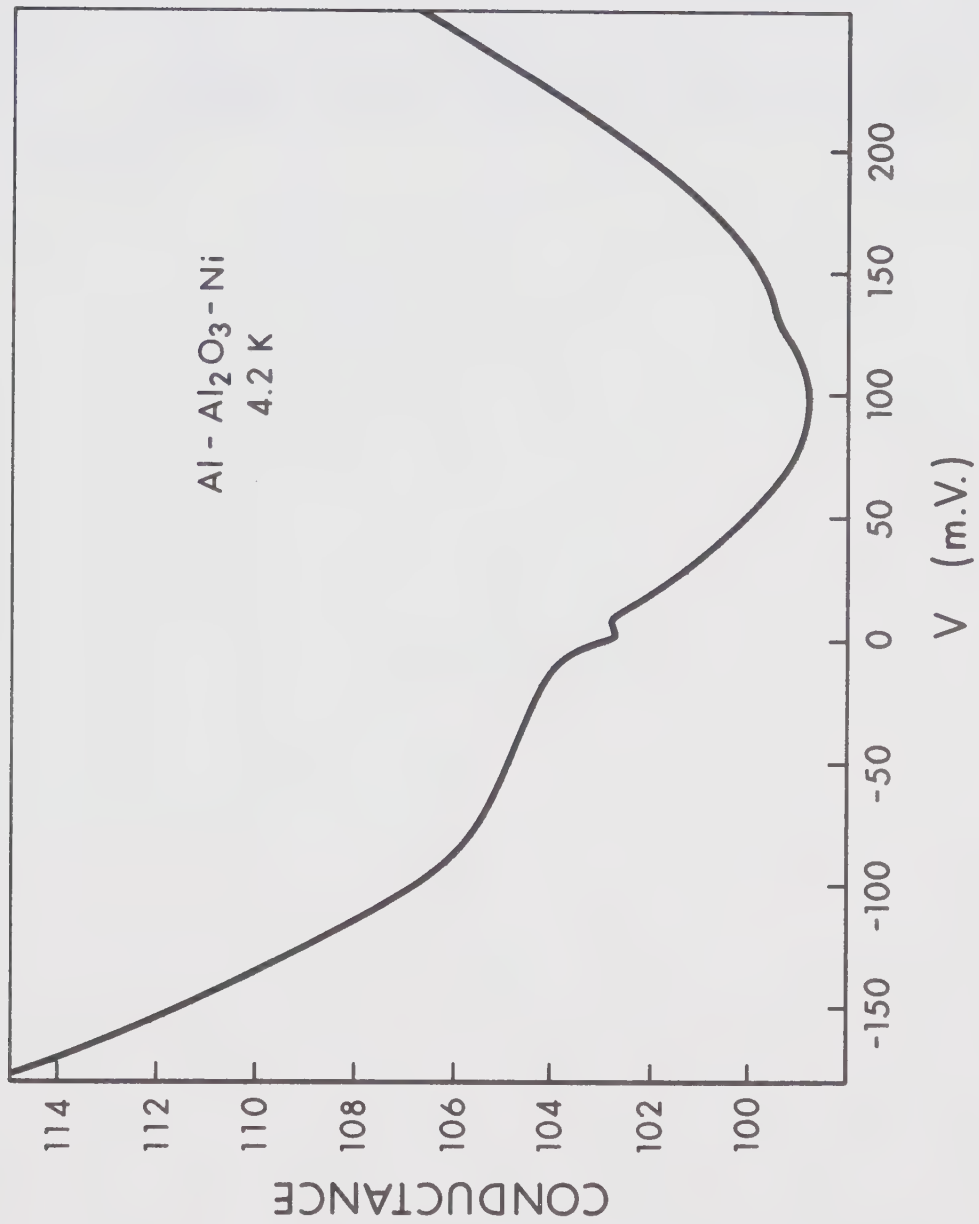
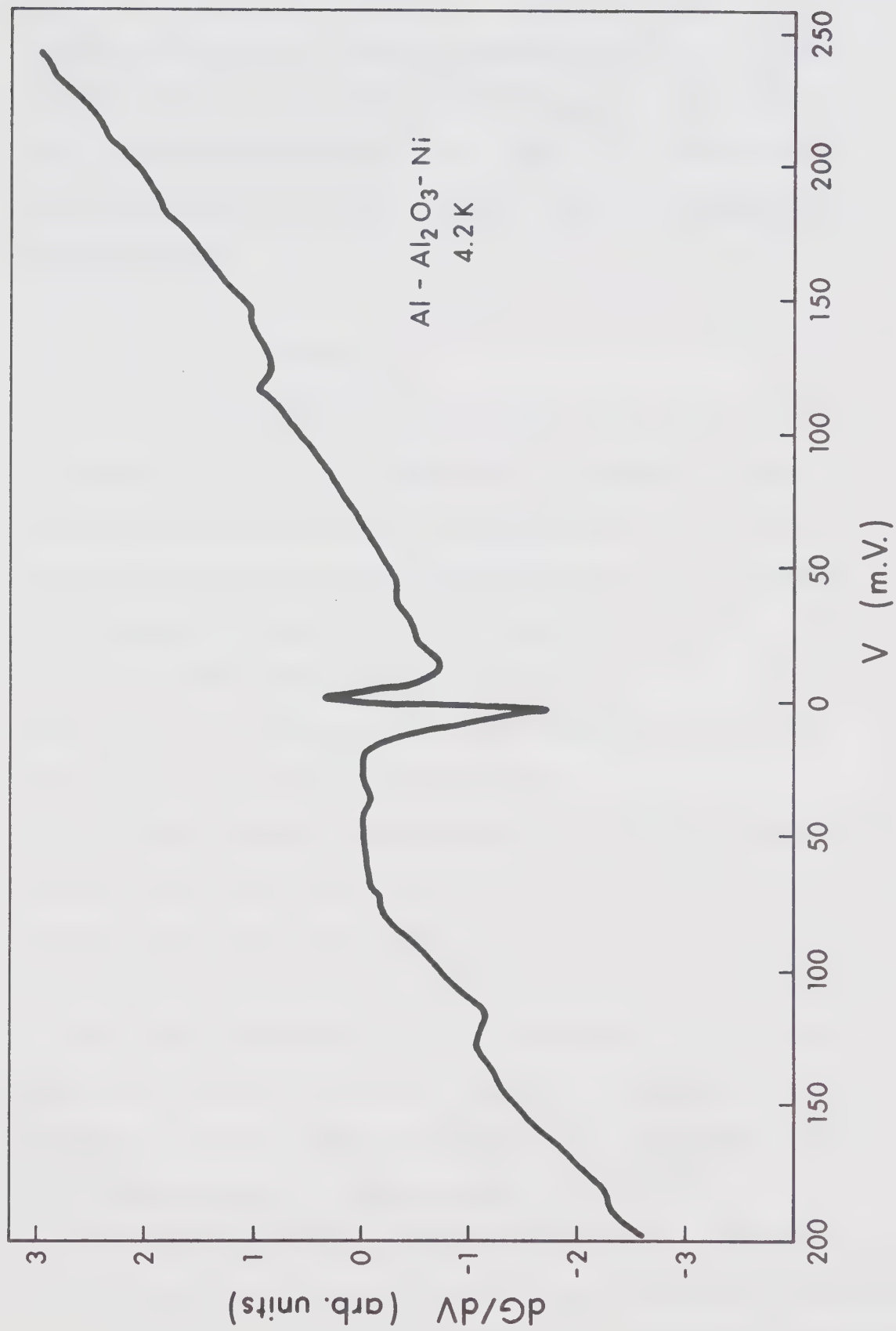


Fig. 4.22

(dG/dV) versus V at 4.2°K for an Al-I-Ni junction.



been associated with magnon excitation of NiO, Tsui et al (1971). It seems that the magnon structure of the magnetic electrode is too weak to be observed in the tunneling conductance which increases rapidly with bias voltage.

4.5 Iron Oxide Barriers

The iron oxide barriers have been grown either thermally or in a glow discharge of oxygen. Tunnel barriers formed by severe thermal oxidation have a large resistance change with temperature and bias voltage. For example, close to the zero bias, a 30 ohms resistance at 70°K increases to 10^4 ohms at 4.2°K; at the zero bias the value of the resistance is beyond the impedance of the present equipment.

Light thermal oxidation at 100°C in air for 10-15 minutes produces barriers which have the tunneling resistance behaviour shown in fig. (4.23). The width of the resistance peak is about 2 m.V. The energy and temperature dependence of the resistance of a tunnel barrier formed in a glow discharge of oxygen is shown in fig. (4.24). These results are in agreement with the measurements of Christopher et al (1968).

The theoretical models, discussed in Chapter 2, show that the origin of the zero bias tunneling anomalies is due to the interaction between the conduction electrons

Fig. 4.23

The dynamical resistance R versus V at different temperature for an $\text{Fe-Fe}_x\text{O}_y\text{-Al}$ junction (the tunnel barrier was formed in air at 100°C for about 10 minutes).

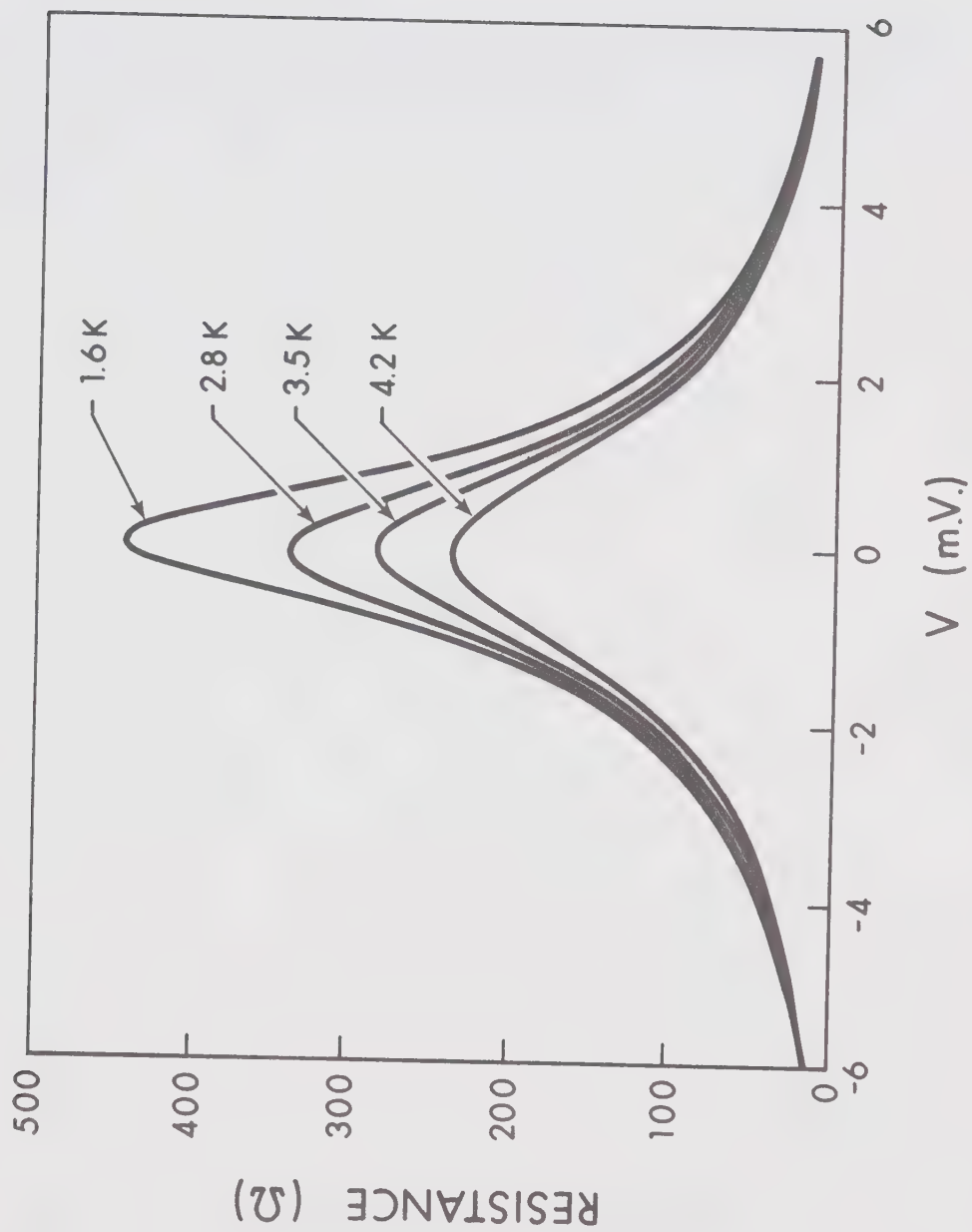
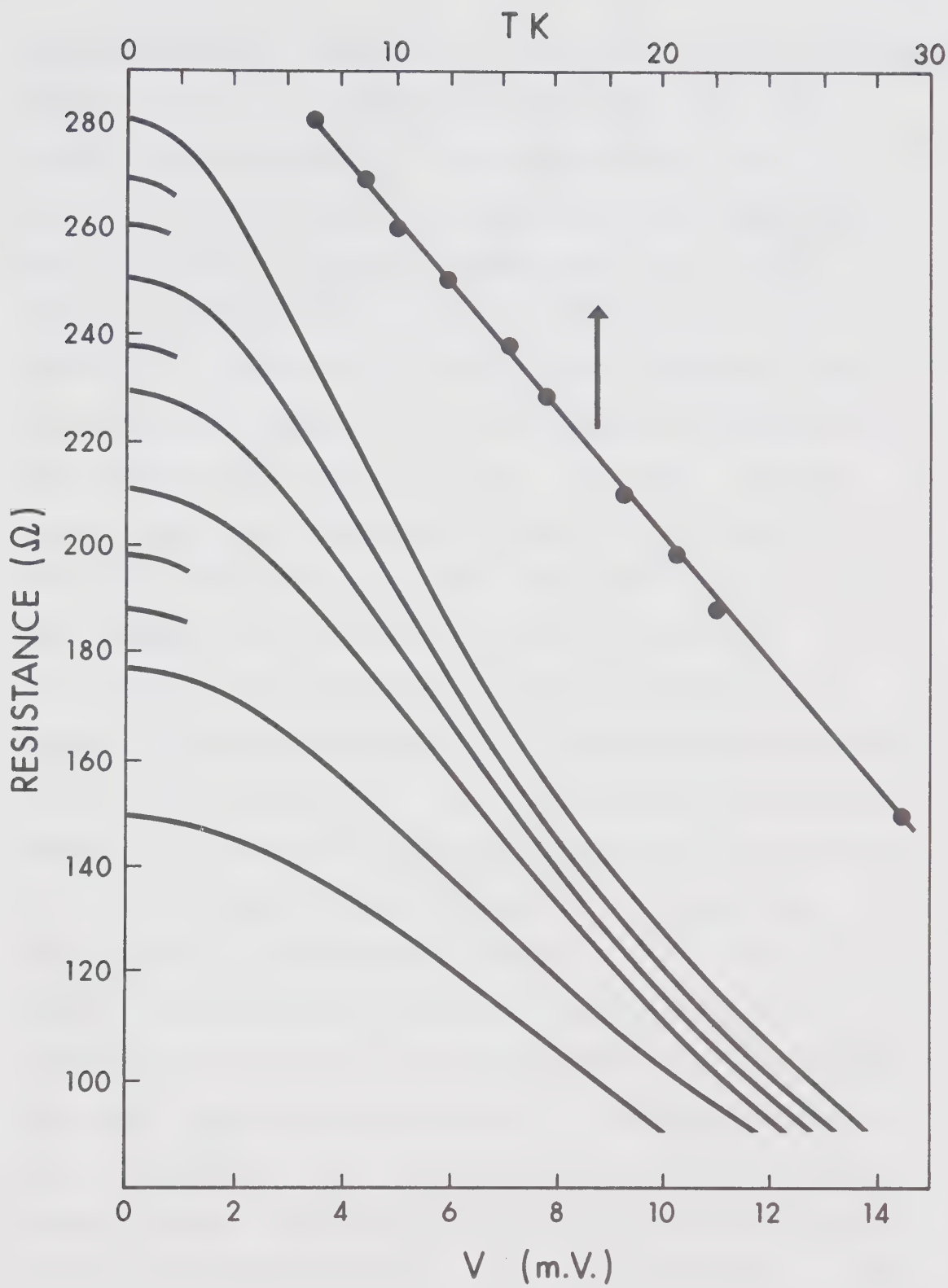


Fig. 4.24

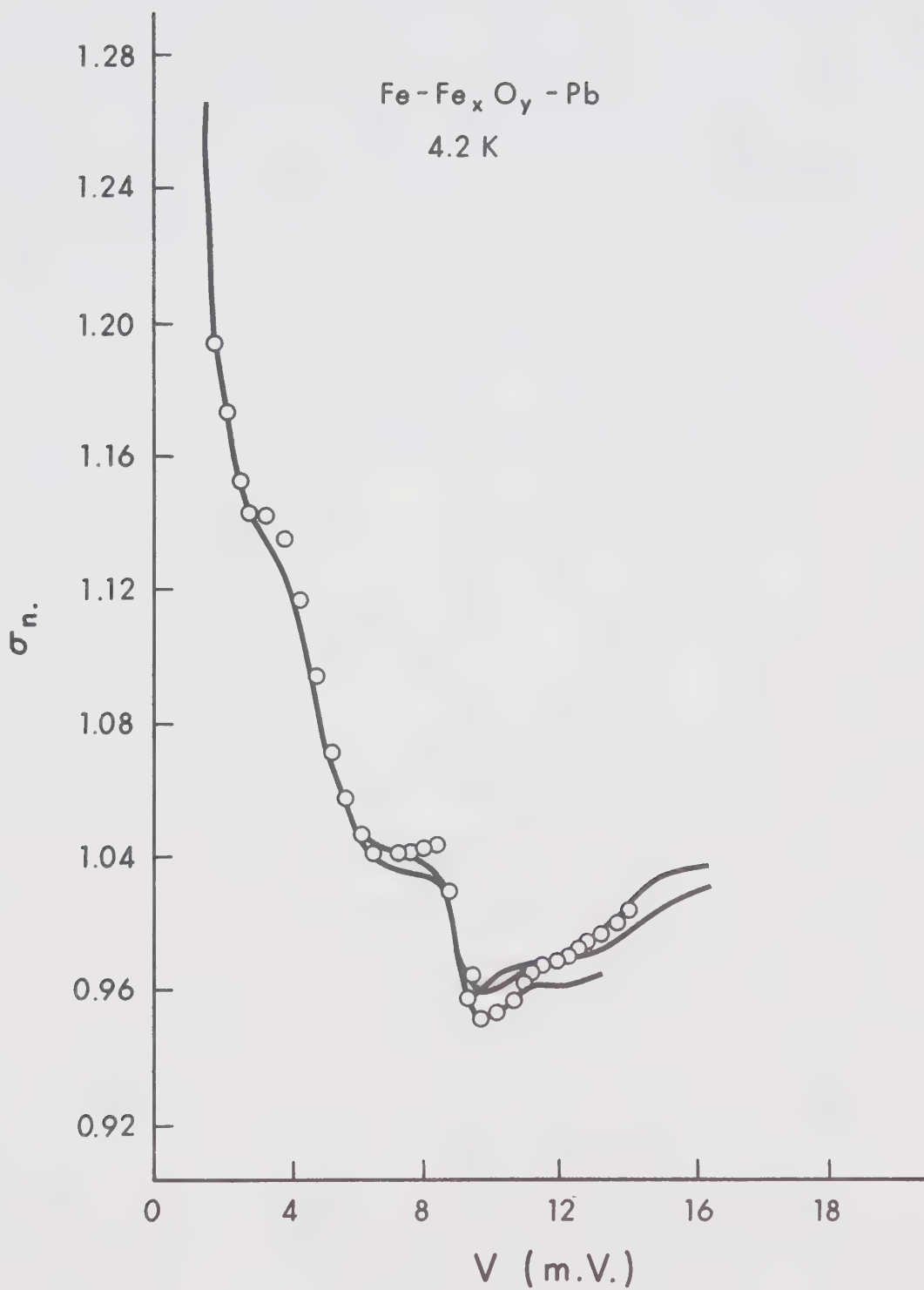
R versus V at different temperatures and $R(V=0)$ versus T for Fe_3O_4 barrier formed in a glow discharge of oxygen.



and the magnetic impurities. Therefore, a pair breaking effect should be evident when one of the electrodes become superconducting. This should result in a decrease of the superconducting transition temperature and a smearing of the gap characteristics. In our results, we found that the energy gap of the Pb and Sn counter electrodes as well as their transition temperatures are similar to those obtained from tunneling measurements of Al-Al₂O₃-Pb (Sn) junctions. Similar results have been reported by Rowell et al (1968) in Cr-CrO-Pb junctions. However, they had found out that the strength of Pb phonon structure is decreased, and had concluded that the energy gap is affected by the anomaly at higher energies. The normalized conductances of different Fe-Fe_xO_y-Pb and Al-Al₂O₃-Pb junctions are shown in fig. (4.25). The phonon structure is slightly affected at higher bias because the junctions have small zero bias resistance anomaly. In the case of a Sn counter electrode on the top of the same Fe_xO_y, the resistance peak anomaly was much larger, and the phonon structure was very much perturbed. The rapid change in the conductance with bias voltage masks out the superimposed phonon structure of Sn. From the above discussions, we conclude that the tunneling anomalies are not necessarily magnetic in origin, but rather due to the structure, the height of the barrier and the electronic

Fig. 4.25

The normalized conductance σ_n versus voltage for Fe-Fe₃O₄-Pb junctions (solid lines) and for Al-Al₂O₃-Pb junction (circles).



behaviour of the barrier oxide-metal interface.

Different types of Fe_xO_y could be formed on the surface of the iron electrode, depending on the parameters of oxidation. Experimental measurements indicate that the main oxide, Fe_3O_4 , has an unusually high conductivity and other electronic behaviour. One of its electrical properties is the order-disorder transition that takes place at 119°K , and the dominant mechanism of conductivity is due to the exchange of electrons between the ferrous and ferric ions in the octahedral lattice sites. Electrical conductivity measurements by Miles et al (1957) indicated that a semiconducting behaviour below 119°K exists with a very low-temperature activation energy of the order of 30 meV. Verwey and Haayman found that excess oxygen lowers the transition temperature and causes the transition to be less sharp. We observed an enormous drop in zero bias resistance between 4.2 and 77°K which may be connected with the ordering transition in magnetic iron oxide Fe_3O_4 . The Fe_2O_3 is a relatively good insulator with a resistivity of the order of $10^{11} \Omega\text{cm}$ and probably has a substantially larger barrier height for tunneling than that of Fe_3O_4 . If the oxidation of the iron proceeds in such a way that a continuous layer of Fe_2O_3 is formed, then the larger barrier height would produce more ideal tunneling characteristics at low voltages.

The magnitude of the zero bias resistance anomaly depends on the counter electrode. It seems possible then that the barrier oxide counter electrode interface forms some sort of glassy semiconducting structure, with the property of a low localized density of states around the Fermi energy which rapidly increases away from the Fermi level. Therefore the available density of states for tunneling electrons which increases with bias voltage could lead to the observed conductance anomaly.

CHAPTER 5

SUMMARY AND CONCLUSIONS

In this thesis we have reported the results of studies on the conductance characteristics of Al-I-Al junctions doped with Ni and Fe impurities. The observed zero bias anomalies have been attributed to the exchange interaction between the conduction electrons and magnetic impurity spins.

We found that a small amount of magnetic dopant can produce a conductance peak anomaly with a Zeeman splitting in a magnetic field. The interaction between the magnetic impurities was found to affect the conductance anomalies even at low concentration. Therefore the extraction of the gyromagnetic ratio g of the localized magnetic moments or its negative shift $-2J\rho$ from the results of the conductance anomaly without considering the interaction between the magnetic impurities may be uncertain.

Upon increasing the amount of magnetic dopant a conductance peak superimposed on a resistance peak anomaly was observed. The conductance peak is due to impurities in the barrier, while the resistance peak is due to impurities in the metallic electrode. This conclusion has been confirmed experimentally by

introducing the magnetic dopant in the form of an impurity layer inside the counter electrode and at different distances from the barrier-electrode interface. A tunneling conductance reduction (resistance peak anomaly) which is larger for impurity layers closer to the interface was observed. The result of this experiment was compared with Mezei and Zawadowski's theory. A Kondo coherence length has been associated with the effective range of the magnetic impurity layers. Much more work has to be done before this conclusion can be considered as final.

The results on Al-I-Ni or Fe junctions do not reflect the electron-magnon or band structure effects predicted by the different theories. However, structure which could be associated with the phonon modes of Fe between 20 and 40 m.V. has been observed.

The tunneling anomalies of Fe-Fe₃O₄-M junctions have been attributed to a small barrier height and the structure of the barrier-metal interface.

REFERENCES

- Abrikosov, A.A. (1965), Phys. 2, 5; 2, 61.
- Abrikosov, A.A. and Gorokov, L.P. (1961), Soviet Phys. 12, 1243.
- Adler, J.G. (1969), Phys. Letters 29A, 675.
- Adler, J.G. and Chen, T.T. (1971), Solid State Commun. 9, 501.
- Ambergaokar, V. and Baratoff, A. (1963), Phys. Rev. Letters 10, 486.
- Anderson, P.W. (1966), Phys. Rev. Letters 17, 95.
- Appelbaum, J.A. (1966), Phys. Rev. Letters 17, 91.
- Appelbaum, J.A., Phillips J.C. and Tzouras, G. (1967), Phys. Rev. 160, 554.
- Appelbaum, J.A. and Brinkman, W.F. (1969), Phys. Rev. 183, 553; 186, 464.
- Appelbaum, J.A. and Brinkman, W.F. (1970), Phys. Rev. B 2, 907.
- Bardeen, J., Cooper L.N. and Schrieffer, J.R. (1957), Phys. Rev. 108, 1175.
- Bardeen, J. (1961), Phys. Rev. Letters 6, 57.
- Bardeen, J. (1962), Phys. Rev. Letters 9, 147.
- Behrndt, K.H. (1966), in Physics of thin films [G. Hass and R.E. Thun, eds.]3, 1; Academic Press Inc., New York (1966).
- Bennett, A.J., Duke, C.B. and Silverstein, S.D. (1968), Phys. Rev. 176, 969.

- Chen, T.T. and Adler, J.G. (1970), Solid State Commun. 8, 1965.
- Chopra, K.L. (1966), J. Appl. Phys. 37, 2249.
- Chopra, K.L. (1968), J. Appl. Phys. 39, 1874.
- Chopra, K.L. (1969), Thin Film Phenomena [McGraw Hill, New York (1969)].
- Christopher, J.E., Coleman, R.V., Isin, A. and Morris, R.C. (1968), Phys. Rev. 172, 485.
- Cohen, M.H., Falicov, L.M. and Phillips, J.C. (1962), Phys. Rev. Letters 8, 316.
- Coles, R.B. (1964), Phys. Letters 8, 243.
- Duke, C.B. (1969) in Tunneling in Solids, Solid State Physics, Supplement 10, 1969.
- Duke, C.B. (1969) in Tunneling Phenomena in Solids (Edited by Elias Burstein, Plenum Press, New York).
- Duke, C.B., Silverstein, S.D. and Bennett, A.J. (1967), Phys. Rev. Letters 19, 315.
- Dumouline, L., Guyon, E. and Rochline, G.I. (1970), Solid State Commun. 8, 287.
- Edelstein, A.S. (1969), Phys. Rev. 180, 505.
- Esaki, L. (1957), Phys. Rev. 109, 603.
- Fisher, J.C. and Giaever, I. (1961), J. Appl. Phys. 32, 172.
- Fowler, R.H. and Nordheim, L. (1928), Proc. Roy. Soc. (London) A119, 173.
- Frenkel, J. (1930), Phys. Rev. 36, 1604.

- Giaever, I. and Zeller, H.R, (1968), Phys. Rev. Letters 20, 1504.
- Golubersuch, D.C. and Heeger, A.J. (1969), Phys. Rev. 182, 584.
- Gupta, H.M. and Upadhyaya, U.N. (1971), Phys. Rev. B 4, 2765.
- Hartman, T.E. (1966), J. Vacuum Sci. Tech. 3, 28.
- Holland, L. (1963), Vacuum Deposition of Thin Films (Chapman and Hall, London, 1963).
- Isin, A., Christopher, J.E, and Coleman, R.V. (1968), J. Appl. Phys. 39, 704.
- Jacklevic, R.C. and Lambe, J. (1966), Phys. Rev. Letters 17, 1139.
- Kasuya, T. (1956), Prog. Theor. Phys. 16, 45.
- Kondo, J. (1964), Prog. Theor. Phys. 32, 37.
- Levistein, H.J. (1949), J. Appl. Phys. 20, 306.
- Lillienfeld, J.E. (1922), Physik Z. 23, 506.
- Lythall, D.J. and Wyatt, A.G.F. (1968), Phys. Rev. Letters 20, 1361.
- Mezei, F. (1967), Phys. Letters 25A, 534.
- Mezei, F. (1969), Solid State Commun. 7, 771.
- Mezei, F. and Zawadowski, A. (1971), Phys. Rev. B 3, 167, 3127.
- Miles, J.L. and Smith, P.H. (1963), J. Electrochem. Soc. 110, 1240.
- Nagaoka, Y. (1965), Phys. Rev. 138A, 1112.

- Neugebauer, C.A. (1959), in Structure and Properties of Thin Films [Neugebauer, C.A., Newkrik, J.B. and Vermilya, D.A. eds.] Wiley, New York (1959).
- Nielsen, P. (1969), Solid State Commun. 7, 1429.
- Nielsen, P. (1970), Phys. Rev. B 2, 3819.
- Oppenheimer, J.R. (1928), Phys. Rev. 31, 66.
- Pocza, J.F. (1967) in Proceeding of the Second Colliquim of Thin Film (Hahn, E. Ed.)
- Poppa, H. (1967), J. Appl. Phys. 38, 3883.
- Rochlin, G.I. and Hansma, P.K. (1970), Phys. Rev. B 2, 1460.
- Rogers, J.S. (1970), Rev. Scient. Instrum. 41, 1184.
- Rowell, J.M. and Shen, L.Y.L. (1966), Phys. Rev. Letters 17, 15.
- Rowell, J.M. (1969), J. Appl. Phys. 40, 1211.
- Rowell, J.M., McMillan, W.L. and Feldman, W.L. (1969), Phys. Rev. 180, 658.
- Sauerbrey, G. (1959), Physik 155, 206.
- Shen, L.Y.L. and Rowell, J.M. (1968), Phys. Rev. 165, 566.
- Sólyom, J. and Zawadowski, A. (1968), Phys. Kondensierten Materie 7, 325; 7, 342.
- Steckelmacher, W. (1966), in Thin Film Microbalance (L. Holland ed.), John Wiley & Sons, Inc., New York (1966).
- Suhl, H. and Wong, D. (1967), Phys. 3, 17.
- Tedrow, P.M. and Meservey, R. (1971), Phys. Rev. Letters 26, 192.

- Tomashov, N.D. (1966), Theory of Corrosion and Protection of Metals, The MacMillan Co., New York (1966).
- Townsend, P., Greogory, S. and Toylor, R.G. (1972), Phys. Rev. B 5, 54.
- Tsui, D.C., Dietz, R.E. and Walker, L.R. (1971), Phys. Rev. Letters 27, 1729.
- Uyeda, R. (1942), Proc. Phys. Math. Soc. Japan 24, 809.
- Vrba, J. and Woods, S.B. (1971), Phys. Rev. B 3, 2243.
- Warner, A.W. and Stachbridge, C.D. (1963), J. Appl. 34, 437.
- Wolf, E.L. and Losee, D.L. (1970), Phys. Rev. B 2, 3660.
- Wyatt, A.F.G. (1964), Phys. Rev. Letters 13, 401.
- Wyatt, A.F.G. (1970), Phys. Rev. Letters 33A, 101.
- Yosida, K. (1957), Phys. Rev. 106, 383; 107, 396.
- Zawadowski, A. (1967), Phys. Rev. 163, 341.
- Zeller, H.R. and Giaever, I. (1969), Phys. Rev. 181, 789.
- Zeller, H.R. and Giaever, I. (1971) in "Proc. of the International Conference on the Science of Superconductivity" [Edited by Frank Chilton, North Holland Publishing Company (1971)].
- Zener, C. (1951), Phys. Rev. 87, 440.

B30043